Naval Research Laboratory

Washington, DC 20375-5320

(2)

NRL/MR/4721—92-6980

X-Ray Laser Program Final Report for FY91

Radiation Hydrodynamics Branch
Plasma Physics Division

September 16, 1992

This work was supported by the Strategic Defense Initiative Organization under Job Title, Ultra Short Wavelength Laser Research

REPORT DOCUMENTATION PAGE

Form Approved
OMB No. 0704-0188

1. AGENCY USE ONLY (*Leave Blank*)	2. REPORT DATE	3. REPORT TYPE AND DATES COVERED
	September 16, 1992	Final 10-1/90 — 9/30/91

4. TITLE AND SUBTITLE

X-Ray Laser Program Final Report for FY91

5. FUNDING NUMBERS

PE - 63220C

6. AUTHOR(S)

Multiple Authorship

7. PERFORMING ORGANIZATION NAME(S) AND ADDRESS(ES)

Naval Research Laboratory
Washington, DC 20375-5320

8. PERFORMING ORGANIZATION REPORT NUMBER

NRL/MR/4721—92-6980

9. SPONSORING/MONITORING AGENCY NAME(S) AND ADDRESS(ES)

Strategic Defense Initiative Organization
T/IS
Washington, DC 20301-7100

10. SPONSORING/MONITORING AGENCY REPORT NUMBER

11. SUPPLEMENTARY NOTES

This work was supported by the Strategic Defense Initiative Organization under Job Title, Ultra Short Wavelength Laser Research.

12a. DISTRIBUTION/AVAILABILITY STATEMENT

Approved for public release; distribution unlimited

12b. DISTRIBUTION CODE

13. ABSTRACT (*Maximum 200 words*)

This report details the progress achieved by the Radiation Hydrodynamics Branch in X-Ray Laser experiments and modeling during FY91. Some of the experimental work discussed was carried out at Sandia National Laboratories in a cooperative program with NRL. It is divided into sections whose authors are separately identified. Topics presented in detail include the first demonstration of a soft x-ray inversion by resonant photopumping, detailed analysis of other photopumped x-ray laser schemes, feasibility of population inversions in fluorine driven by ultra short pulse lasers, fully time dependent radiation transport modeling, and analysis of pumping mechanisms in neonlike lasers.

14 SUBJECT TERMS

X-ray laser
Neonlike lasers
Time-dependent transport
Population inversion
Ultra short pulse lasers
Spectroscopy
Pulsed power
Resonant photoexcitation

15. NUMBER OF PAGES

142

16. PRICE CODE

17. SECURITY CLASSIFICATION OF REPORT	18. SECURITY CLASSIFICATION OF THIS PAGE	19. SECURITY CLASSIFICATION OF ABSTRACT	20. LIMITATION OF ABSTRACT
UNCLASSIFIED	UNCLASSIFIED	UNCLASSIFIED	SAR

CONTENTS

EXECUTIVE PROGRAM SUMMARY

This NRL Memorandum Report describes the research accomplishments of the Radiation Hydrodynamics Branch, in part in collaboration with Sandia National Laboratories, during Fiscal Year 1991. It consists of 6 sections whose authors are separately identified at the beginning of each section.

Perhaps the most noteworthy achievement this past year was the first-ever demonstration of a population inversion in the x-ray region pumped solely by resonant photoexcitation. Last year's report discussed a time - integrated neon spectrum which suggested inversion. This year's first section presents detailed time- resolved spectra of He - like neon pumped by both (resonant) sodium and (non-resonant) magnesium, which spectra prove the existence of the inversion. Also, this achievement (using Sandia National Laboratories' 10 - megampere Saturn accelerator) represents the first population inversion driven by a Z-pinch. The major goal of the continuing Saturn experiments is to detect and measure the gain of the 231 Å laser line. We believe the feasibility of creating x-ray inversions by resonant photoexcitation has now been demonstrated. Success in demonstrating gain will open the door to a new and radically different class of x-ray lasers with large output energies. As this report was being prepared, we received the news that the material in Sec. I has been accepted for publication in the Feb. 10, 1992 Physical Review Letters.

The following two sections of this report are also concerned with resonantly photopumped ultrashort wavelength lasers, but of considerably different design. Sec. II presents the first detailed analysis of the Al XI - Mg IX scheme proposed by Krishan and Trebes in 1984. Although the atomic physics of these ions is more complicated than that of the simple He - like stages of sodium and neon, we conclude that this scheme is as promising as Na-Ne, and might well be suitable as a "tabletop" device for smaller machines because of the ease of fabrication of Al - Mg targets. In Sec. III, a class of lasers featuring "automatic" pump resonance is discussed. In this method, a hot, dense neonlike krypton shell pumps a cooler, more tenuous lasant inner krypton plasma. The advantags of the scheme are that all the pump lines automatically match in wavelength (no accidental coincidence is required as for Na-Ne or Al -Mg), and , the low density interior plasma is configured to minimize x-ray refraction effects which degrade beam quality. Large output

energies and long lasing times (several nsec or more) are additional attractive features of this laser when configured on an accelerator as a coaxial Z pinch.

One of the most exciting new technologies which has emerged in the past 3 years or so is that of the high-power, femtosecond-duration optical laser. Potential applications are numerous and have been widely discussed in the literature. The current conventional wisdom is that such devices are the number one candidate for producing cheap, room-sized "tabletop" x-ray lasers. Section IV presents a detailed study of radiation energetics and target coupling for the interaction of an ultrabright laser pulse with a planar fluorine target. Section V describes the development and validation of the first fully time-dependent radiative transfer model which can be employed in analysis of laser plasmas. Since the velocity of light is 0.3 μm / fsec, in many of the ultrashort pulse laser heated plasmas, the light travel time is comparable to the heating or cooling time. It is anticipated that this model will be coupled to a realistic , multilevel atomic data base in FY92. Taken together, the capabilities detailed in Secs IV and V constitute a firm analytical base for the design of an eventual compact, high-output x-ray laser.

In the concluding Sec. VI, one of the most baffling continuing mysteries of x-ray laser experiments is rigorously analyzed. Ever since neonlike x-ray lasers were first demonstrated in 1984, it has been generally observed that the strongest predicted laser transition, that arising from an excited J=0 level, is anomalously weak. Many explanations have been offered, with as yet no consensus developed in the community. Sec VI presents a near-exhaustive analysis of the possibilities which are not yet scientifically ruled out. While this major contribution cannot be adequately summarized here, one of the authors' most important findings concerns the effect of inability to calculate collision rate coefficients to better than factors of two or three. The authors have discovered several instances in the literature where the accuracy of a key monopole collision rate has been seriously challenged, contrary to many existing claims of excellent accuracy for this fundamental atomic parameter. Their study, among other approaches, varies this rate through plausible values and concludes that this rate must be measured, and, if lower than the present consensus values, could explain this persistent mystery.

Demonstration of Population Inversion by Resonant Photopumping in a Neon Gas Cell Irradiated by a Sodium Z Pinch

J. L. Porter, R. B. Spielman, M. K. Matzen, E. J. McGuire, L. E. Ruggles and M. F. Vargas

Sandia National Laboratories, Albuquerque, NM 87185

J. P. Apruzese, R. W. Clark and J. Davis

Naval Research Laboratory, Washington, D.C. 20375-5000

Abstract

The broadband radiation emitted from a Na z pinch is used to photoionize Ne to the He-like ground state and radiation from the Na $1s^2$-1s2p $^1P_1$ transition is used to resonantly photoexcite the Ne $1s^2$-1s4p $^1P_1$ transition. Time-resolved and time-integrated spectral measurements of the Ne K-shell emission demonstrate the first population inversion driven by a z pinch. This is the first experiment in any medium to demonstrate a soft x-ray inversion pumped solely by resonant photoexcitation.

Article

Research conducted during the past 10 years has demonstrated that pulsed-power drivers are capable of efficiently creating very energetic radiation sources with a variety of spectral distributions.[1] Many have suggested that these drivers can be used for applications such as creating photopumped x-ray lasers[2], imploding inertial confinement fusion capsules,[3] and studying the photoionization kinetics of plasmas in intense radiation fields.[4] A serious potential problem with using pulsed-power drivers is that the powerful electrical

Manuscript approved July 20, 1992.

pulse (currents of many MA and voltages of many MV) flowing within millimeters of the various "targets" may obscure the effects of the radiation drive and hopelessly complicate the execution of this class of experiment. In this Letter we show that these problems are separable and present the first unambiguous experimental demonstration of population inversion driven by a z pinch, and the first soft x-ray inversion pumped solely by resonant photoexcitation in any medium.

We are performing photopumping experiments using the sodium/neon resonant photoexcitation x-ray laser scheme. This scheme, which has received extensive theoretical study,[5-8] employs radiation from the $1s^2$-$1s2p\ ^1P_1$ transition at 11.0027 Å in He-like Na to resonantly photoexcite the Ne $1s^2$-$1s4p\ ^1P_1$ transition at 11.0003 Å in He-like Ne. Electron and ion collisions are predicted to transfer a large fraction of the excited 4p singlet population to the 4d and 4f levels. The line calculated to have the highest gain is the $1s3d\ ^1D_2$ - $1s4f\ ^1F_3$ transition at 231 Å. This resonance is attractive because of the excellent match between the Na and Ne resonant transitions, the intrinsic strength of the Na pump line, and the relative ease in creating a large population of Ne ions in the He-like ground state.

To produce a bright Na pump line one needs a high density ($> 10^{19}$ ions cm^{-3}), high temperature (> 300 eV) Na plasma in order to both maximize the radiation rates and insure that a large population of Na ions are in excited He-like states. The Ne lasant plasma, however, needs to be at a lower density ($\approx 10^{18}$ ions cm^{-3}) and temperature (< 100 eV) in order to both maximize the population of Ne ions in the He-like ground state and minimize collisional excitation of the lower lasing level.

In our experimental arrangement (see Fig. 1) such divergent conditions have been achieved. We create the Na plasma by imploding an array of 16, 20-mm-

long, 75-μm-diameter Na wires using the Saturn accelerator[9] as a z-pinch driver. Saturn implodes the Na wire-array load with a peak current of 10 MA in an electrical pulse with a peak power of 20 TW and a 40-nsec FWHM. The total broadband radiation output from this plasma is measured to be 400 kJ in a pulse with a peak power of 10 TW and a 40-nsec FWHM. Measurements show that 90% of this radiation is emitted at energies less than 1 keV. Since the final pinch diameter is observed to be 2.5 mm (implying ion densities of 4×10^{20} cm^{-3}), we assume that the broadband radiation from this plasma can be approximated by the emission from a 89-eV blackbody (simply the blackbody equivalent temperature for the measured radiating area and power). 6 kJ of energy is typically observed to be radiated in the 11 Å Na pump line in a pulse with a peak power of 200 GW and a 20-nsec FWHM. This pulse is basically Gaussian in shape until about 25 nsec after the peak, at which time a "foot" appears that slowly decays away. Approximately 16% of the energy and power which is radiated between 1-3 keV appears in the 11 Å pump line. The pump line-width has been measured[10] with a high-resolution time-integrating spectrometer and found to be approximately 20 mÅ. Calculations of this opacity broadened line width, based on the above-cited diameter and density and the calculated range of He-like Na fraction, result in a predicted line width of 10-20 mÅ. Since the ionization balance and thus the opacity of this line vary with time, a definitive measurement of the pump line width will require a high-resolution time-resolving spectrometer. This difficult measurement has not been made to date.

We use the broadband radiation from the Na pinch to photoionize the Ne to the He-like ionization state. The ionization balance in the Ne is dominated by the Na z-pinch radiation field and not the Ne electron temperature. Independent simulations of these experiments by Sandia National

Laboratories, the Naval Research Laboratory,[11] and Lawrence Livermore National Laboratory[12] show that 53-80% of the Ne ions are in the He-like ground state even though the Ne electron temperature is only 25-30 eV.

The target used in these experiments is located 20 mm away from the z-pinch axis (outside the current return posts) and consists of Ne at a pressure of 10 Torr (4×10^{17} atoms cm^{-3}) contained within a "gas cell" target. The viewing and illumination windows of this target are made of free standing, 5000-Å-thick Lexan ($C_{16}H_{14}O_3$). The illumination window which faces the Na pinch is 10-mm long and 3-mm wide. The two viewing windows which face the lasant spectrometers are circular in shape with a diameter of 6 mm. Radiation-hydrodynamic calculations predict that the Lexan illumination window is heated by the broadband radiation from the Na pinch and expands, compressing a few-hundred-micron-thick region of the Ne to densities suitable for lasing ($\approx 10^{18}$ ions cm^{-3}) at the time of peak Na 11 Å pump emission. This compressed region is approximately one mean free path thick to the 11 Å pump line. Not only is this target both designed and measured to achieve suitable laser conditions, but as discussed later, our measurements indicate that it contains no current and associated instabilities. This eliminates a major difficulty of pulsed-power driven x-ray lasers. While the present 20 mm separation facilitates clean diagnosis and is sufficient to demonstrate population inversion, the small solid angle subtended by the sodium flashlamp can be significantly improved in future experiments. The use of more advanced targets could lead to gain in the 4-2 and 3-2 transitions which have shorter wavelengths and higher quantum efficiency.

The total broadband radiated energy and power from the Na pinch is measured with an unfiltered, thin-film resistive bolometer. The radiated energy and power above 1 keV is measured with a filtered bolometer, a time-

integrating convex KAP crystal spectrometer, and an array of three absolutely-calibrated, filtered x-ray diodes.[13] A 12-frame, time-resolving, x-ray pinhole camera is used to monitor the implosion quality of the Na pinches.

The K-shell emission between 9-14 Å from the Ne lasant is monitored simultaneously with time-resolving and time-integrating elliptical crystal (RAP) spectrometers (see Fig. 1). The time-resolving spectrometer is located 1.2 m from the target and uses a 7-frame, microchannel-plate-intensified, x-ray framing camera as the detector.[14] The time-integrating spectrometer is located 0.35 m from the target and uses Kodak 2497 x-ray film. We insert metal tubes between the x-ray laser target and each spectrometer to guard against any Na contaminant radiation entering the line-of-sight of these spectrometers. The ends of these baffles are placed inside counterbored holes located at both the x-ray laser target and the entrance port of the spectrometers. To insure that no Na contaminant radiation was observed by these lasant spectrometers, we conducted a "null" shot by replacing the Ne with N at 10 Torr. A nominal Na pinch was produced on this shot and no lines were observed on either of the lasant spectrometers.

We looked for an enhancement of the He-like Ne $1s^2$-1s4p line relative to the He-like Ne $1s^2$-1s3p line to demonstrate that the Na pinch photopumps the Ne plasma. The three independent kinetics calculations have shown that if an inversion exists between these two transitions (i.e. the 1s-4p line is brighter than the 1s-3p line), then at the Ne densities encountered in these experiments, an inversion also exists between the 1s4f and 1s3d singlet levels. The exact magnitude of the gain, however, is uncertain. The kinetics calculations differ in the predicted He-like fraction, oscillator strengths of the pumped and laser transitions, width of the laser transition, and level of detail in modeling the excited states. Uncertainties of 10-60% in these factors lead to the very

sensitive prediction of gain varying from 0.2 to 1.5 cm^{-1}. Additional experimental uncertainties arise from the width of the 11 Å pump line at peak power and the details of the soft photoionizing spectrum.

To ensure that the enhanced emission observed in the $1s^2$-1s4p line is due to resonant photopumping by the Na 11 Å pump line, we performed a second type of "null" shot. In this "null" shot the Na wire-array load was replaced with a Mg wire-array load in an attempt to generate the same broadband and general keV radiation as a Na pinch but eliminate the 11 Å Na pump line.

Figure 2a shows typical time-integrated and time-resolved Ne spectra from a shot with a Na pinch and a Ne-filled target. The time-integrated spectrum has been corrected for the spectrometer response[15] (using tabulated values for the film response, filter transmission, crystal reflectivity, and spectrometer geometry) and background light. In addition, the time-resolved spectra were also corrected for the gold photocathode response and the variation in gating voltage (and hence detector gain) between frames. For this shot, each gating pulse was 4 nsec wide and spaced 5 nsec apart (center to center). Since the framing camera was run at very high gain (≈1 kV across the microchannel plate), the bright $1s^2$-1s2p line might be slightly saturated on some frames. The high gain also resulted in "noisier" time-resolved data than time-integrated data.

As can be seen from Fig. 2a, the He-like Ne $1s^2$-1s4p line is about twice as bright as the $1s^2$-1s3p line, demonstrating an inversion between the 1s4p and 1s3p singlet levels. Integration of these spectra gives an intensity ratio for the $1s^2$-1s4p line to the $1s^2$-1s3p line of 1.7 for the time-integrated spectrum and a ratio of 2.4 at the time of peak emission of the Na 11 Å pump line. This pattern was observed on each of three Na-pumped shots. The three independent simulations predict this line ratio to be between 1.4 and 2.2 at the time of peak Na 11 Å pump emission. The spontaneous decay rate of the $1s^2$-1s3p line

exceeds that of the $1s^2$-1s4p transition by a factor of 2.4. Even with the effects of self-absorption, population inversion is required to make the 4p transition twice as bright as the 3p, as is observed here.

The excited state density of the pumped 1s4p level, N(4p), may be inferred from the measured power P (photons sr^{-1} sec^{-1}) of the 11 Å Ne line from $N(4p)=4\pi P/AV$ where A is the line's decay rate (10^{12} sec^{-1}) and V is the observed Ne volume. By normalizing the absolute energy measured with the time-integrating spectrometer to the relative time history measured with the time-resolving spectrometer, we estimate that $P=4 \times 10^{20}$ photons sr^{-1} sec^{-1}. The observed volume is the product of the observed window length (3 mm), the depth of penetration of the Na pump radiation into the Ne, and the depth into the Ne seen by the time-integrating instrument. The latter two quantities are inversely proportional to the line optical depth and therefore to the He-like fraction f. As a result, N(4p) is proportional to f^2. If f=0.53 is assumed (LLNL model, Ref. 12), we infer $N(4p)=2.0 \times 10^{13}$ cm^{-3}, compared to the Ref. 12 calculation of 3.0×10^{13} cm^{-3}. However, the f of 0.8 predicted by the NRL and SNL models leads to $N(4p)=4.5 \times 10^{13}$ cm^{-3}, compared to the corresponding model calculations of 5.9×10^{13} and 2.9×10^{13} cm^{-3}. Therefore, taking into account the dependence of the viewing volume on f, the measured power of the photopumped line is consistent with all 3 models to within 35%.

Another interesting feature of the time-resolved spectra shown in Fig. 2a is the general time history of the Ne K-shell lines. Note that no lines appear until frame 3 of the time-resolved data. If the ionization balance and the excitation of the Ne plasma were dominated by stray currents or by high energy electron beams flowing in this plasma, then one would expect these lines to appear much earlier in time since this shot had a 65 nsec implosion time (time from 10% of maximum current to stagnation). The fact that these K-shell lines follow

the pinch's keV radiation pulse (and not the current pulse) indicates that both the ionization balance and the excitation of the Ne plasma are dominated by the radiation field produced by the Na pinch.

Figure 2b shows the time-integrated and time-resolved Ne spectra from the Mg/Ne "null" shot. For this shot the gating pulses on the time-resolving spectrometer were 8 nsec wide and spaced 5 nsec apart (center to center), resulting in some overlap between adjacent frames. The main feature to note from this spectrum is the fact that the $1s^2$-1s4p line is no longer brighter than the $1s^2$-1s3p line. The spectrally integrated intensity ratio of the $1s^2$-1s4p line to the $1s^2$-1s3p line is 1.0 for both the time-integrated spectrum and frame number 4 of the time-resolved spectra. This observation, combined with the fact that no Na radiation was observed on the Na/N "null" shot, confirms our interpretation of resonant photopumping as the cause of the observed inversion between the $1s^2$-1s4p and $1s^2$-1s3p lines in the Na/Ne shots. Another interesting feature of the Ne spectra from the Mg/Ne shot is the relative brightness of the $1s^2$-1s5p, $1s^2$-1s4p, and $1s^2$-1s3p lines. The integrated line intensities of these spectral lines are in the ratio 1.0:1.7:1.7 for the time-integrated spectrum and 1.0:1.3:1.3 for frame number 4 of the time-resolved spectra. This is suggestive of recombination from H-like Ne ions in the cold, moderate density Ne plasma. A population of H-like ions is known to exist on this shot since the H-like Ne 1s-2p resonant line is observed on frames 3-6 of the time-resolved spectra.

It is important to note that no H-like lines have ever been observed on Na-pumped shots. Moreover, the $1s^2$-1s5p line is absent when a Na plasma is the pump. It can be shown that the three-body recombination rate scales as $n^{5.33}$ for the plasma conditions discussed here, where n is the principal quantum number. This scaling is deduced from a detailed balancing of collisional ionization (using the Lotz ionization formula[16]) with three-body

recombination. The absence of n=5 radiation during the Na-pumped shots, as well as the lack of H-like lines or any recombination continuum, rules out recombination as a pump mechanism for the inversion. In contrast, the Mg-pumped shots exhibit the H-like Ne 1s-2p line and the recombination continuum, as well as a strong He-like Ne $1s^2$-1s5p line, which are all characteristic of recombination. The keV lines from Mg are all of sufficient energy to ionize He-like Ne and were also emitted with 40% more power than those of Na, fully consistent with the above picture. Analysis of the (somewhat noisy) slope of the recombination continuum of the Mg shot yields an electron temperature of 30 eV, consistent with the radiation-hydrodynamic simulations of these experiments.[11]

In summary, we have made time-integrated and time-resolved spectral measurements which demonstrate population inversion by resonant photopumping in the Na/Ne x-ray laser system. Success in demonstrating gain on this or other laser transitions would open the door to a class of x-ray lasers with large output energies and lasing times of several nsec or longer.

We would like to thank B. Hammel for the many early discussions which ultimately led to these experiments. We are also indebted to T. Hussey, W. Hsing, F. Young, C. Deeney, J. McGurn, S. Lopez, D. Derzon and the Saturn operations crew. The targets were supplied by Luxel Inc. of Friday Harbor, WA. The Sandia authors would also like to thank J. P. VanDevender for his continued support of these experiments. This work was supported by SDIO/T/IS and the U.S. Department of Energy under Contract DE-AC04-76DP00789.

References

[1] N. R. Pereira and J. Davis, J. Appl. Phys. **64**, R1 (1988).

[2] M. K. Matzen *et al.*, J. Phys. Colloq. (Paris) **47**, C6-135 (1986).

[3] J. P. VanDevender and D. L. Cook, Science **232**, 831 (1986).

[4] M. J. Eckart, private communication.

[5] A. V. Vinogradov, I. I. Sobelman, and E. A. Yukov, Sov. J. Quantum Electron. **5**, 59 (1975).

[6] P. L. Hagelstein, Plasma Phys. **25**, 1345 (1983).

[7] J. P. Apruzese and J. Davis, Phys. Rev. A. **31**, 2976 (1985).

[8] S. J. Stephanakis *et al.*, IEEE Trans. Plasma Sci. **16**, 472 (1988).

[9] R. B. Spielman *et al.*, 1989 Proc. 2nd Int. Conf. on Dense Z Pinches, eds. N. R. Pereira, J. Davis, and N. Rostoker (New York, American Institute of Physics) pp 3-16.

[10] P. Burkhalter *et al.*, in Record 1991 IEEE Int. Conf. Plasma Sci., Williamsburg, VA ,1991, p. 212.

[11] J. P. Apruzese *et al.*, in Proceedings of the 2nd International Colloquium on X-Ray Lasers, York, England, ed. G. J. Tallents (Bristol, IOP) pp. 39-42 (1991).

[12] J. Nilsen and E. Chandler, Phys. Rev. A **44**, 4591 (1991).

[13] F. C. Young, S. J. Stephanakis, and V. E. Scherrer, Rev. Sci. Instrum. **57**, 2174 (1986).

[14] B. A. Hammel and L. E. Ruggles, Rev. Sci. Instrum. **59**, 1828 (1988).

[15] B. L. Henke and P. A. Jaanimagi, Rev. Sci. Instrum. **56**, 1537 (1985).

[16] W. Lotz, Z. Phys., **216**, 241 (1968).

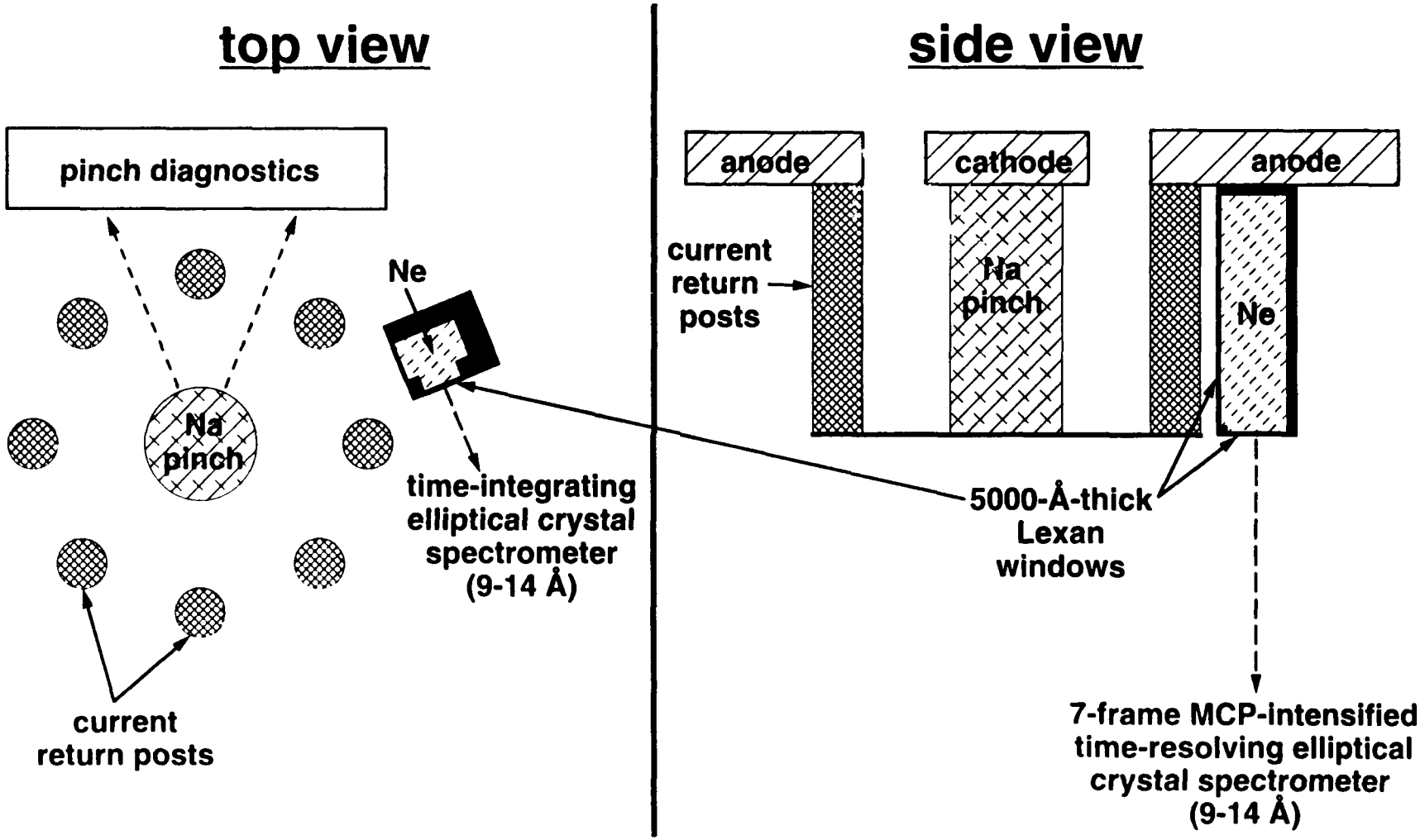

Fig. 1. Schematic diagram of the experiment.

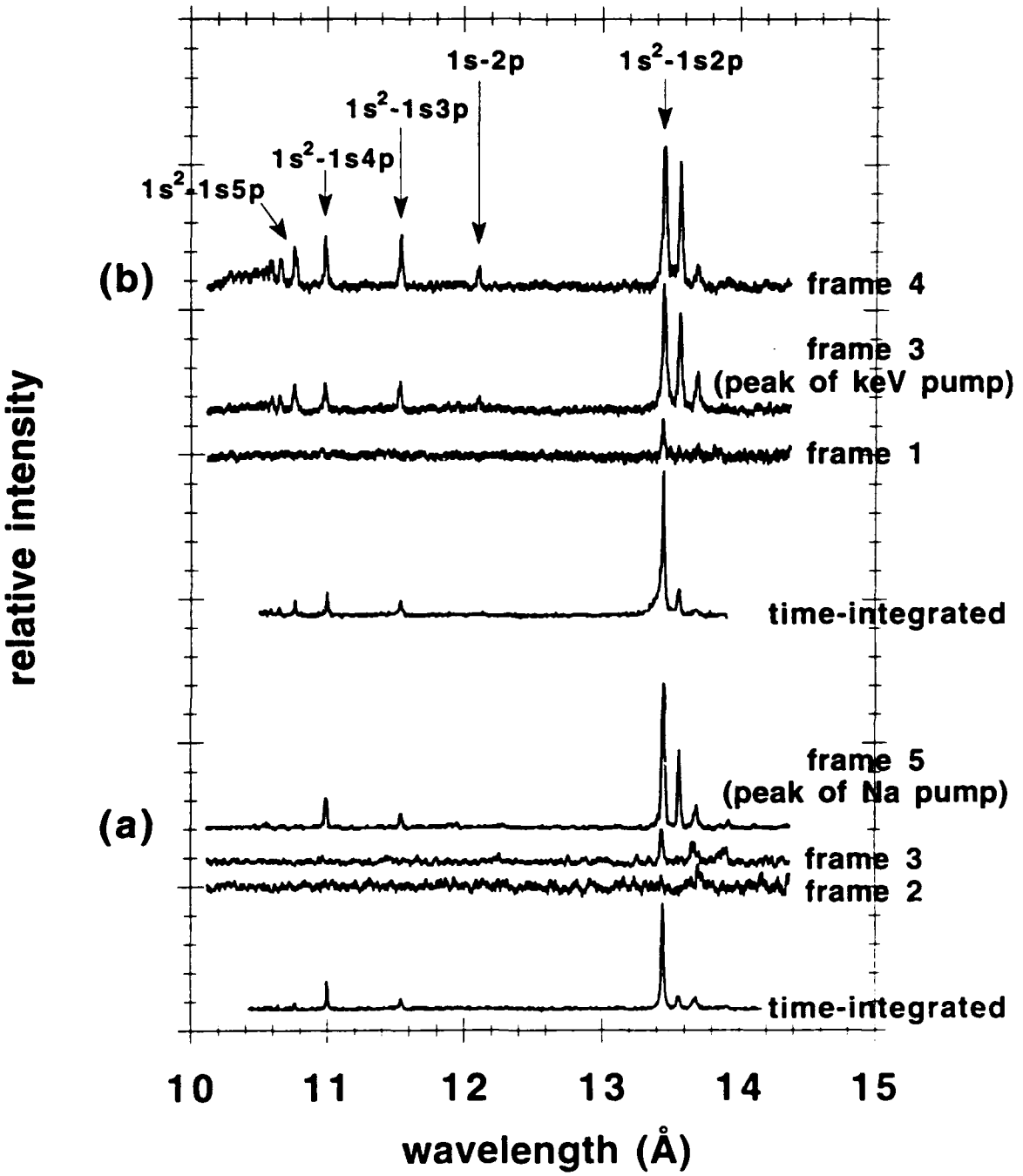

Fig. 2. Time-integrated and time-resolved Ne spectra for **(a)** a typical Na pinch/Ne target shot and **(b)** the Mg pinch/Ne target "null" shot. Time increases with increasing frame number.

ACHIEVABLE PUMP POWER AND GAIN IN THE Al XI - Mg IX PHOTORESONANT X-RAY LASER

J. P. Apruzese and M. Buie*

Radiation Hydrodynamics Branch
Plasma Physics Division
Naval Research Laboratory
Washington, D. C. 20375

Abstract - The aluminum-magnesium photoresonant x-ray laser scheme is investigated using detailed atomic models for both elements. The aluminum pump source is assumed to be a Z pinch driven by a current of several MA. It is found that monochromatic pump powers of 100 GW/eV are obtainable within the 48 Å aluminum pump line over a broad range (125-400 eV) of pump plasma temperatures. The gain in Mg IX is calculated assuming separations of 1 or 2 cm from the pump plasma. The highest gain appears in the $2s3d\ ^1D_2 - 2s4f\ ^1F_3$ line at 228 Å. However, photoionization as well as resonant photoexcitation appears to be crucial to the success of this scheme. If photoionization by lines other than the pump line is neglected, Mg IX does not exist below ~ 60 eV. In the 60-100 eV Mg plasma temperature range, collisional excitation from low-lying states to the lower laser level severely degrades the gain. However, when photoionization of Mg by all of the strong Al XI lines is taken into account, Mg IX is found

to exist at much lower temperatures, leading to respectable gain of ~ 3 cm^{-1} at 1 cm Al-Mg separation.

* Current address: Dept. of Nuclear Engineering, Univ. of Michigan, Ann Arbor, Michigan 48109

I. INTRODUCTION

In 1984 Krishnan and Trebes analyzed[1] a series of six Be-like ions whose $2s^2\ {}^1S_o$ - $2s4p\ {}^1P_1$ transitions are closely resonant with various possible pump lines in ions ranging from Mn VI to Al XI. The Be-like lasant ions range in atomic number from 6 (C III) to 12 (Mg IX). By exposing a plasma containing the Be-like ion to the resonant radiation from the pump ion, gain in 4-3 singlet transitions may be achieved through pumping of the $1s^2 2s4p\ {}^1P_1$ level. The lowest-atomic-number resonant pair, C III - Mn VI has already been successfully demonstrated[2], resulting in the shortest laser wavelength (2163 Å) yet achieved by resonant photoexcitation, with the possible exception of the recent neonlike titanium experiments at the University of Rochester and Lawrence Livermore National Laboratory[3]. The highest-atomic-number resonant pair, Al XI-Mg IX, had been previously proposed by Seely[4] and discussed by Dixon and Elton.[5]

Of course, many other resonant photoexcitation schemes to obtain gain in the soft x-ray region have been proposed[6-16]. One of the most attractive and highly developed of these is the 11 Å resonance[6,8-10] between the Na X $1s^2$ -$1s2p\ {}^1P_1$ and Ne IX $1s^2$ - $1s4p\ {}^1P_1$ lines where experimental evidence of both fluorescence and population inversion has been produced[12,15,16]. Previous analyses of this sodium-neon scheme have emphasized the need for considerably different conditions in the pumping sodium and pumped neon plasmas. Indeed, conditions in the experiments demonstrating fluorescence and population inversion are consistent with the requirement for a sodium plasma much hotter

and denser than the neon. The Be-like scheme has one obvious advantage over the sodium-neon approach; higher quantum efficiency. As seen below, there are also disadvantages. It is the purpose of this paper to report a detailed analysis of the Al XI - Mg IX resonant laser, and quantify the design requirements for a demonstration of gain.

II. ATOMIC MODELS AND CALCULATIONS

A. Aluminum pump plasma

The resonant pump line is the Al XI $1s^2 2s\ ^2S_{1/2}$-$1s^2 3p\ ^2P_{1/2}$ transition at 48.338 Å (256.49 eV), nearly perfectly coincident with the pumped Mg IX line $1s^2 2s^2\ ^1S_0$ - $1s^2 2s4p\ ^1P_1$ at 48.340 Å (256.48 eV). The J = 3/2 component of the Al XI resonance doublet is located at 48.297 Å (256.71 eV). This J = 3/2 line is separated by 43 mÅ (8 Doppler widths at an ion temperature of 150 eV) from the pumped transition, but, if sufficiently broadened, may participate in the pumping. Any attempt to calculate the pumping rate must therefore include multifrequency radiative transfer to resolve the doublet and obtain monochromatic power.

The atomic model employed in our calculations for aluminum is a subset of the comprehensive structure described in Ref. 17. For obvious reasons, Al XI and nearby stages are emphasized. In the key Li-like Al XI species, the following levels are modeled: $(1s^2)2s^2S$, $2p^2P$, $3s^2S$, $3p^2P$, $3d^2D$, 4s, 4p, 4d, 4f, and a consolidated n=5 state. Note that the J=1/2 and J=3/2 levels of the $3p^2P$ level are lumped together; in calculating the emergent line power profile for this doublet the J-sublevels are assumed to be statistically populated. The Al plasma is assumed to be a uniform cylinder of specified density and temperature in collisional-radiative equilibrium (CRE). The populations are

computed by solving the steady-state rate equations coupling the levels, including photon transport initially performed using a multicell coupling escape probability technique described in Refs. 18 and 19. Once the populations are computed by using this efficient technique, the detailed line profile of the pump doublet is obtained by a one-step multifrequency recomputation of the radiative transfer within the two closely spaced lines assuming Voigt profiles. Approximately 200 frequency points are employed in this final phase of the calculation.

B. Pumped magnesium plasma

The magnesium atomic model has been constructed along lines similar to that of aluminum, with the obvious exception that the Be-like lasing stage is emphasized. In calculating level energies, oscillator strengths, and collision rates for Mg IX, 17 different configurations are allowed to mix. The levels, their statistical weights, and energies calculated for Mg IX using the atomic structure code of Cowan[20] are presented in Table I. The magnesium plasma is assumed optically thin in all cases considered below. The effects of line trapping on gain are neglected although this effect may be non-negligible at the higher densities considered, for realistic plasma sizes. Such an investigation is beyond the scope of this paper and is reserved for the future. Lines which may exhibit gain with sufficient resonant pumping of the 4p singlet level are principally the 4-3 singlet and triplet allowed transitions. In calculating the gain for the various candidate lines, statistical equilibrium among the singlet and triplet sublevels is assumed. By examining the results of the gain calculations described below, it is evident that the most attractive laser line by far is the $2s3d\ ^1D_2$ - $2s4f\ ^1F_3$ transition calculated to lie at 228 Å. Other candidate laser lines are predicted to have maximum gain more than a factor of 3 below that of this line. All further discussion of achievable gain therefore refers to the $2s3d\ ^1D_2$ - $2s4f\ ^1F_3$ transition.

III. RESULTS

A. Aluminum plasma pump power

Fine aluminum wires have long served as a source of plasma in multi-megampere Z pinch experiments (see, e.g., Refs. 21 and 22 and references therein). However, by far the most effort using aluminum has been expended in studying and analyzing the behavior of its K shell lines. Fortunately, some recent experiments using the 3-4 MA Double EAGLE generator of Physics International Company[23,24] provide considerable insight and guidance for the optimization of L shell radiation which includes the 48.3 Å Al XI pump line. In a series of shots in which the product of the Al wire array mass (M) and the square of its initial radius (R_o^2) remained approximately constant, the behavior of L-shell and K-shell radiation was observed. Keeping M R_o^2 constant (while separately varying M and R_o) keeps the energy coupling from the generator to the imploding load constant and approximately optimum. It was observed in these experiments[23,24] that the L shell radiation maximized at a wire mass load of 474 μg/cm, and that the diameter of the L shell emitting region was approximately 4.2 mm. Therefore, as a means of assessing the achievable pump power, a series of calculations was performed assuming a 2-cm long cylindrical aluminum plasma of diameter 4.2 mm containing 948 μg. This corresponds to an atomic density of 7.6×10^{19} cm^{-3}. The temperature was varied independently from 75 to 600 eV to observe the effect on the emitted power of the resonant pump line at 48.338 Å (256.49 eV) and other lines.

Results for three temperatures for the Al XI $2s^2S_{1/2}$ - $3p^2P_{1/3,3/2}$ doublet are shown in Fig. 1. In the optically thin limit the non-pumping J = 3/2 component at 48.297 Å (256.71 eV), oscillator strength (0.22) is twice as

strong as the J = 1/2 pump line. For the 400 eV profile depicted in Fig. 1, this is nearly the case. At such a relatively high temperature, the Li-like stage is nearly burned through, and the optical depth of the lines are of order unity. The two doublet components are distinct, with the J = 3/2 line not quite twice as strong as the J = 1/2. As lower temperatures are assumed, more Li-like Al results in higher optical depth. Since the J = 3/2 component has twice the opacity of the J = 1/2, the emitted intensity of the two lines tends to equalize, as is clearly seen for the 250 eV temperature case in the center of Fig. 1. At still lower temperatures (150 eV), opacity broadening, self reversal, and the relatively lower optical depth between the two components produces the three-pronged profile also seen in Fig. 1. The most important implication of these results for resonant photopumping is that monochromatic powers near 100 GW/eV (10^{13} photons sec^{-1} Hz^{-1}) are achieved for a broad range of temperatures (125 - 400 eV). As the Li-like stage is depleted at higher temperatures, the reduced opacity of the line keeps the pump power from falling until the line is thin and there is virtually no Al XI remaining. In the gain calculations described in the next section, the pump power (to 4π) has been fixed at 100 GW/eV, a reasonable estimate of the capabilities of an optimized Al array driven by several MA.

Before presenting the Mg gain, one final feature of these Al calculations merits discussion. Li-like Al emits several strong lines from 33 to 55 Å, including the pump doublet discussed above. Some of these lines can photoionize lower stages of Mg, affecting the ionization balance of the lasant species as a function of temperature. Table II presents the total power in the more important photoionizing lines as calculated at a temperature of 125 eV. Their influence on Mg is discussed below.

B. Magnesium gain without photoionization

It is assumed that a suitable Mg plasma can be placed in close proximity to the Al pinch. In fact, separations of 1-2 cm in similar experiments have been demonstrated[15]. The Mg plasma may require energy input other than the x-rays from the Al pinch, for instance a modest-current pulser or laser driver. In the present work, we assume the temperatures and densities for optically thin Mg plasma and calculate the gain in the 228 Å laser transition given the Al photoresonant power. The pump rate from the Be-like ground state is

$$P(\sec^{-1}) = \int F_\nu \, \sigma_\nu d\nu = F_\nu \int \sigma_\nu d\nu = \frac{\pi e^2}{mc} F_\nu f \qquad (1)$$

where F_ν is the monochromatic pump flux, assumed constant across the pumped line profile, σ_ν is the photoabsorption cross-section, and f is the absorption oscillator strength of the pumped transition (= 0.155). For a 2-cm Al-Mg separation, F_ν = 2×10^{11} photons cm^{-2} sec^{-1} Hz^{-1}, for our calculated pump strength of 10^{13} photons sec^{-1} Hz^{-1} and 50 cm^2 dilution. Using Eq. (1) a pump rate of 8.2×10^8 sec^{-1} is obtained. For a 1 cm separation, this rate increases by about a factor of 4, to 3.3×10^9 sec^{-1}.

Since the $1s^2\ 2s^2\ {}^1S_0$ Be-like ground state forms the lower level of the pumped transition, it is important to optimize its fractional population to obtain an efficient laser. Figure 2 displays the calculated Be-like ground state fraction as a function of temperature and ion density. In this case, the only external radiation effect included is the photoresonant pumping at an assumed separation of 2 cm. Inspection of Fig. 2 reveals that the maximum fractional population is less than 5%, near 90 eV and 10^{16} ions cm^{-3}. Furthermore, gain in the 228 Å 2s3d ${}^1D_2$ - 2s4f ${}^1F_3$ transition (not shown) does not exceed 0.03 cm^{-1} anywhere in the density-temperature plane. The key to this result is found in the energy-level structure of Mg IX, Table I. There are 5

terms within 61.2 eV of the ground state having a total statistical weight of 27, as opposed to unity for the $1s^2 2s^2\ {}^1S_0$ ground level. Therefore, it is virtually impossible to obtain a large fractional ground state population. Moreover, the lower laser level (only 220 eV from the ground) is susceptible to collisional excitation from the ground state as well as the highly populated levels within 61.2 eV of the ground. The fact that the Be-like ground state maximizes near T = 90 eV has the consequence that the lower laser level is easily populated via collisional excitation. In summary, if resonant photoexcitation from the Al pinch is the only external radiation considered, gain in Mg IX is very low ($< 0.03\ cm^{-1}$) due to the small achievable population of the pumped Be-like ground state as well as strong collisional excitation of the lower laser level.

C. Gain calculations including photoionization

We find that this laser shows substantially improved gain when photoionization of Mg due to L-shell Al lines is considered. This allows the Be-like stage to maximize at much lower temperatures, reducing collisional excitation to the lower laser level and narrowing the gain line Doppler width. The ground state ionization potentials for Mg VI, VII and VIII are, respectively, 187, 225, and 266 eV. Also the ionization potential from the critical $2s2p^2$ first excited level of B-like Mg VIII is 229 eV. According to Table II, many of the powerful lines of Li-like Al are sufficiently energetic to ionize these stages toward the desired Mg IX ground state. The effect of these lines on the Mg ionization balance is revealed in the contour plots of Figs. 3 and 4, where the Be-like ground state fractional population is plotted vs. ion density and temperature with photoionization included. Note that, for both the 2 cm separation (Fig. 3) and 1 cm (Fig. 4), the Mg IX ground state fraction maximizes at much lower temperatures, 10-20 eV. The effect on gain for both the

2 cm case (Fig 5) and 1 cm (Fig. 6) is very positive. For the 1 cm separation gains exceeding 3 cm^{-1} are possible near ion densities of 10^{18} cm^{-3}, and for 2 cm, the gain is a more modest 0.4 cm^{-1}, peaking at somewhat lower densities. Ion densities above 10^{18} cm^{-3} have not been considered due to the probable deleterious effects of line trapping for realistic plasma sizes at such higher densities.

The importance of photoionization of Mg by Al XI lines to the overall ionization balance is demonstrated by comparing rates obtained from well-known simple formulations for both photoionization and collisional ionization. Consider the ionization from the $1s^2 2s 2p^2$ levels of B-like Mg to the pumped Be-like ground state. The ionization potential of 229 eV permits very efficient photoionization by the Al XI 2p-3d and 2s-3p lines at 237 and 257 eV, respectively. According to Table II, the combined power of these lines is 185 GW, giving a flux at a distance of 1 cm of 3.7×10^{26} photons cm^{-2} sec^{-1}.

Multiplying this flux by the screened hydrogenic Kramers-Gaunt edge cross section of 3.6×10^{-19} cm^2 gives a photoionization rate of 1.3×10^8 sec^{-1}. By contrast, at 45 eV, the collisional ionization rate coefficient obtained from the Lotz formulation [25] is 4.8×10^{-12} cm^3 sec^{-1}. Even at the highest electron densities considered here, 10^{19} cm^{-3}, the corresponding rate of 4.8×10^7 sec^{-1} is nearly a factor of 3 below that of photoionization. At lower temperatures and densities, the disparity is much greater.

The effect of ionization and collisional excitation on gain is illustrated by close study of Fig 6 at an ion density of 3.6×10^{17} cm^{-3}. At a temperature of 12 eV, gain of 2 cm^{-1} is predicted, whereas at 65 eV, only 0.045 cm^{-1} is expected. The fractional population of the upper laser level is given within a factor of 2 under these conditions by a simple kinetics model

$$f(2s\ 4f\ {}^1F_3) = f(g) \cdot P \cdot (7/16) / A \qquad (2)$$

where f(g) is the pumped Be-like ground state fraction, P is the photoresonant

pump rate (3.3×10^{9} sec^{-1}), 7/16 is the statistical weight of the 4f level divided by that of all of the 2s4f singlet levels, and A is the weighted inverse lifetime of the n=4 singlets (1.6×10^{11} sec^{-1}). Note from Fig.4 that f(g) is reduced from 6.5×10^{-2} to 6.2×10^{-3} as the temperature increases from 12 to 65 eV. According to Eq. (2), this would reduce the gain from 2 cm^{-1} to 0.19 cm^{-1}. The increase in line Doppler width accounts for a further reduction of a factor of 2.3. The final factor of 2 reduction required arises from the increase in lower laser level population. At 12 eV, the 4f $^1F_3$ population exceeds that of 3d $^1D_2$ by a factor of 5.6; at 65 eV this ratio is reduced to 2.2 (as given by the detailed calculations). This is not surprising as the collisional excitation rate from the Be-like ground state increases 5 orders of magnitude between 12 and 65 eV. The above simple considerations provide a useful guide and scoping tool for the kinetics as revealed by the detailed calculations.

IV. CONCLUDING DISCUSSION

Our detailed calculations of photoresonant pump power in Al XI as well as gain in Mg IX reveal that photoionization by nonresonant Al lines is required along with the resonant photopumping to obtain useful gain. The photoionization allows the Mg IX to exist at relatively low electron temperatures greatly reducing deleterious collisional excitation to the lower laser levels. It is instructive to compare this scheme to the well-known photoresonant Na X - Ne IX system.[6,8-10] Such a comparison is clarified and facilitated by the fact that the gain lines have nearly the same wavelength and oscillator strength-indeed, they are both 3d $^1D_2$-4f $^1F_3$ transitions. However, the quantum efficiency of the Al-Mg system exceeds that of the Na-Ne scheme by a factor of 4.4. That is, one pumping of the Ne IX upper laser level requires a photon 4.4 times more energetic than that required to pump Mg IX. Moreover, this clear advantage for Al-Mg is offset by the difficulty of obtaining a large fraction of Mg IX ions in the pumped $1s^2 2s^2$ ^1S_o ground state, due to the proximity of many other levels of

much higher statistical weight. By contrast the Ne IX pump ground level ($1s^2$ ^1S_o) is isolated from all overlying levels by nearly a kilovolt and at least 50% of the neon ions can be placed in this state in a properly prepared plasma. The end result, even when many other atomic physics details are included, is that the two systems are about equally attractive.

V. ACKNOWLEDGMENTS

The authors have benefitted immensely from discussions with M. Krishnan (Science Research Laboratories) and C. Deeney (Physics International Company). The encouragement of J. Davis (Naval Research Laboratory) throughout this work is greatly appreciated. This research was supported by SDIO/T/IS.

REFERENCES

1. M. Krishnan and J. Trebes, Appl. Phys. Lett. 43, 189 (1984); also in Laser Techniques in the Extreme Ultraviolet, S. E. Harris and T. B. Lucatorto, Eds. (AIP, New York, 1984), p.514.

2. N. Qi and M. Krishnan, Phys. Rev. Lett. 59, 2051 (1987).

3. T. Boehly, M. Russotto, R. S. Craxton, R. Epstein, B. Yaakobi, L. B. Da Silva, J. Nilsen, E. A. Chandler, D. J. Fields, B. J. Mac Gowan, D. L. Matthews, J. H. Scofield, and G. Shimkaveg, Phys. Rev. A 42, 6962 (1990).

4. J. F. Seely, private communication to R. H. Dixon and R. C. Elton (1983).

5. R. H. Dixon and R. C. Elton, J. Opt. Soc. Am. B 1, 232 (1984).

6. A. V. Vinogradov, I. I. Sobelman, and E. A. Yukov, Kvant. Electron. (Moscow) 2, 105 (1975) [Sov. J. Quantum Election 5, 59 (1975)].

7. B. A. Norton and N. J. Peacock, J. Phys. B 8, 989 (1975).

8. P. L. Hagelstein, Plasma Phys. 25, 1345 (1983).

9. J. P. Apruzese, J. Davis, and K. G. Whitney, J. Appl. Phys. 53, 4020 (1982).

10. J. P. Apruzese and J. Davis, Phys. Rev. A 31, 2976 (1985).

11. R. C. Elton, T. N. Lee, and W. A. Molander, Phys. Rev. A 33, 2817 (1986).

12. S. J. Stephanakis, J. P. Apruzese, P. G. Burkhalter, G. Cooperstein, J. Davis, D. D. Hinshelwood, G. Mehlman, D. Mosher, P. F. Ottinger, V. E. Scherrer, J. W. Thornhill, B. L. Welch, and F. C. Young, IEEE Trans. Plasma Sci. 16, 472 (1988).

13. R. C. Elton, Phys. Rev. A 38, 5426 (1988).

14. J. Nilsen, Phys. Rev. Lett. 66, 305 (1991).

15. J. L. Porter, R. B. Spielman, M. K. Matzen, E. J. McGuire, T. W. Hussey, C. Deeney, R. R. Prasad, and T. Nash, 1990 IEEE Int. Conf. on Plasma Science, IEEE Catalog No. 90CH2857-1, p. 148 (1990).

16. J. P. Apruzese, R. W. Clark, J. Davis, J. L. Porter, R. B. Spielman, M. K. Matzen, S. F. Lopez, J. S. McGurn, L. E. Ruggles, M. Vargas, D. K. Derzon, T. W. Hussey, and E. J. Mc Guire, to be published in Proceedings of the 2nd International Colloquium on X-Ray Lasers (IOP Publishing, Bristol, 1991).

17. D. Duston and J. Davis, Phys. Rev. A 23, 2602 (1981).

18. J. P. Apruzese, J. Quant. Spectrosc. Radiat. Transfer 25, 419 (1981).

19. J. P. Apruzese, J. Quant. Spectrosc. Radiat. Transfer 34, 447 (1985).

20. R. D. Cowan, The Theory of Atomic Structure and Spectra (University of California Press, Berkeley, 1981).

21. M. Gersten, W. Clark, J. E. Rauch, G. M. Wilkinson, J. Katzenstein, R. D. Richardson, J. Davis, D. Duston, J. P. Apruzese, and R. Clark, Phys. Rev. A 33, 477 (1986).

22. N. R. Pereira and J. Davis, J. Appl. Phys. 64, R1 (1988).

23. J. L. Giuliani, J. E. Rogerson, C. Deeney, T. Nash, R. R. Prasad, and M. Krishnan, J. Quant. Spectrosc. Radiat. Transfer 44, 471 (1990).

24. C. Deeney, private communication (1991).

25. W. Lotz, Z.Phys. 216, 241 (1968).

TABLE I: Levels, their statistical weights, and energies in the Be-like magnesium atomic model.

Level	Statistical Weight	Energy (eV)
$1s^2 2s^2\ {}^1S_o$	1	0.
$1s^2 2s2p\ {}^3P$	9	17.8
$1s^2 2s2p\ {}^1P$	3	32.4
$1s^2 2p^2\ {}^3P$	9	45.6
$1s^2 2p^2\ {}^1D$	5	50.2
$1s^2 2p^2\ {}^1S$	1	61.2
$1s^2 2s3l\ {}^3SPD$	27	199.3
$1s^2 2s3l\ {}^1SPD$	9	201.1
$1s^2 2p3l\ {}^3SPDF$	81	220.4
$1s^2 2p3l\ {}^1SPDF$	27	222.8
$1s^2 2s4l\ {}^3SPDF$	48	257.8
$1s^2 2s4l\ {}^1SPDF$	16	258.4
$1s^2 2s5l$	100	283.7
$1s^2 2s6l$	144	297.4

TABLE II: Total power output of various photoionizing transitions in Li-like aluminum. Length of Z pinch is 2 cm, diameter 4.2 mm, ion density $7.6 \times 10^{19}_{cm^{-3}}$, and temperature 125 eV. Doublets and other closely spaced lines are lumped together.

Transition ($1s^2$ core)	Energy (eV)	Power (GW)
2p-3s	228	28
2p-3d	237	98
2s-3p	257	87
2p-4s	314	20
2p-4d	317	143
2s-4p	338	76
2p-5l	354	19
2s-5l	376	14

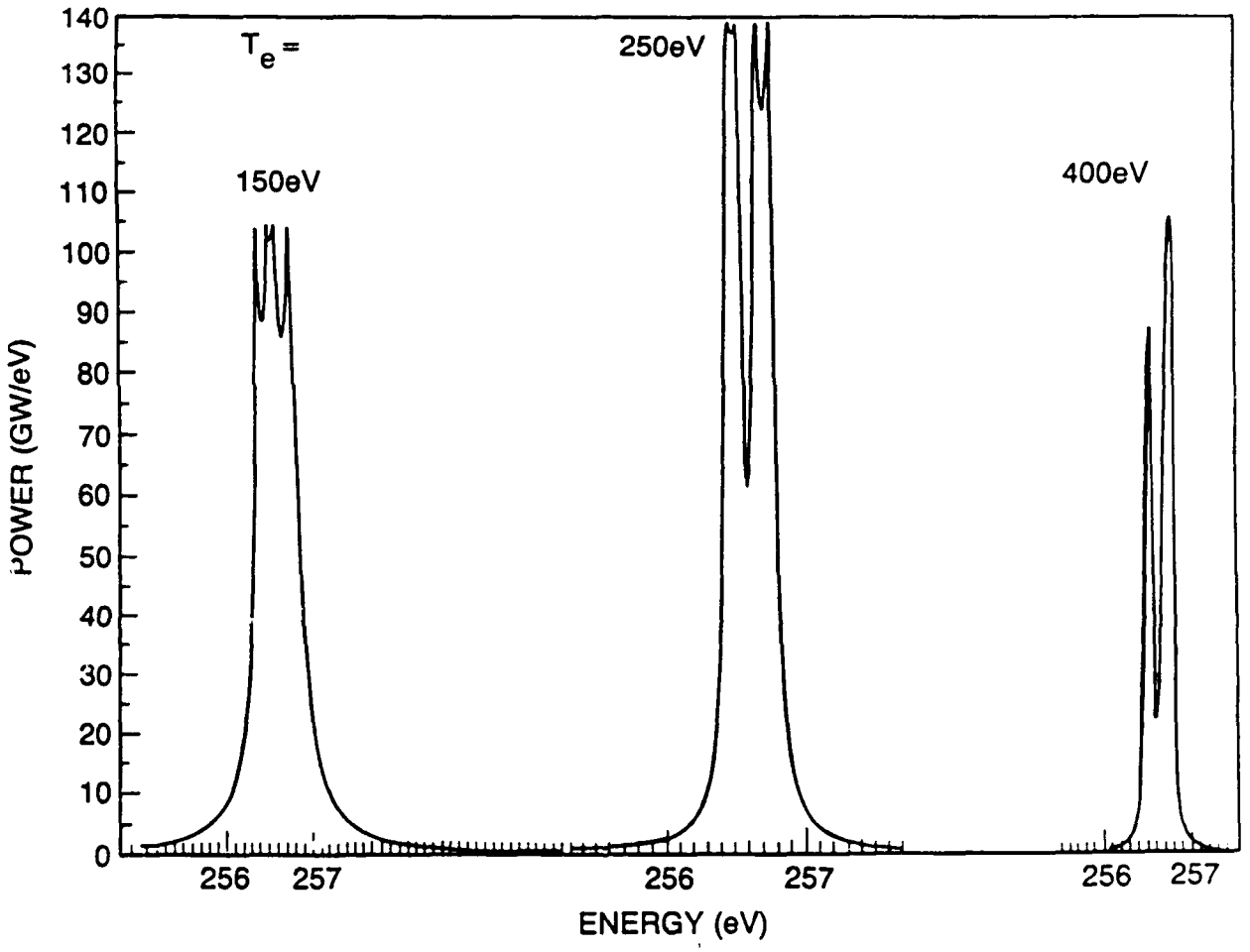

Fig. 1. Power output line profile for the Al XI 2s $^2S_{1/2}$ - 3p $^2P_{1/2,3/2}$ pump line doublet for an assumed 2 cm long Z pinch with ion density 7.6 x 10^{19} cm^{-3}. Temperatures for the 3 cases are indicated. The pumped Mg transition lies at 256.48 eV.

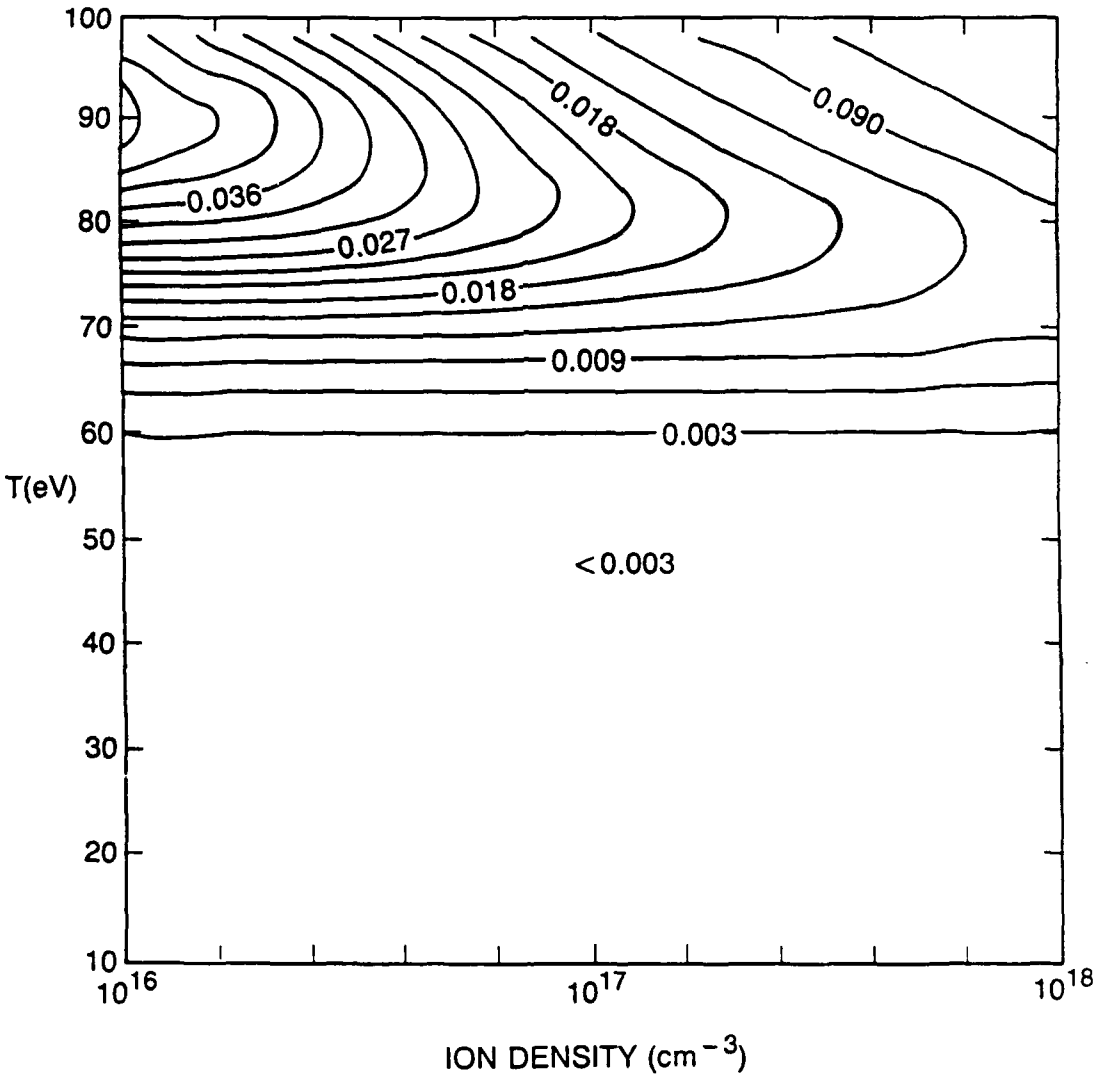

Fig. 2. Be-like ground state fraction for an optically thin Mg plasma vs. ion density and temperature. Distance of Mg plasma from Al Z pinch is 2 cm. Resonant pumping of Mg IX 2s4p level is included, but not photoionization of Mg by the Al radiation.

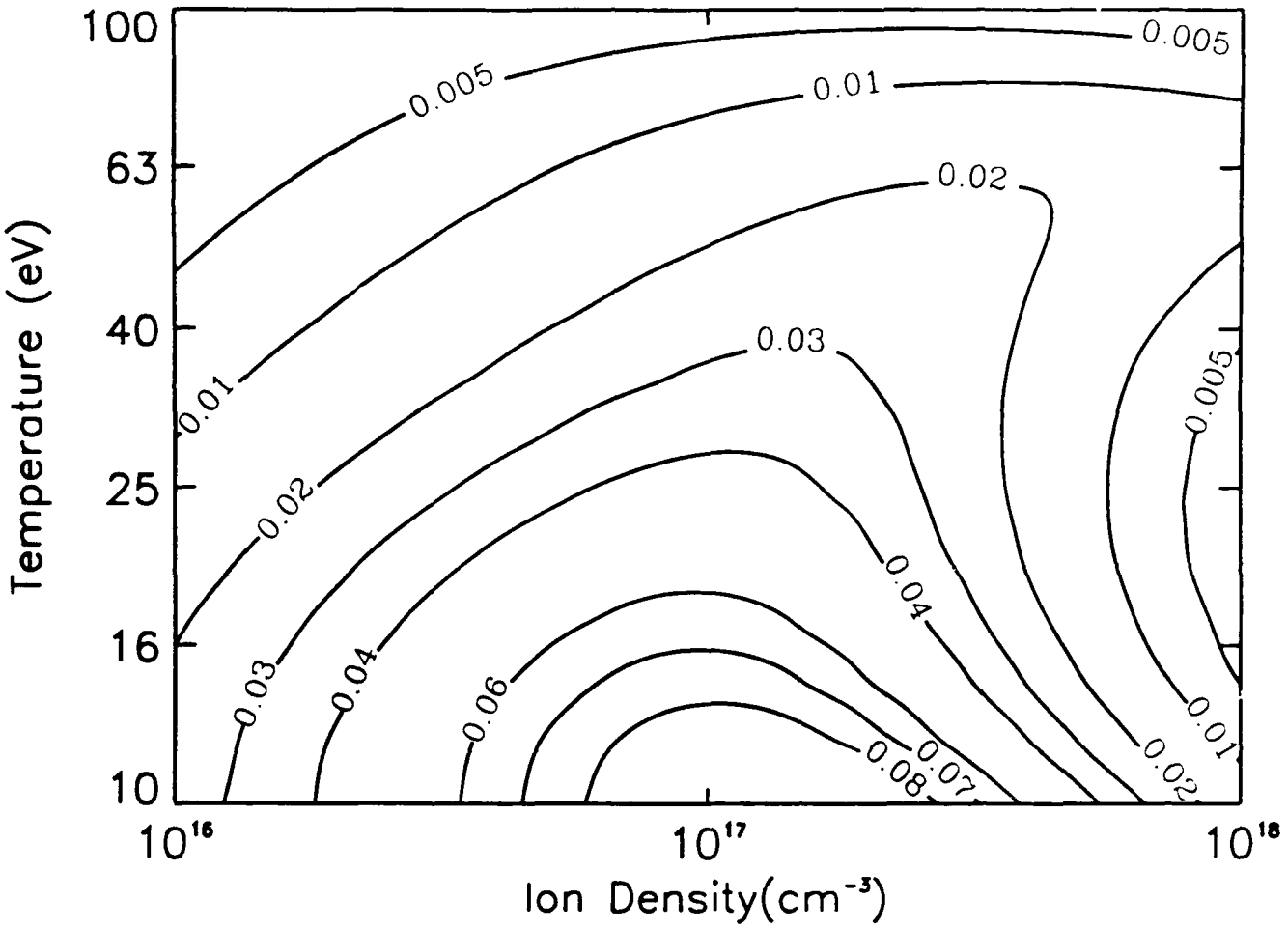

Fig. 3. As in Fig. 2, except that photoionization of the various Mg stages by the Al lines listed in Table II is included.

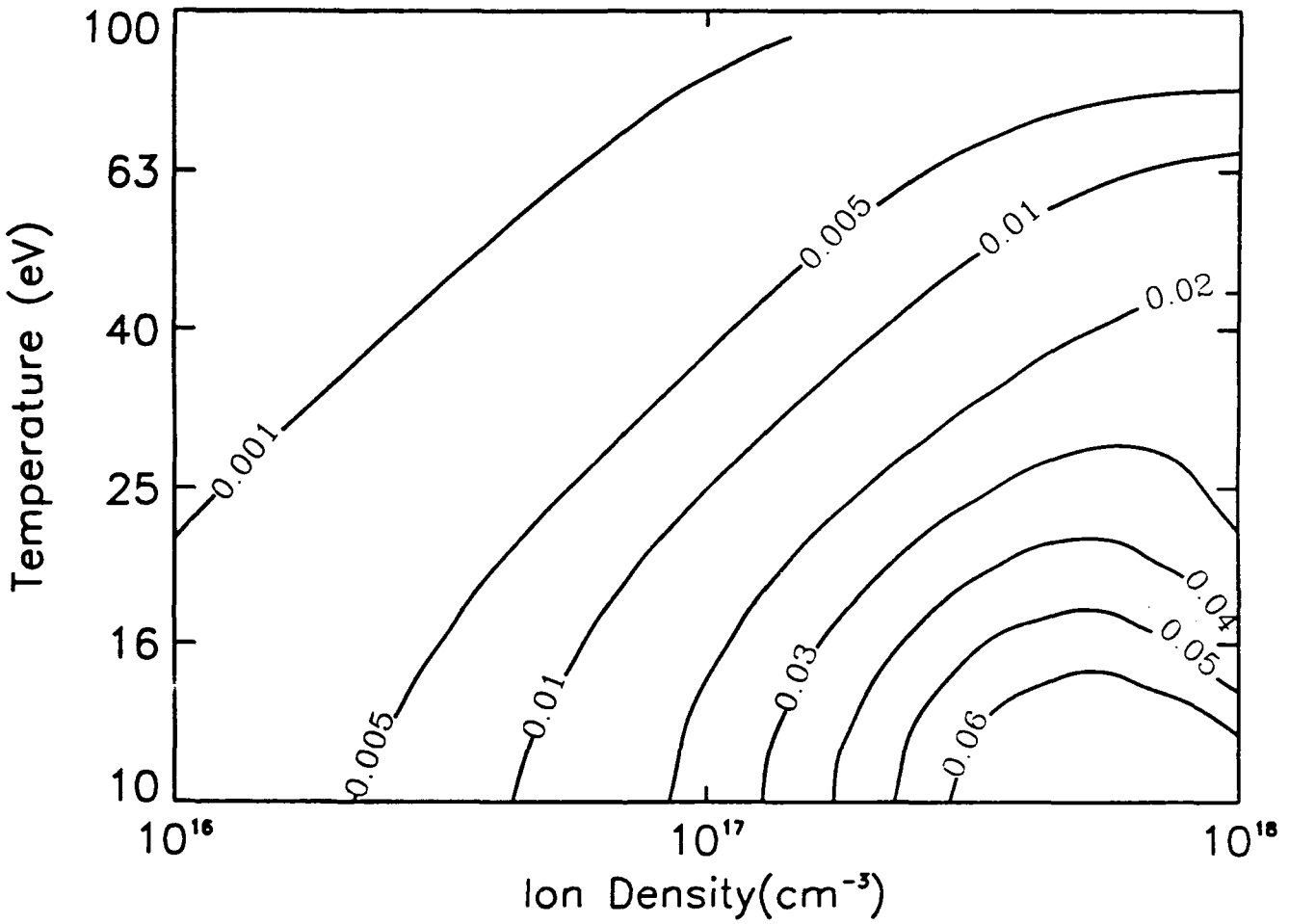

Fig. 4. As in Fig. 3, except that the Al-Mg plasma separation is reduced to 1 cm.

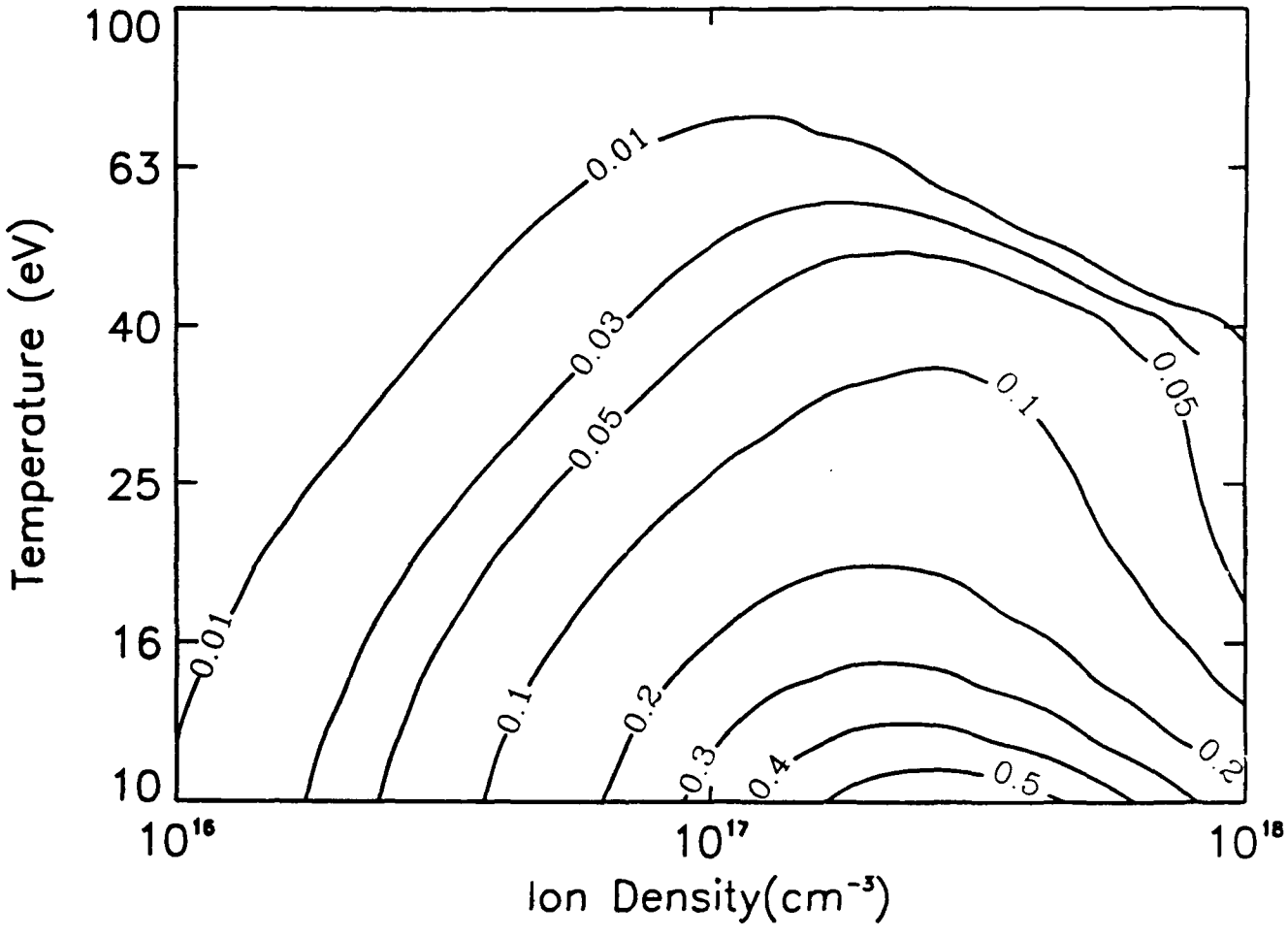

Fig. 5. Gain coefficient for the Mg IX 2s3d $^1D_2$ - 2s4f $^1F_3$ transition near 228 Å is shown as a function of ion density and temperature for an Al-Mg separation of 2 cm, with both photoionization and resonant photopumping included.

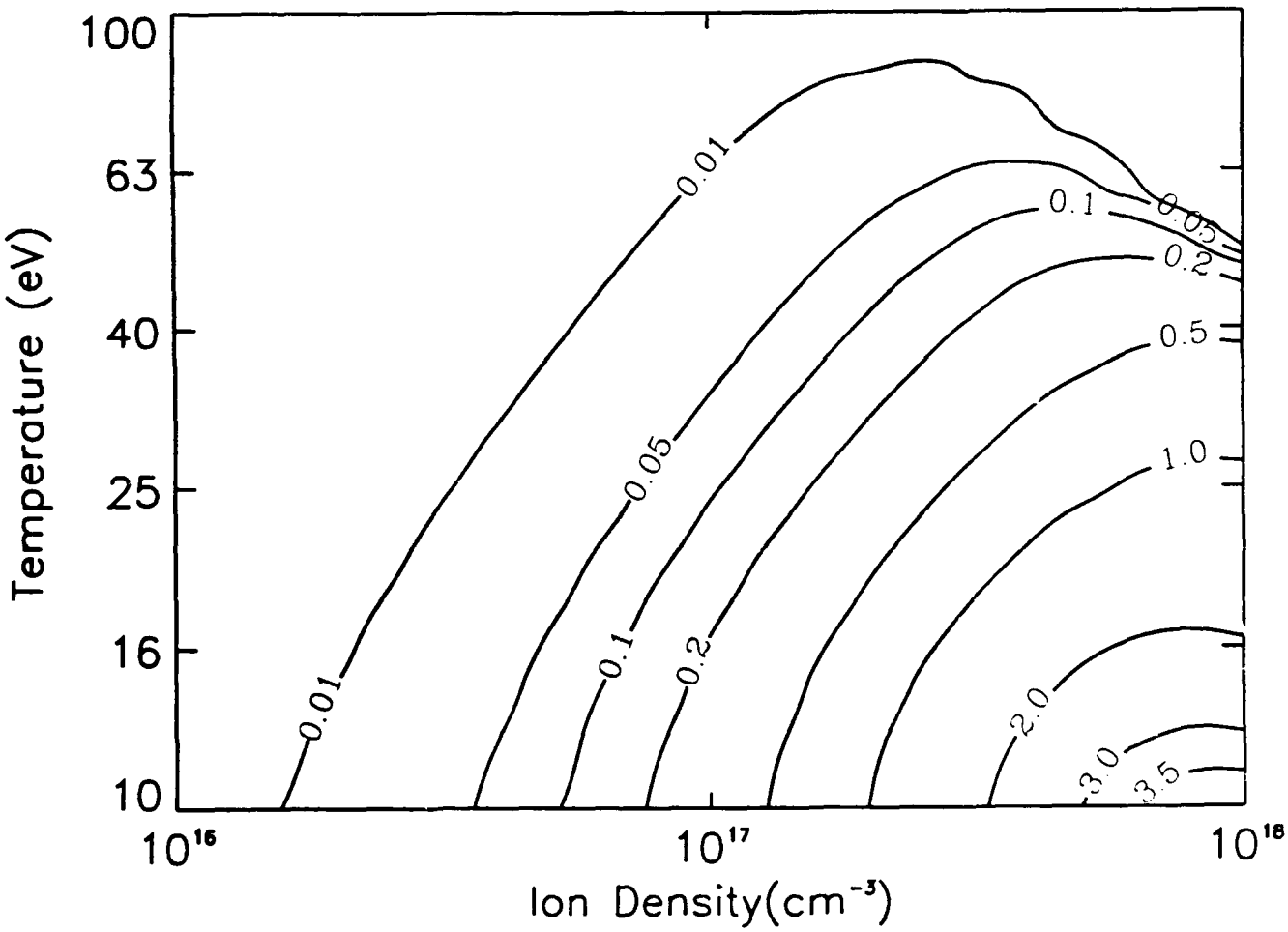

Fig. 6. As in Fig. 5, except that the Al-Mg separation is 1 cm.

Design Considerations for Z-Pinch Driven Photoresonant X-Ray Lasing in Neonlike Krypton

J. W. Thornhill, J. P. Apruzese, J. Davis, and R. W. Clark

Naval Research Laboratory

Radiation Hydrodynamics Branch

Plasma Physics Division

Washington, D.C. 20375-5000

Abstract

A neonlike x-ray laser photoresonant pumping scheme is explored. An attractive design is a coaxial z-pinch consisting of an inner krypton lasant plasma surrounded by a carbon shell that itself is surrounded by a stagnated krypton plasma. The photoresonant radiation emitted from the outer plasma passes inwardly through the carbon shell and photoexcites lasant electrons to the 3s, 3d, and 4d levels. It is calculated that monochromatic pump powers of 30 GW/cm-eV can be achieved for the 4d neonlike resonance line while powers of 100 - 200 GW/cm-eV are attainable for the 3s and 3d resonance lines. The gain in several neonlike 3s-3p transitions is calculated as a function of temperature and density of the lasant plasma. Reasonable gain in only the 3p-3s (J=0-1) transition is obtained for high density, high temperature lasant conditions. This gain, which is driven by monopole excitation from the ground state to the 3p J=0 level, is nearly independent of the presence of pump radiation. For low density, low temperature lasants, optimal gain is obtained in the 3p-3s (J=2-1) transitions. Under these conditions, the pump radiation is necessary to photoionize and photoexcite the lasant plasma to the neonlike stage while

radiative decay from the resonantly pumped 4d level to the 3p (J=2) states provides the major upper lasing level pump mechanism.

I. INTRODUCTION

One of the major limitations of photoresonant laser schemes is the wavelength requirement that the pumping and pumped transitions lie within a linewidth of one another. There are a number of candidate resonant pairs that meet this requirement.[1-4] However, an assured way of achieving this goal is to use ions of the same kind for both the pump source and lasant. Recent work[5-6] has shown that the potential of photoresonant pumping by like ions to produce gain in the x-ray region compares favorably to that of other photoresonant schemes as well as to collisional excitation or recombination schemes driven by high powered lasers or z-pinches.

In this investigation we build upon the analytical work of Chichkov and Fill[5-6] and discuss the results of a numerical model of their proposed coaxial z-pinch configuration laser in which the inner core lasant plasma is being pumped by a stagnating outer plasma, consisting of the same element as the core. In particular, a neonlike krypton photoresonant scheme is analyzed. In the absence of photoresonant pumping the neonlike 3p (J=0) level is populated primarily by direct monopole excitation of the $2p^6$ ground state, see Fig. 1, whereas the other 3p levels are populated by recombination from the ground state of fluorinelike krypton as well as d-- excitation from the upper levels. The presence of pump radiation produces two main effects which alter the populations of the 3p states. First, enhanced photoexcitation and photoionization ionize low density plasmas to the neonlike state at much lower temperatures than are required without photo-pumping. Also, the photoresonant pumping of the 4d level with

subsequent radiative decay to the 3p states provides for a strong upper (J=2) lasing level pump mechanism. As mentioned by Chichkov and Fill,[5-6] the advantage of this scheme is that it operates at electron densities too low to cause collisional de-excitation of the laser transition or refraction of the amplified beam. In addition, the quasi-metastability of the upper lasing level provides inversion without filtering of the 3s resonance radiation, which populates the lower lasing level.

The z-pinch model developed to study this scheme has been simplified by assuming that the pump plasma has already stagnated against a cold carbon shell that surrounds and isolates the core lasant plasma from hydrodynamic effects. The radiation from the outer plasma passes inwardly through the massive carbon shell and photoexcites and photoionizes electrons of the core plasma. It is assumed that the core plasma can be independently heated either Ohmically, by division of the current driving the z-pinch, or else by a laser combined with radiation from the pump plasma.

The details of the z-pinch configuration and the multi-material radiation hydrodynamics models used in the simulation are discussed in Section II. Section III-A describes the calculation of the pump powers and section III-B presents results for the temperature and density dependence of the effective charge and gain in the neonlike 3p-3s (J=0-1) transition at 172 Å and the (J=2-1) transition at 186 Å (Fig. 1). The results for gain achieved in the (J=2-1) 184 Å transition are not discussed, but they are very similar to the results for the (J=2-1) 186 Å transition. A contrast of lasant characteristics with and without the influence of the pump plasma as well as a discussion of the role that opacity plays in limiting the achievable gain are also provided in Section III-B. A summarizing discussion follows in Section IV.

II. MODEL DESCRIPTION

This model describes a static situation that is assumed to be representative of the conditions realized during the stagnation phase of a z-pinch experiment. In our model the cylindrical plasma is divided into three regions (Fig. 2). The first region contains the lasant krypton plasma and it extends from the origin to 0.1 cm. It has uniform density and temperature profiles. Since the lasant plasma is independently heated, its temperature is freely specified. Region 2 is a thin column extending from 0.1 cm to 0.10024 cm, it consists of 400 μg/cm of solid state density carbon at 5 eV. If this were a dynamic Z-pinch simulation, the purpose of the carbon in hydrodynamically isolating the core plasma could be tested. However, since this calculation is static, it is assumed that the carbon has done its job and that the outer krypton pump plasma has stagnated onto the carbon shell. At this stage the main effect of the carbon is to somewhat attenuate via inner-shell absorption the radiation field emanating from the stagnated outer plasma. The third region, which extends from 0.10024 cm to 0.15 cm, contains a krypton pump plasma that has uniform temperature and density profiles characteristic of a stagnated plasma.

The analysis proceeds in two stages. First, a multi-level non-LTE ionization and radiation transport calculation that self-consistently couples all of the regions of the z-pinch configuration is performed. This is an extensive model that is briefly described in Appendix I. Because it is too expensive computationally, there is insufficient neonlike krypton level structure represented in this model to do a credible laser gain calculation. Instead, the gain calculation is performed by passing the following lasant plasma data along to a more detailed multi-level gain model that completes

the second stage of the calculation, this data includes: the electron and ion densities, ground state populations of neonlike and fluorinelike krypton, and the pump powers of the 3s $(3/2,1/2)_1$, 3s $(1/2,1/2)_1$, 3d $(3/2,5/2)_1$, 3d $(1/2,3/2)_1$, and 4d neonlike resonance lines [$(j_1,j_2)_J$ notation] emanating from the outer plasma, see Fig. 1. This gain model is similar to the neonlike selenium model described in Ref. 7, but scaled to neonlike krypton. A static local approximation is used to transport radiation. The pump powers, attenuated by $e^{-\tau_\nu x}$, where τ_ν is the frequency-dependent optical depth and x is the distance into the core plasma, are included as source terms in the gain model for populating the 3s, 3d, and 4d levels.

III. RESULTS

A. Krypton plasma pump power

At stagnation the krypton pump plasma is specified to have a mass loading of 273 μg/cm, an ion density of 5.0×10^{19} cm^{-3}, and temperature of 500 eV. Good pumping rates over a wide range of temperatures and densities were found. The chosen conditions represent typical values that are believed to be attainable (similar values have been obtained for nickel wire experiments performed at Physics International Corp.)[8] using existing pulse power machines, i.e, Sandia National Laboratories' Saturn machine, Physics International's Double Eagle Machine, or Maxwell Laboratories' Blackjack 5 device.

The powers of the 3s, 3d, and 4d resonance lines of the pump plasma are shown in the theoretical spectrum displayed in Fig. 3. For illustration purposes an enlargement of the 3s $(3/2,1/2)_1$ resonance line is shown in Fig.

4. According to this figure, monochromatic powers near 170 GW/eV-cm are achievable for the 3s $(3/2,1/2)_1$ resonance transition. Similar to the calculation of Ref. 9, the pump rate for the 3s $(3/2,1/2)_1$ level (for example) from the neonlike ground state is calculated as

$$P(sec^{-1}) = \int F_\nu \sigma_\nu d\nu = F_\nu \int \sigma_\nu d\nu = (\pi e^2/mc) F_\nu f \qquad (1)$$

where F_ν is the monochromatic pump flux, assumed constant across the pumped line profile, σ_ν is the photoabsorption cross-section, and f is the absorption oscillator strength of the pumped transition (=0.136). Assuming negligible attenuation of the pump radiation by the carbon shell and that the core plasma sees the full 2π steradians of radiation field from the pump, $F_\nu = 2.7 \times 10^{12}$ photons/(cm^2-sec-Hz). Using Eq. (1) a pump rate of 9.7×10^9 sec^{-1} is obtained. The pump rates, energy levels, and oscillator strengths for the other 3s, 3d, and 4d levels are presented in Table I. The pump rate to the 4d state, which ultimately populates the upper 3p (J=2) lasing levels by radiative decay is 8.29×10^9 sec^{-1}. Whether this factor is sufficient to produce or enhance gain is examined in the next subsection.

B. Calculation of gain in krypton

The effective charge as a function of temperature and density of the lasant plasma for the case in which the radiation field emitted from the pump plasma is turned off is shown in Fig. 5. These results are taken from the innermost zone of the lasant plasma, but, they also represent typical values throughout the core. This figure illustrates that increasing the core ion density allows the neonlike krypton state (z = 25) to be attained at progressively lower temperatures. The principal cause of this behavior is

ladder ionization. As density increases, the increased excited state populations are ionized to the next highest ground stage, requiring a lower ionization potential than ground-to-ground ionization.

When the pump plasma is present, photoionization and photoexcitation produce a dramatic rise in the ionization state of the low density lasant plasmas. This is clearly seen in Fig. 6, where the effective charge as a function of density and temperature is shown. A comparison of Fig. 5 and Fig. 6 reveals that the low density, $N_i = 10^{17}$ cm^{-3}, plasma increases from an ionization stage of z = 22 (without pump) to z = 26.5 (with pump) at a temperature of only 250 eV. In fact, Fig. 6 demonstrates that the simulations for the 10^{17} cm^{-3} plasma should be performed at lower temperatures or lower pump powers because the neonlike krypton stage is partially burned through at 250 eV. Low temperature and density results are discussed below. The contrasting behavior between the state of the lasant plasma with and without a pump field is an excellent example of the trade-off between collisional versus radiative effects, i.e., the state of low density (less collisional) plasmas are significantly affected by the pump field, whereas, higher density (collisional) plasmas are only minimally altered.

When there is no pump plasma, significant gain is only achieved for the high density, 10^{19} cm^{-3}, plasmas principally because only they attain sufficient population in the excited neonlike states, see Fig. 5. The gain in the 3p - 3s (J=0-1) transition at 172 Å is plotted in Fig. 7 for the inner zone of the lasant plasma as a function of temperature. This gain is nearly uniform from the center to within 100 μm of the edge of the lasant plasma. At the very edge of the lasant plasma reduced opacity of the 3s $(1/2,1/2)_1$ resonance line does lead to factors of 2 - 3 enhancement of gain over that displayed in Fig. 7. Gain in excess of unity was achieved in the

(J=2-1) transition only at the very edge of the plasma. Again, this phenomenon is the result of reduced trapping of the 3s $(1/2,1/2)_1$ resonance line. This gain is not shown, but it has a value of 2.25 cm^{-1} at 700 eV and linearly extrapolates to zero at a temperature of 450 eV.

These static model results are in reasonable accord with predictions from the Livermore model[10] that was used to simulate neonlike selenium laser experiments. In particular, both models show that monopole excitation of the upper 3p J=0 level exceeds the indirect excitation of the 3p J=2 levels such that gain in the neonlike selenium 183 Å (J=0-1) transition is substantially larger than in the 209 Å (J=2-1) transition. These model results are in opposition to the experimentally observed amplifications of 5 cm^{-1} for the (J=2-1) transition and negligible gain in the (J=0-1) transition.[11] This 'mystery of the missing (J=0-1) line'[11] has led to some controversy as to whether the Livermore experiments achieved the predicted plasma conditions necessary to produce high gain in the (J=0-1) transition and whether the atomic models are flawed.[7] This controversy has somewhat abated due to new experiments which showed 2 - 3 cm^{-1} gain in the (J=0-1) transition of selenium.[12] In addition, the Livermore model has been updated by including detailed dielectronic recombination to the excited states of neonlike selenium[13-17] (with the exception of an effective dielectronic recombination rate to the ground state, these individual processes are not included in our model). This addition has increased the predicted strengths of the (J=2-1) lines relative to the (J=0-1) line. However, the Livermore model still predicts larger gain in the (J=0-1) transition.[12] Another CRE selenium model that includes dielectronic recombination to the excited states[18] as well as excitation and ionization coefficients derived from the same data base as the Livermore model has confirmed the prediction that the (J=0-1)/(J=2-1) gain ratio is larger than unity for the 183 and 209 Å transitions but it

predicts the ratio to be less than unity for the (J=0-1) 169 Å and (J=2-1) 206 Å transitions. This atomic model, the Livermore model, and the one used in our work all have common features and well as some that are still controversial. These unresolved experimental, atomic data, and calculational issues do not affect photon pump rates and therefore do not negate the utility of evaluating the effects of photoresonant pumping on a neonlike gain calculation.

The gain results are now discussed for the case in which the pump is on but the explicit pump rates to the 3s, 3d, and 4d levels, listed in Table I, are unattenuated as the pump radiation travels into the core. The enhanced pumping of the 3p J=0 state by direct radiative decay of the 4d level does lead to slightly larger (J=0-1) gain coefficients than displayed in Fig. 7 for the non-photo-pumped lasant plasma. The additional ionization and enhanced upper laser level pumping associated with the pump plasma also produce unity (J=0-1) gain coefficients for temperatures in excess of 350 eV in moderate density, 10^{18} cm^{-3}, plasmas. However, the most dramatic increase in gain occurs for the (J=2-1) 186 Å transition. This is illustrated in Fig. 8 where excellent gain, > 2 cm^{-1}, is achieved for temperatures in excess of 300 eV. There are several phenomena that play a role in producing gain under these plasma conditions. First, since opacity scales with ion density, the trapping of the 3s to ground state resonance lines is substantially lower for a plasma with an ion density of 10^{18} cm^{-3} as opposed to 10^{19} cm^{-3}. Secondly, pumping excites the plasma to the neonlike stage at lower temperatures than without the pump, see Figs. 5 and 6; this reduces the line Doppler width and also promotes recombination from the fluorinelike stage. Third, radiative decay of the resonantly pumped 4d level is the dominant mechanism for populating the upper lasing 3p J=2 level.[5-6] The presence of resonant photo-pumping to the 4d level effects a three order of magnitude

enhancement of the creation rate to the 3p J=2 level. For the 10^{17} cm^{-3} plasma, (J=2-1) 186 Å gain is limited by low neonlike ground state populations due to burn through, i.e. the simulations were performed at too high lasant temperatures.

Gain results from the calculations that include the attenuation of the pump rates due to resonance absorption in the core plasma are now examined. These calculations are the most representative of an actual z-pinch configuration soft x-ray laser. Since the opacity of the 4d resonance line is greater than 60 cm^{-1} (200 cm^{-1}) in a plasma having an ion density of 10^{18} cm^{-3} (10^{19} cm^{-3}) and a temperature in excess of 400 eV , it is not surprising that at sufficiently high ion density the upper lasing level pump rates are attenuated a short distance into the core plasma. The attenuation is sufficient that the gain results for the (J=0-1) transition are virtually identical to the case without any pump plasma (Fig. 7), except at the very edge of the plasma where the 4d resonance line is unattenuated. This point is also clearly demonstrated by comparing the 186 Å (J=2-1) gain results at the center of the outer zone (Fig. 9), which is only 67 μm from the edge of the lasant plasma, with the unattenuated results (Fig. 8). The gain at 67 μm is reduced by attenuation to half the value found at the very edge of the 10^{18} cm^{-3} lasant plasma. Attenuation is so complete at the very center of the 10^{18} cm^{-3} lasant plasma that there is no gain in the 186 Å transition. For the 10^{17} cm^{-3} plasma, the ion density is low enough that attenuation of the pump only produces a 40 percent decrease in gain from the outer compared to the inner zone. This is encouraging because by choosing a low lasant density and temperature (Fig. 10), gain coefficients in excess of unity over a large, 1 mm, radial expanse are obtainable. At these temperatures the radiation from the pump source alone may be sufficient to heat the lasant plasma. The major drawback to using a low temperature lasant plasma is that,

as revealed by a time dependent ionization dynamics calculation, the pump plasma needs to be present for prohibitively long, 100 ns, time periods in order to photoionize a plasma with ion density of 10^{17} cm^{-3} and temperature of 50 eV to the neonlike state. By contrast, a 10^{17} cm^{-3} plasma at 300 eV requires only about 20 ns to reach the neonlike stage. These photoionization times imply that the low density gains shown in Figs. 8 and 9 are conservative because there will be a substantial interval of time during photoionization when conditions will be more favorable for gain than indicated by the steady state effective charge of ~ 26.5 shown in Fig. 6.

IV. SUMMARY AND DISCUSSION

This work was intended to be a preliminary assessment, not a full optimization determination, for investigating the potential of realizing lasing via neonlike krypton photoresonant excitation in which ions of the same kind serve as both the lasant and pump source. The scheme is for a coaxial z-pinch configuration in which the inner core lasant is pumped by a stagnated outer shell plasma. Gain coefficients as a function of density and temperature of the lasant plasma as well as whether or not the pump plasma is present are calculated for the 3p-3s (J=0-1) transition at 172 Å and the 3p-3s (J=2-1) transition at 186 Å.

It is calculated that monochromatic powers of 30 GW/eV-cm for 4d resonance radiation are achievable by stagnating a pump plasma onto a massive carbon shell that hydrodynamically isolates the lasant plasma but is transparent to the resonant radiation. This radiation pumps the 4d states of the lasant plasma. The subsequent radiative decay from the 4d to the 3p level provides for the major upper lasing level pump mechanism for the J=2 states. Although the J=0 level population can be enhanced by radiative decay

of the pumped 4d level, under most (J=0-1) gain conducive plasma conditions, the most important J=0 level populating mechanism is direct monopole excitation from the ground state.

Significant gain coefficients for the 3p-3s (J=0-1) transition were found only for high ion density, 10^{19} cm^{-3}, and high electron temperature (> 500 eV) lasant plasmas. Under these conditions, gains of the order 2 cm^{-1} were present throughout the interior of the lasant plasma; at the edge of the plasma the gain was a factor of 2-3 larger because of reduced opacity in the lower lasing level 3s resonance transition. Because of the dominance of collisional processes in these high density plasmas, the gain was nearly independent of the presence of pump radiation.

For high density lasant plasmas, opacity effects limit gain in the 186 Å 3p-3s (J=2-1) transition to only the outer edge of the plasma. For moderate and low density plasmas the pump field is essential for photoionizing the plasma to the neonlike state as well as resonantly photopumping the 4d level populations. Radiative decay of the 4d to the 3p J=2 state is the principal creation mechanism for the J=2 upper lasing level. Attenuation of the photoresonant 4d pump radiation limits significant gain to only the outer 100 μm of a lasant plasma with an ion density of 10^{18} cm^{-3}. The gain at this density for temperatures of 300 - 700 eV is between 1- 2 cm^{-1}, except at the very edge of the plasma where it is factors of 2-3 larger because of negligible attenuation of the pump radiation as well as reduced opacity. At lower densities, 10^{17} cm^{-3}, gains of the order 1 - 2 cm^{-1} are achieved over a broad radial expanse at very low lasant temperatures, of the order 50 eV. The disadvantage of the low density lasant plasma is the pump plasma has to provide photoionizing/pumping radiation for the long time span needed to ionize the lasant plasma to the neonlike state. The advantages of the low

density lasant plasma are the radiation from the pump source alone may be sufficient to heat the lasant plasma, and refraction effects are minimized.

Acknowledgements

We thank Dr. K. G. Whitney and the referee for their valuable comments and Dr. P. C. Kepple for providing the krypton rate table. This work was supported by the Strategic Defense Initiative Office of Innovative Science and Technology.

Appendix I

The ionization dynamics is calculated using the multi-material collisional-radiative-equilibrium (CRE) radiation and atomic physics models developed at NRL.[19-24] In addition to all of the ground states of carbon and krypton, there are 136 excited levels of krypton represented by the model. There is not any excited state structure of carbon included in the model since the neonlike resonance lines of krypton lie above the carbon K edge, thus, neglecting excited state structure should produce an overestimate of the inner-shell absorption and result in a conservative gain calculation.

Since optical pumping by such mechanisms as photoionization and photoexcitation allow plasmas separated in space to affect each other's level populations, these processes must be self-consistently modeled by transport of the radiation field. In this calculation, a multi-frequency transport model is employed to calculate the level populations of the core plasma as they are redistributed by the pump plasma's radiation field. This model transports 1400 frequency bins that span the total frequency space over which the bound-bound, bound-free, and free-free radiation is emitted from the krypton and carbon plasmas. The model includes 58 spectral lines mostly from the fluorinelike, neonlike, and sodiumlike krypton ionization stages. A Voigt line profile is assumed, and there are 12 frequency bins resolving each line. In addition there are 2 frequency bins designated for each bound-free edge. Transporting the radiation required zoning the plasma regions; in our model we used 4 zones to model the core, 3 zones to model the carbon shell, and 4 zones to model the pump plasma. All the zones of a particular region contain the same mass.

References

1. P. L. Hagelstein, Plasma Phys. 25, 1345 (1983).

2. A. V. Vinogradov, B. N. Chichkov, and E. A. Yukov, Sov. J. Quant. Electron. 14, 444 (1984).

3. M. Krishnan and J. Trebes, Appl. Phys. Lett. 45, 189 (1984).

4. R. C. Elton, T. N. Lee, and W. A. Molander, Phys. Rev. A 33, 2817 (1986).

5. B. N. Chichkov and E. E. Fill, Optics Communications, 74, 202 (1989).

6. B. N. Chichkov and E. E. Fill, Phys. Rev. A 42, 599 (1990).

7. J. P. Apruzese, J. Davis, M. Blaha, P. C. Kepple, and V. L. Jacobs, Phys. Rev. Lett. 55, 1877 (1985).

8. C. Deeney, T. Nash, P. D. Lepell, K. Childers, M. Krishnan, K. G. Whitney, and J. W. Thornhill, J. Quant. Spectrosc. Radiat. Trans. 44, 457 (1990).

9. J. P. Apruzese and M. Buie, J. Appl. Phys, 70, 1957 (1991).

10. M. D. Rosen, P. L. Hagelstein, D. L. Matthews, E. M. Campbell, A. U. Hazi, B. L. Whitten, B. MacGowan, R. E. Turner, R. W. Lee,

G. Charatis, Gar. E. Busch, C. L. Shepard, and P. D. Rockett, Phys. Rev. Lett. 54, 106 (1985).

11. D. L. Matthews, P. L. Hagelstein, M. D. Rosen, M. J. Eckart, N. M. Ceglio, A. U. Hazi, H. Medecki, B. J. MacGowan, J. E. Trebes, B. L. Whitten, E. M. Campbell, C. W. Hatcher, A. M. Hawryluk, R. L. Kauffman, L. D. Pleasance, G. Rambach, J. H. Scofield, G. Stone, and T. A. Weaver, Phys. Rev. Lett. 54, 110 (1985).

12. R. A. London, M. D. Rosen, M. S. Maxon, D. C. Eder, and P. L. Hagelstein, J. Phys. B: At. Mol. Phys. 22, 3363 (1989).

13. M. D. Rosen and P. L. Hagelstein, "Short Wavelength Coherent Radiation Generation and Applications," (Am. Inst. Phys. Conf. Proc. No. 147) ed. D. J. Attwood and J. Bokor (New York: AIP) p110 (1986).

14. M. H. Chen, Phys. Rev. A 34, 1073 (1986).

15. B. L. Whitten, A. U. Hazi, M. H. Chen, and P. L. Hagelstein, Phys. Rev. A 33, 2171 (1986).

16. P. L. Hagelstein, M. D. Rosen, and V. L. Jacobs, Phys. Rev. A 34, 1931 (1986).

17. P. L. Hagelstein and R. K. Jung, At. Nucl. Data Tables 37, 121 (1987).

18. K. G. Whitney, A. Dasgupta, M. Blaha, and M. C. Coulter, "The Influence of 3d Metastability on the Dynamics of the 3s and 3p Multiplet States

in Neonlike Krypton," (Am. Phys. Soc. Plasma Phys. Annual Meeting), Bull. of Am. Phys. Soc. 2354 (1991).

19. D. Duston and J. Davis, Phys. Rev. A 23, 2602 (1981).

20. J. Davis, J. Quant. Spectrosc. Radiat. Trans. 14, 549 (1974).

21. V. L. Jacobs, J. Davis, P. C. Kepple, and M. Blaha, Astrophys. J. 211, 605 (1977).

22. V. L. Jacobs and J. Davis, Phys. Rev. A 18, 697 (1978).

23. D. Duston, R. W. Clark, J. Davis, and J. P. Apruzese, Phys. Rev. A 27, 1441 (1983).

24. R. W. Clark, J. Davis, and F. L. Cochran, Phys. Fluids 29, 1971 (1986).

TABLE I: Total power output and pump rates of important photoresonant transitions in Ne-like krypton [$(j_1,j_2)_J$ notation]. The mass of the source plasma is 273 μg/cm, the temperature is 500 eV, and the ion density is 5×10^{19} cm^{-3}. The 4d level is representative of a number of fine structure split levels that are lumped according to statistical equilibrium.

Transition to $(1s^2 2p^6)$ from	Energy (eV)	Oscillator Strength	Power (10^{11} W/cm-eV)	Pump Rate P(10^9 sec^{-1})
3s $(3/2,1/2)_1$	1652	0.136	1.72	9.67
3s $(1/2,1/2)_1$	1708	0.095	1.72	6.78
3d $(3/2,5/2)_1$	1790	1.66	1.18	74.5
3d $(1/2,3/2)_1$	1846	2.0	1.33	98.6
4d	2309	0.88	0.32	8.29

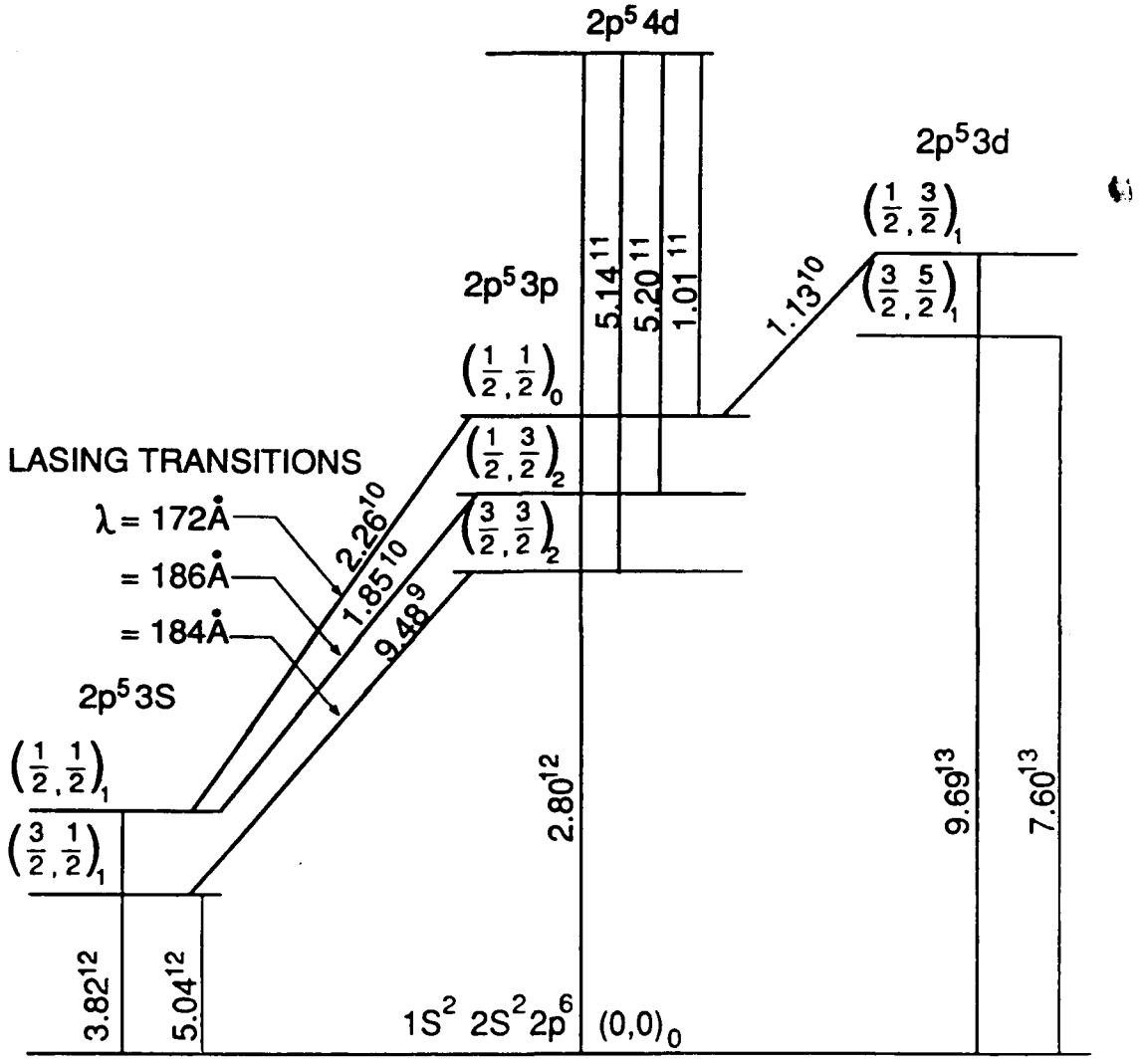

Fig. 1 Energy level diagram [$(j_1,j_2)_J$ notation] and oscillator strengths for important lasing and resonance transitions for neonlike krypton. The 4d level is representative of a number of fine split levels that are lumped according to statistical equilibrium.

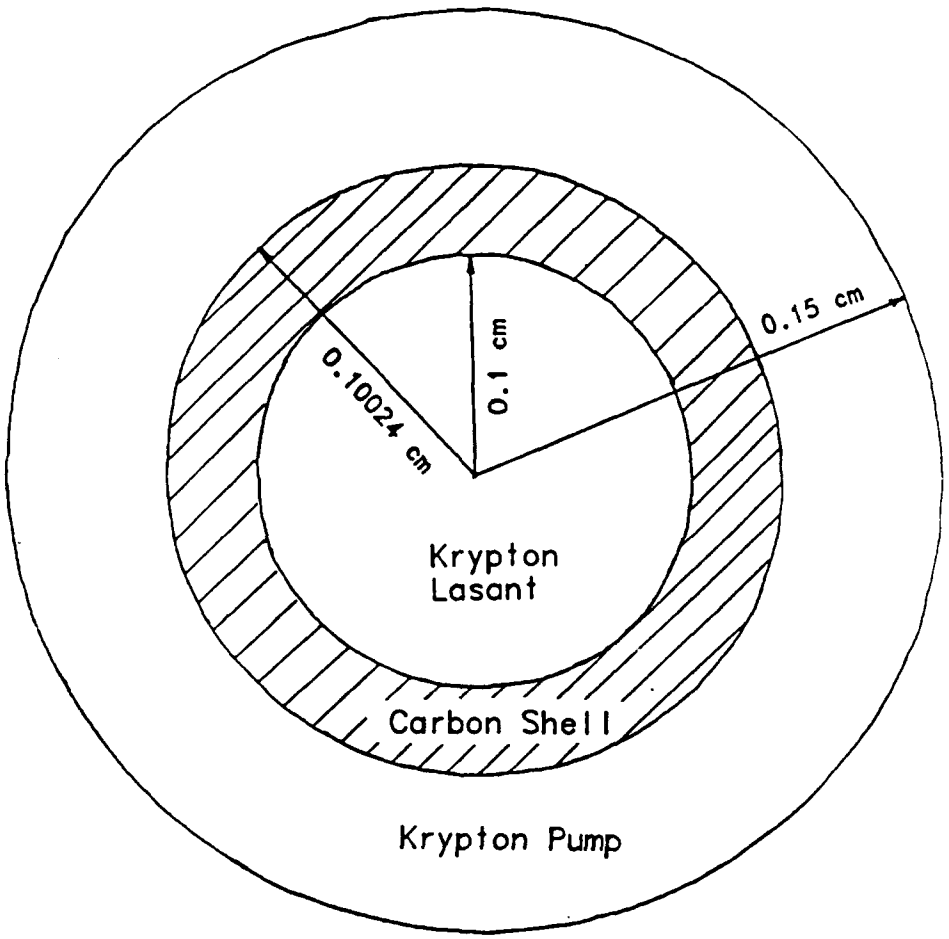

Fig. 2 Schematic diagram of z-pinch coaxial laser.

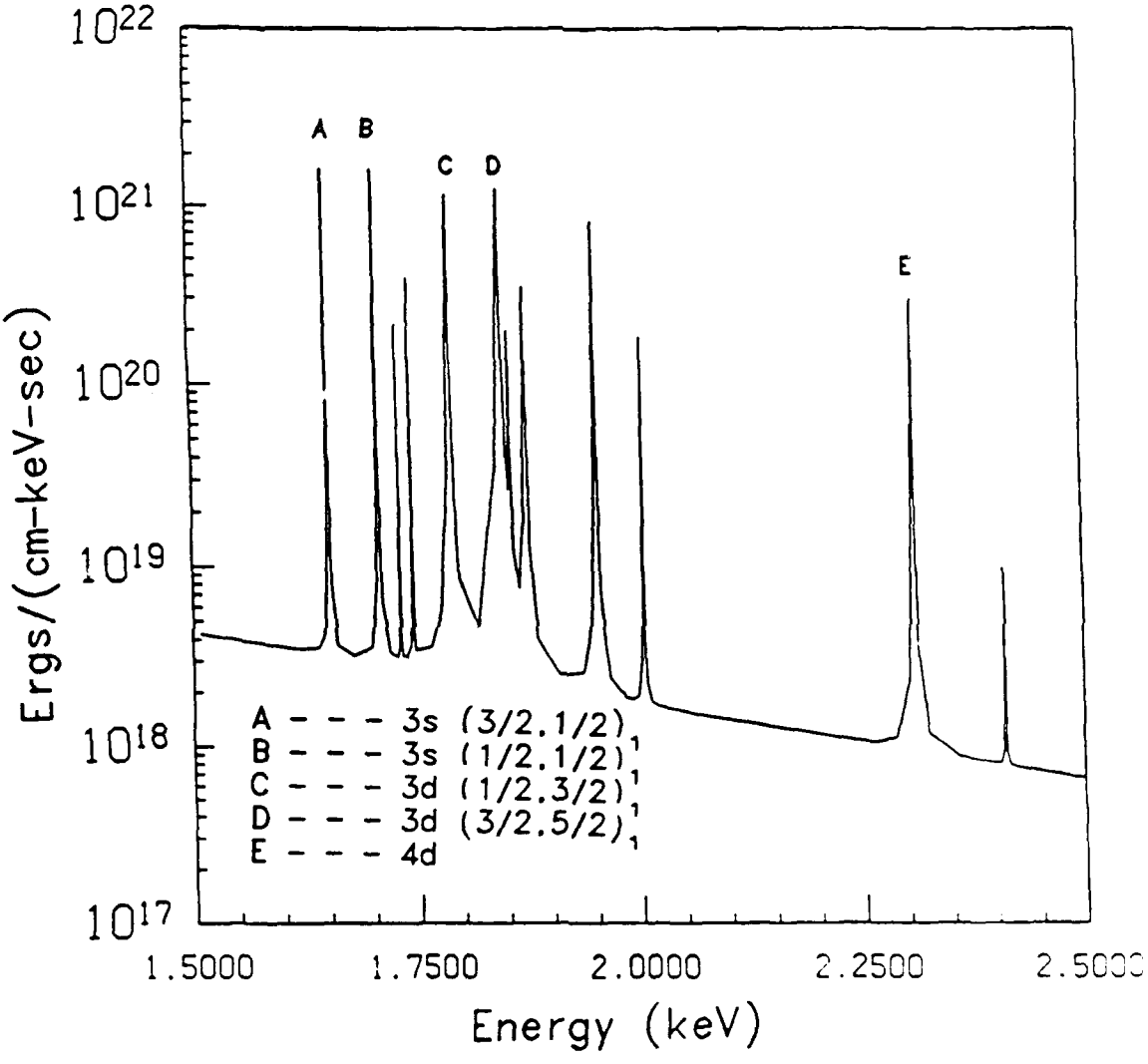

Fig. 3 Spectrum of neonlike krypton resonance lines emitted from the pump plasma.

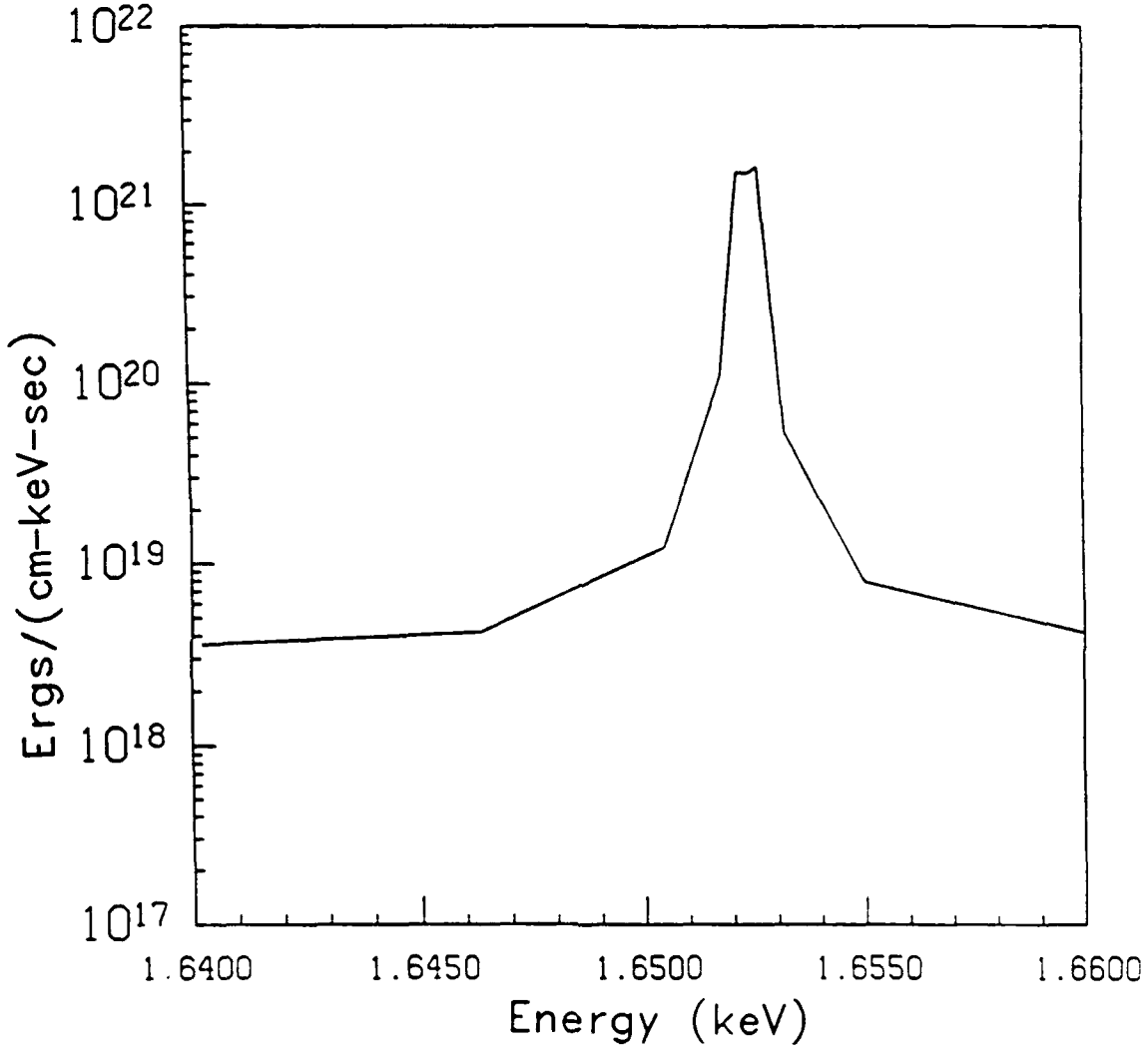

Fig. 4 Emitted spectral profile of $3s(3/2,1/2)_1$ - ground state transition of neonlike krypton emitted from the pump plasma.

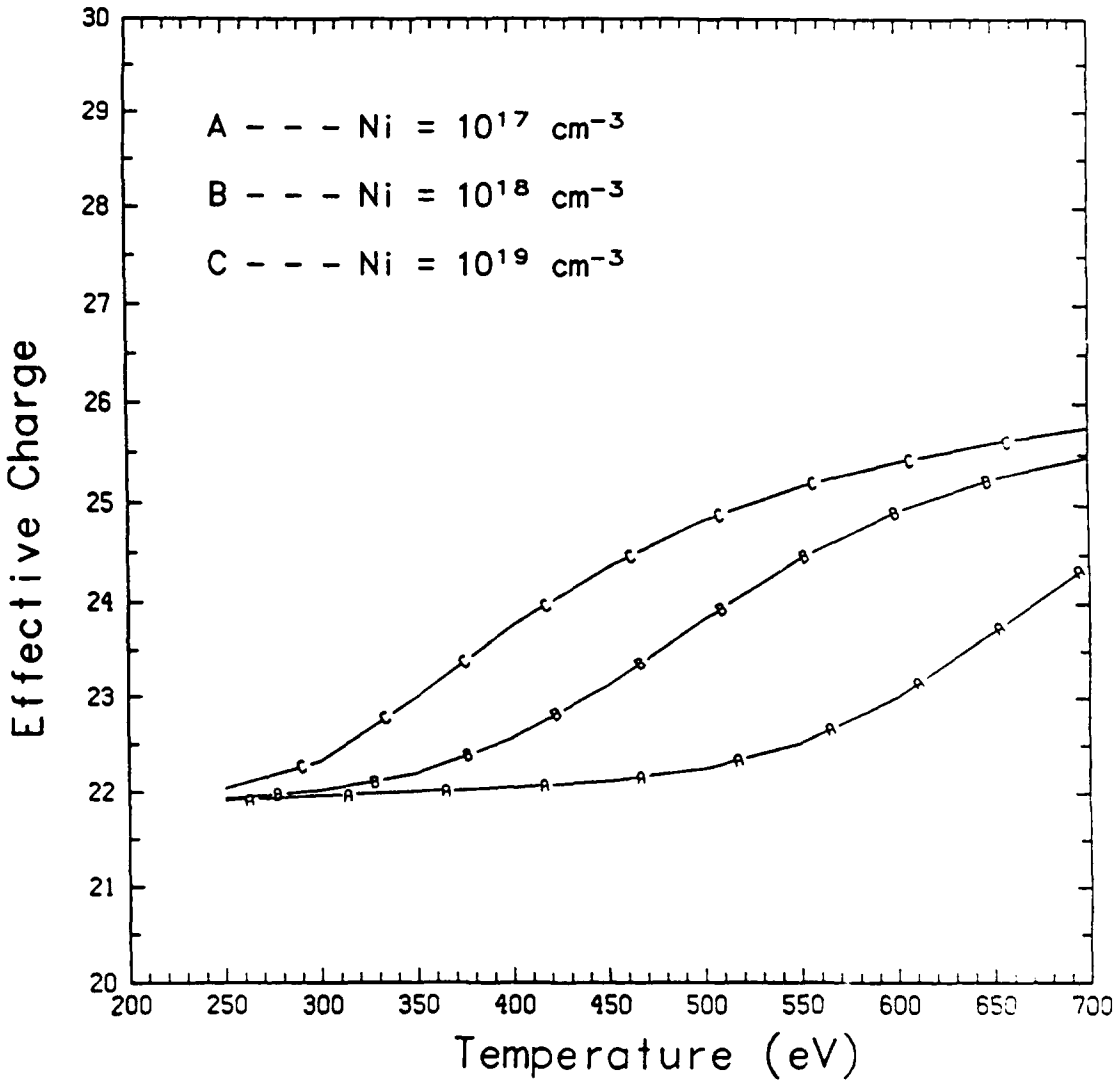

Fig. 5 The effective charge as a function of density and temperature of the lasant plasma. Radiation from the pump plasma is turned off.

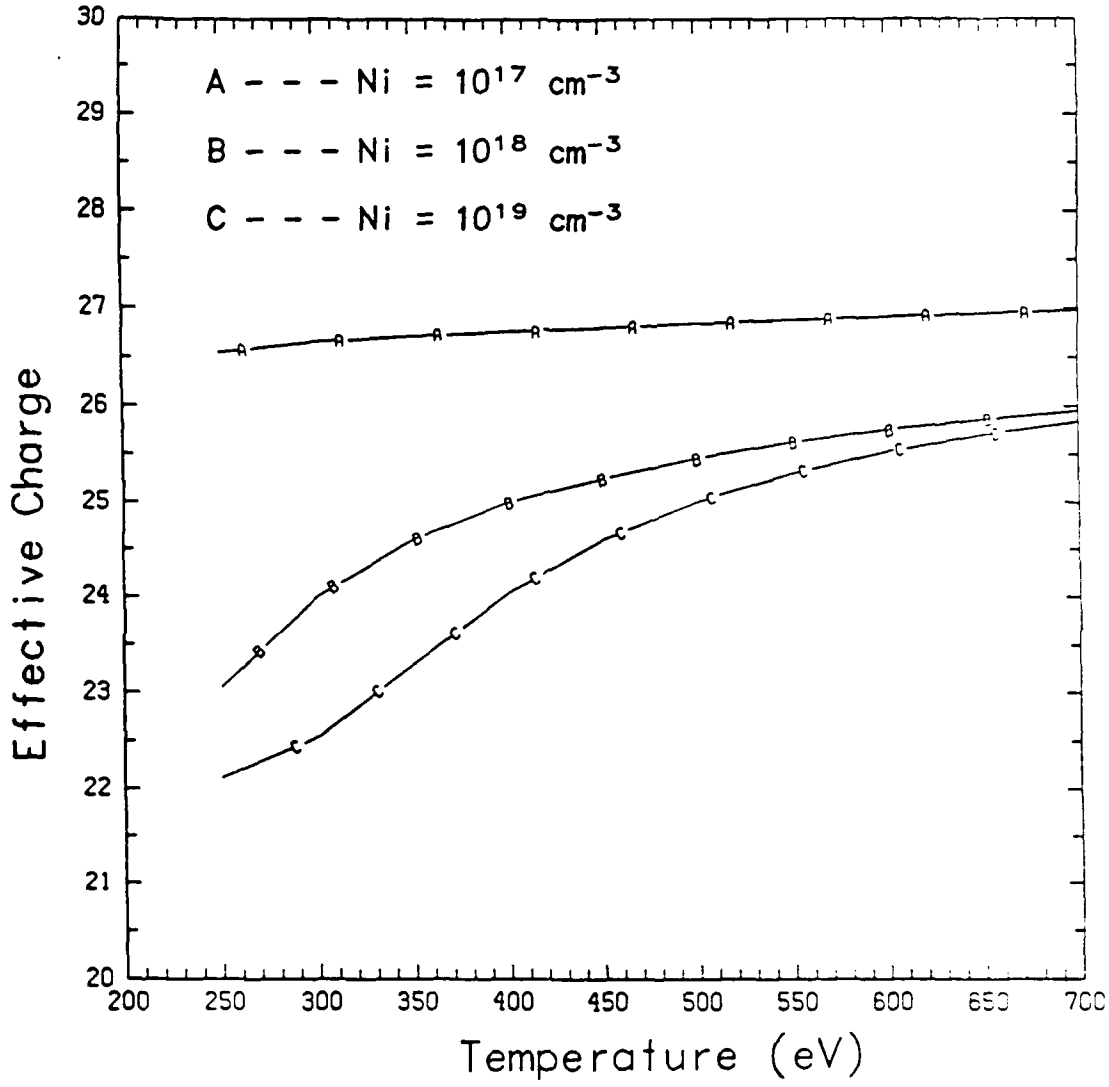

Fig. 6 The effective charge as a function of density and temperature of the lasant plasma. Radiation from the pump plasma is turned on.

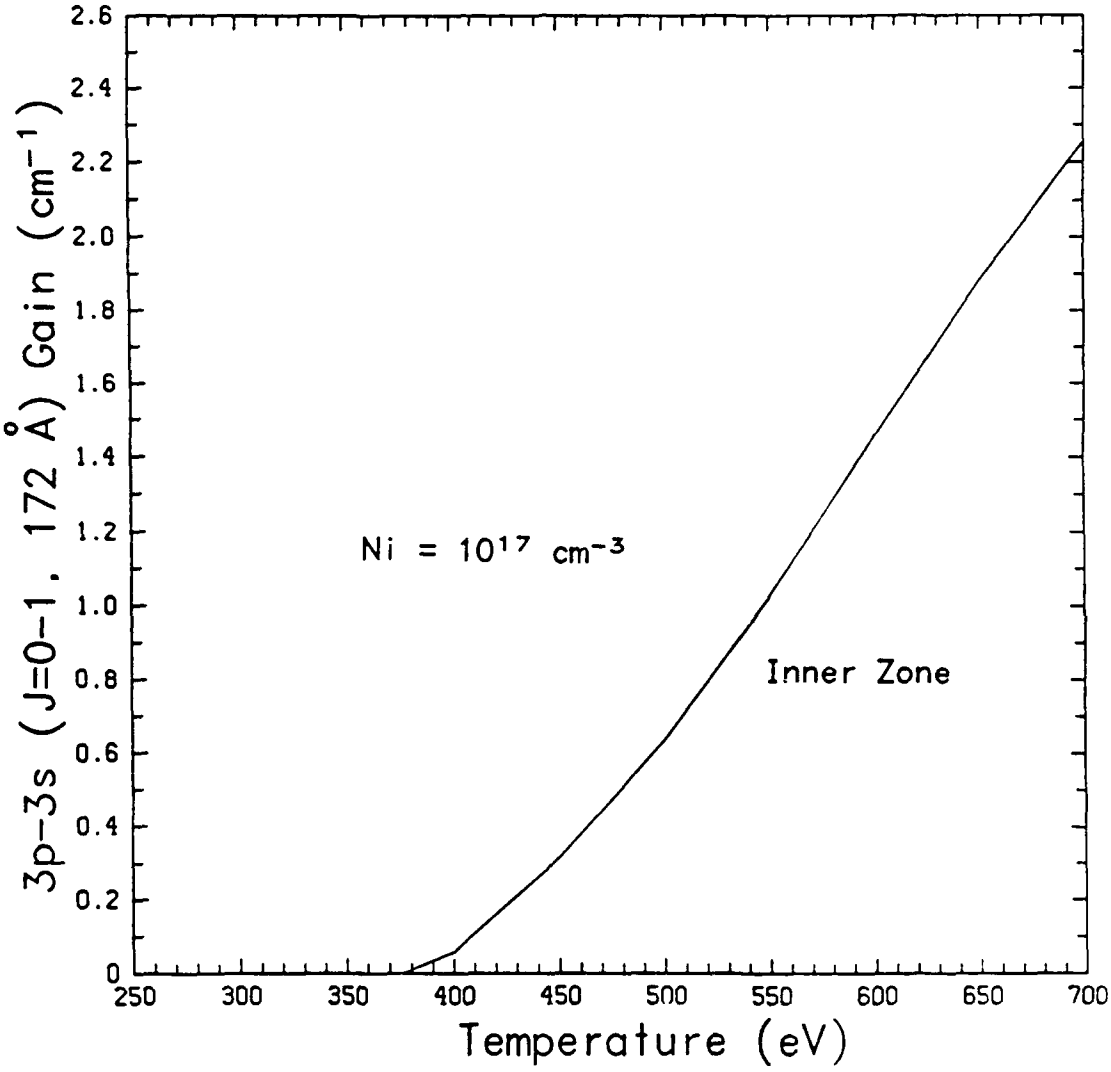

Fig. 7 3p-3s (J=0-1) gain coefficients as a function of temperature for the inner zone of a 10^{19} cm^{-3} ion density lasant plasma. Radiation from the pump plasma is turned off. The radius of the lasant plasma is 0.1 cm

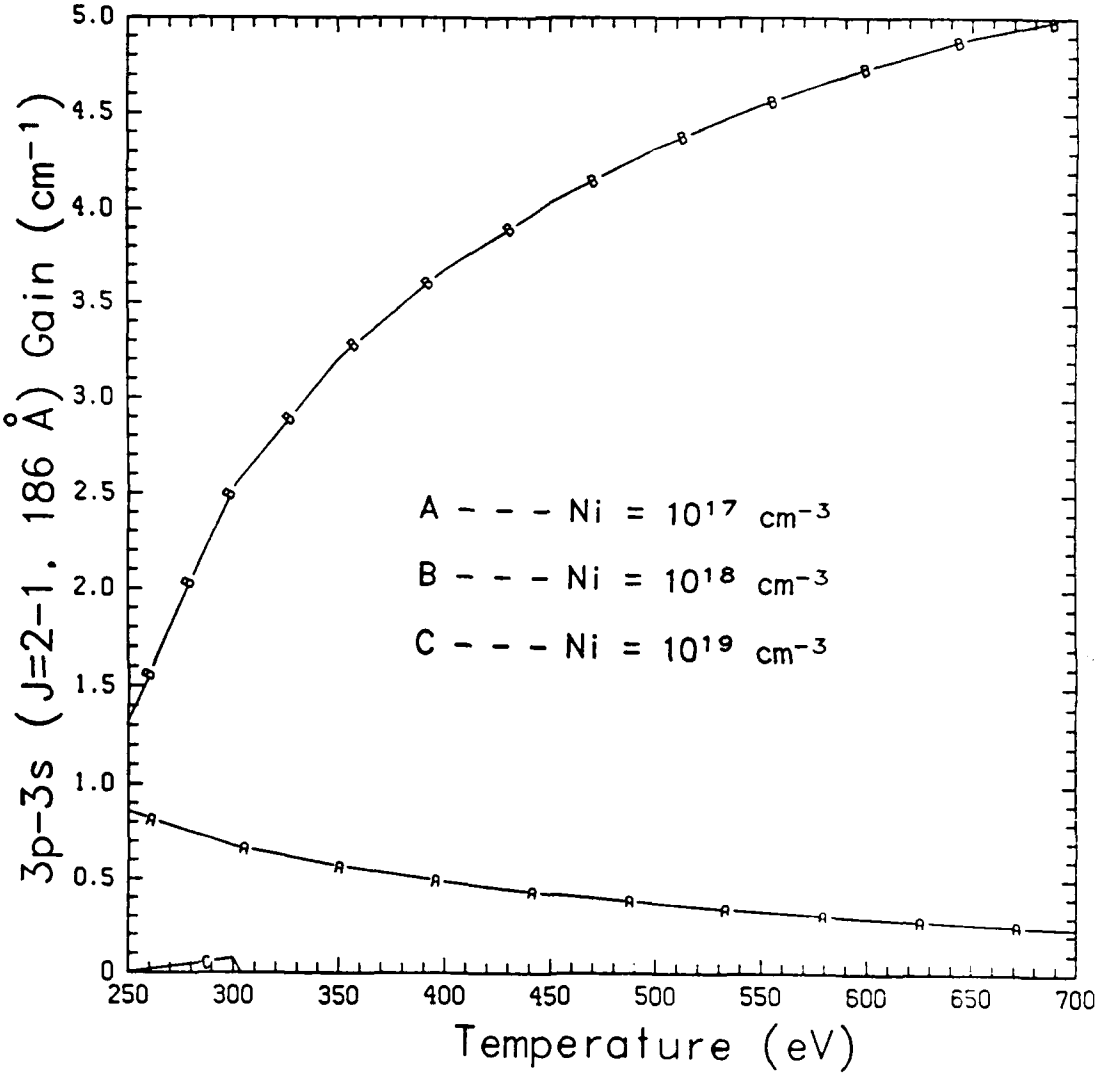

Fig. 8 3p-3s (J=2-1) 186 Å gain coefficients as a function of temperature and density of the lasant plasma. The pump plasma is present but there is no attenuation of the Ne-like ground state pump rates to the 3s, 3d and 4d levels. The radius of the lasant plasma is 0.1 cm.

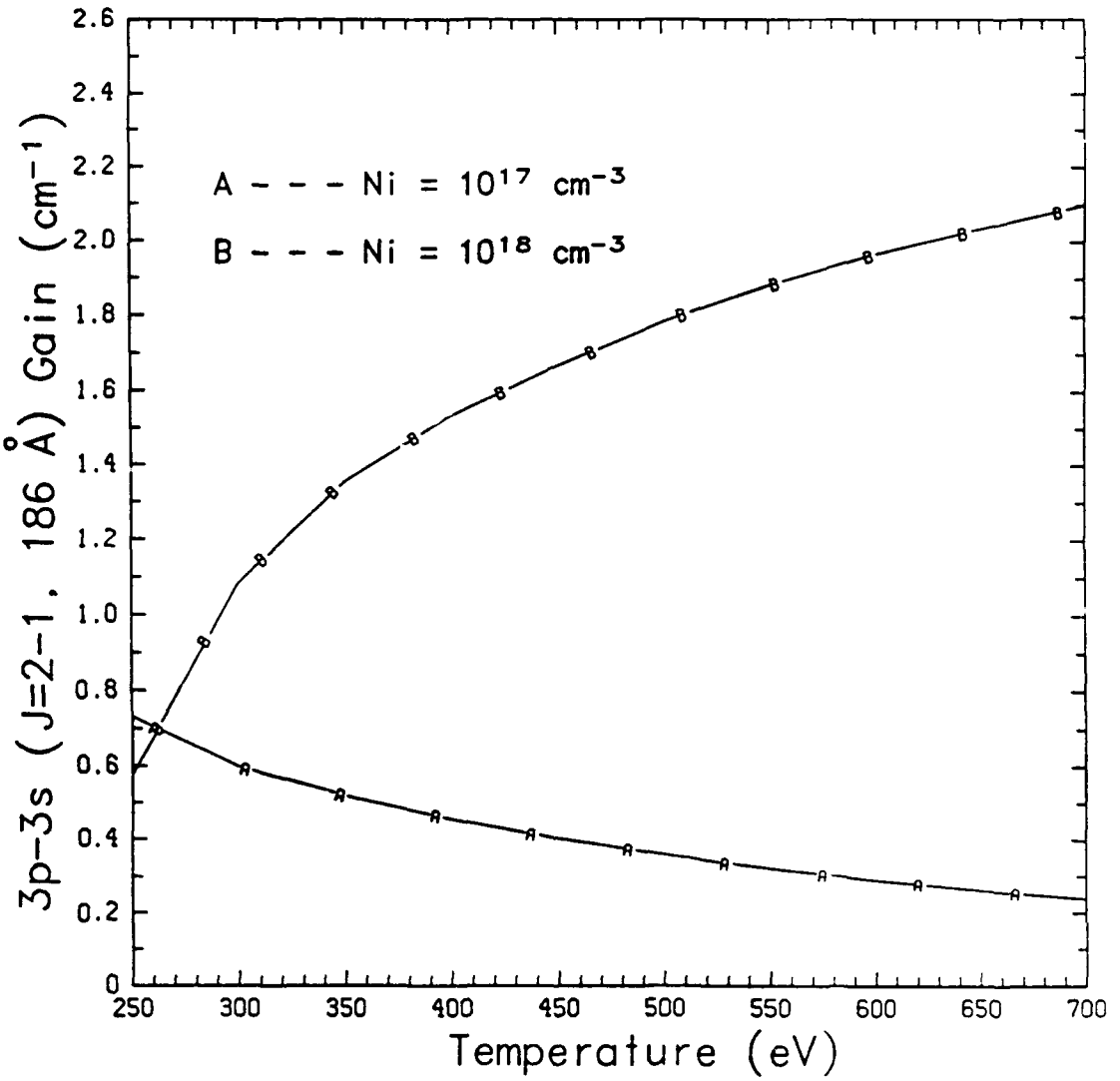

Fig. 9 3p-3s (J=2-1) 186 Å gain coefficients as a function of temperature and density for the outer zone of the lasant plasma. The pump plasma is present and there is attenuation of the Ne-like ground state pump rates to the 3s, 3d, and 4d levels. The radius of the lasant plasma is 0.1 cm.

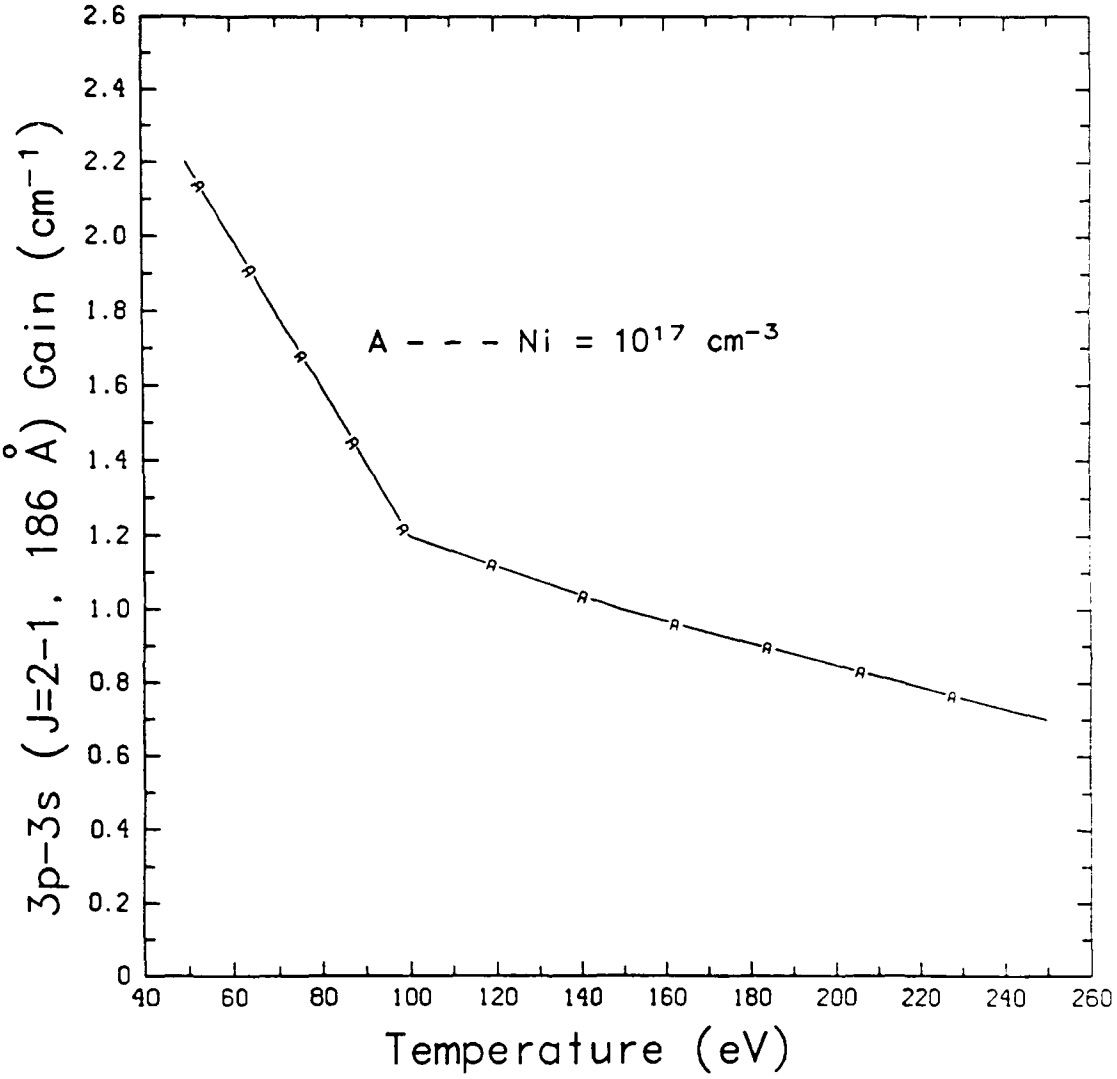

Fig. 10 3p-3s (J=2-1) 186 Å gain coefficients as a function of temperature for the outer zone of the low density lasant plasma. The pump plasma is present and there is attenuation of the Ne-like ground state pump rates to the 3s, 3d, and 4d levels. The radius of the lasant plasma is 0.1 cm.

Ultra Short Pulse Laser Produced Fluorine Plasma

J. Davis, R.W. Clark, and J. Giuliani

Radiation Hydrodynamics Branch

Plasma Physics Division

Naval Research Laboratory

Washington, D.C. 20375

Abstract

The interaction of an intense ultra bright laser pulse with a planar fluorine target is investigated. The interaction is numerically simulated using a 1-D time-dependent non-LTE radiation hydrodynamics model, including the effects of the ponderomotive force, self-consistently coupled to a wave equation describing the beam-plasma coupling. The target is shown to be highly reflective for the intensities considered but still allows sufficient energy to be coupled to produce substantial heating. A time history of the evolving plasma is presented and discussed as well as the role played by the ponderomotive force. The feasibility of creating conditions conducive to population inversions and gain in selected transitions in helium- and hydrogen-like fluorine is also investigated.

Introduction

The interaction of nanosecond pulsed lasers with a variety of targets has been under intensive investigation for over three decades. The major

emphasis of the research was focused on laser fusion experiments dedicated to creating a laser produced plasma with self sustained fusion reactions. Although interest remains high for the eventual success of the laser fusion program, a number of other activities are emerging as a result of recent technological advances in laser development. One of these activities is due to the application of chirped pulse amplification making it possible to produce ultra short pulse lasers with pulsewidths of 10's to 100's of femtoseconds and intensities in excess of 10^{18} watts/cm^2. This newly evolving technology is introducing a number of innovative, interesting and exciting activities involving the interaction of ultra short pulse lasers with matter, including x-ray laser research, laser produced hohlraum physics, harmonic generation, subnanosecond spectroscopy, and the interaction of intense laser fields with individual atoms and molecules, just to mention a few. The interaction of these intense lasers with a planar target makes it feasible to investigate solid state plasmas in the strongly coupled plasma regime and preliminary results suggest the possibility of tailoring the x-ray pulse emitted from the hot dense plasma before hydrodynamic blowoff begins to disassemble the target. Once expansion of the high density blowoff plasma occurs it can cause a rapid cooling of the leading edge of the plasma resulting predominantly in collisional recombination into the upper excited levels of the recombined ion creating the possibility of population inversions. In this paper we investigate the interaction of an ultra short laser pulse with a planar fluorine target with the focus of the research directed toward characterizing the radiative properties of the plasma as well as determining whether the plasma can support population inversions and lasing in selected transitions in highly

ionized excited states as a result of recombination resulting from rapid cooling.

Model

The numerical simulations are based on a 1-D time-dependent non-LTE radiation hydrodynamics model self-consistently coupled to a Helmholtz wave equation describing the interaction of the laser pulse which is assumed to be normally incident on the target. The atomic model contains all the ground states and selected excited states distributed throughout various stages of ionization. In particular, the hydrogenlike manifold contains excited states up to and including the n=10 level, the heliumlike ionization stage up to and including the n=5 singlet and triplet levels, and the lithiumlike stage contains doublet level structure up to and including n=5. The remaining ionization stages contain only ground states. The ionization dynamics is based on a time-dependent collisional radiative model self-consistently coupled to a probability of escape radiation transport scheme. Ionization lowering is included to account for the disappearance of excited levels in the very dense regions of the plasma. The spectral line profile functions are represented by Voigt functions. For an in-depth discussion of the non-LTE radiation hydrodynamics model the reader is referred to references 1 and 2. The absorption of a laser pulse normally incident on the target is calculated by solving the Helmholtz wave equation for a multi-layered medium. In this way we self-consistently characterize the incident, reflected and transmitted waves in each numerical zone in the medium. The conductivity was calculated using the

Drude model. The initial ionization was produced by multiphoton effects but was rapidly dominated by inverse bremsstrahlung heating.

Results

The reflective properties of the solid density planar fluorine target irradiated by a normally incident 248 nm KrF laser pulse with a peak intensity of $3X10^{17}$ watts/cm^2 and a pulse duration of 650 femtoseconds is shown in Fig.1 as a function of time. The incident laser intensity I is normalized to I_0 (in this case I_0=3x10^{17}watts/cm^2). Most of the incident laser energy is reflected from the surface; about 97% as shown by the curve labeled Reflect. The normalized time integrated energy absorbed is represented as the ($\int$(Incident-Reflected)dt/$\int$(Incident)dt) and reaches a peak value of about 3 % at 1/2 psec. In Fig.2 the energy deposited into the target at 0.755 psec (which is at the end of the laser pulse) is shown as a function of position (the original position of the target's surface was 0.5μ). Also shown is the ratio averaged over an optical cycle of the local electric field, <E>, to the amplitude of the incident field, E_0. The oscillatory nature of <E> simply mirrors the alteration of the wavenumber k due to target absorption - reflection. The behavior of the mass density, ρ, is also shown as is R_{critic}, which where the plasma frequency equals the laser frequency. Note the increase in density at about 0.3μ due to the shock wave launched into the material as a result of the deposition. The laser energy is not completely reflected at R_{critic} but penetrates a skin depth further into the target.

The competition between the gas and ponderomotive pressure is shown in Fig.3 near the peak of the laser pulse at 0.355 psec. The ponderomotive

force exhibits behavior directly related to the square of the electric field and exceeds the gas pressure in the leading edge of the blowoff plasma. The sudden increase in both the ponderomotive and fluid accelerations beyond 0.7μ is due to the low density in the region. At this intensity the ponderomotive force plays a substantial role in the plasma evolution. Figs. 4 and 5 show the dynamic evolution of the plasma at two times: after the peak of the laser pulse at 0.359 psec and the end of the laser pulse at 0.759 psec, respectively. Note the change in the horizontal axis in Figure 5 at late time. The break in the velocity curve represents material moving outward (righthand portion) and inward (lefthand portion), respectively . The peak temperature occurs around the peak of the laser pulse and is in excess of 2 keV. At later times the plasma is cooler, and shows a pronounced drop in temperature near 1.0μ. The dE/dt_{rad} curve represents the total radiated power density over all wavelengths, but is certainly dominated by short wavelengths where the plasma is hot.

Emission spectra are shown in figures 6 and 7 for two times: after the peak of the laser pulse at .359 psec and at the end of the pulse at .759 psec, respectively. The earlier spectrum (fig. 6) is hotter, and there is less K-shell recombination radiation. Near the peak of the laser pulse, about 20% of the radiated power comes from spectral lines (predominately from the resonance lines of hydrogen- and helium-like fluorine), about 40% comes from recombination (largely K-shell) and about 40% from bremsstrahlung. Most of this radiation emanates from the "transition" region, where the temperature is several hundreds of eV, and the plasma is near solid density. Because this region is of nearly infinitesimal thickness, radiation moving in the forward direction is nearly optically thin. The latter spectrum (fig. 7) is characteristic of a

cooler, denser plasma. However, it is still dominated by hydrogen- and helium-like radiation, and the fraction of the emission from spectral lines, recombination and bremsstrahlung is approximately the same. Finally, the time-integrated emission spectrum is shown in figure 8. Not surprisingly, it is very similar to the spectrum near the peak laser deposition (fig. 6).

Finally, for the conditions considered here population inversions were **not** observed in any of excited states of hydrogen-, helium-, or lithium-like fluorine. It may be possible to create population inversions leading to gain at higher laser intensities and/or different geometries with higher Z materials. Both possibilities will be investigated.

Acknowledgements

We would like to thank Dr. P. Kepple for making the atomic data base available. This work was supported by SDIO/T/IS and ONR.

References

1.D.Duston, R.Clark, J.Davis and J.Apruzese, Phys. Rev.27A, 1441, 1983.

2.D.Duston, R.Clark and J.Davis, Phys. Rev. 31A, 3220, 1985.

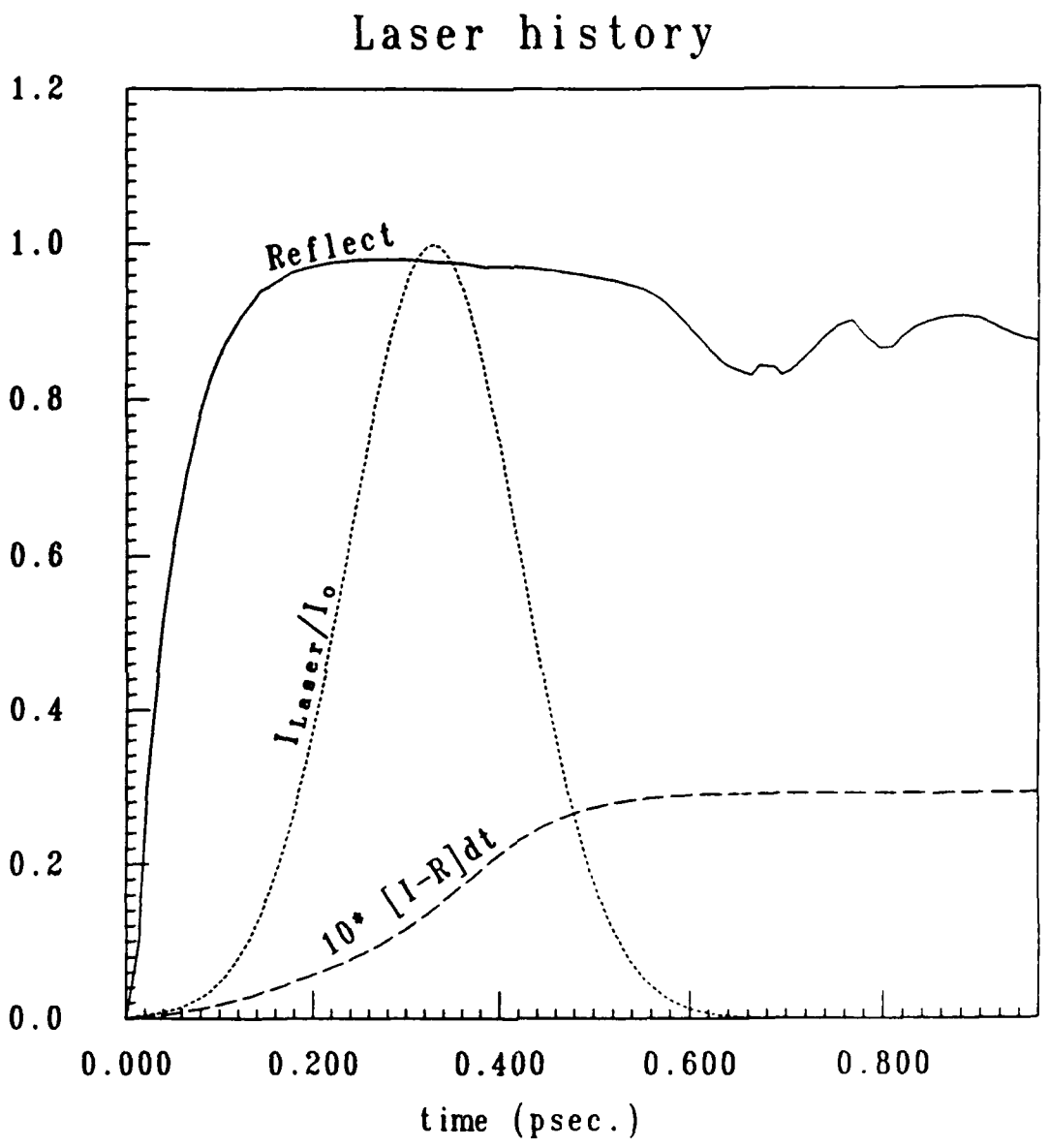

Fig. 1. Time history of the laser deposition.
Incident laser intensity I_{Laser} is normalized with respect to the peak intensity I_o. The reflection coefficient $Reflect$ is the reflected intensity I_{Ref} divided by the incident I_{Laser}. The normalized time integrated energy absorbed is given by $\int[I_{Laser} - I_{Ref}]dt / \int I_{Laser}dt$. It is plotted x10 for legibility.

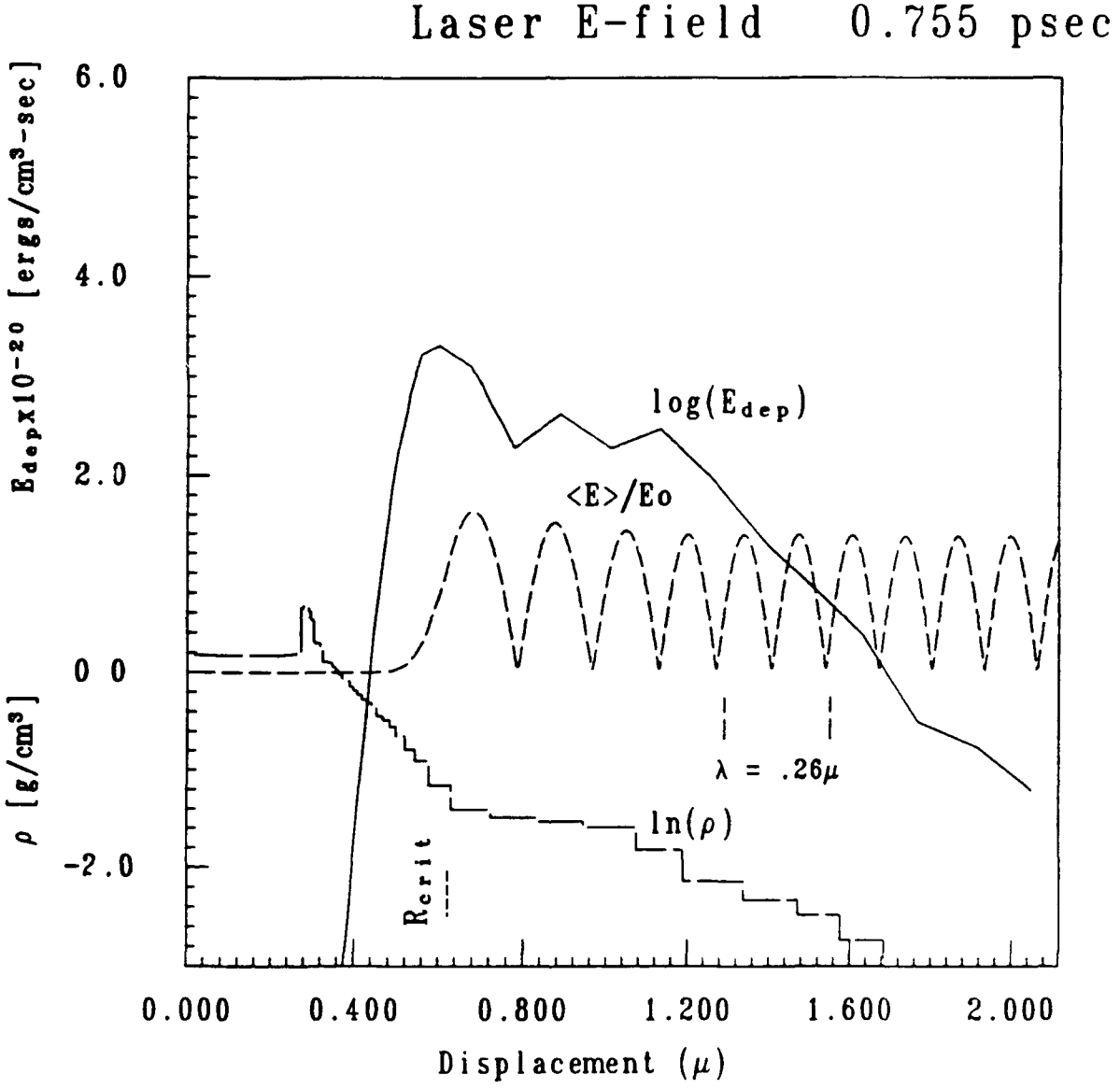

Fig. 2. Laser electric field at 0.755 picoseconds.
The local electric field, averaged over an optical cycle, $< E >$ is shown normalized to the amplitude of the incident field E_o. The mass density ρ is shown in a stepwise manner to indicate the spatial resolution of the simulation in the deposition region. The logarithm of the rate of energy deposition into the target E_{dep} is plotted, and the location of the critical surface R_{crit} is shown.

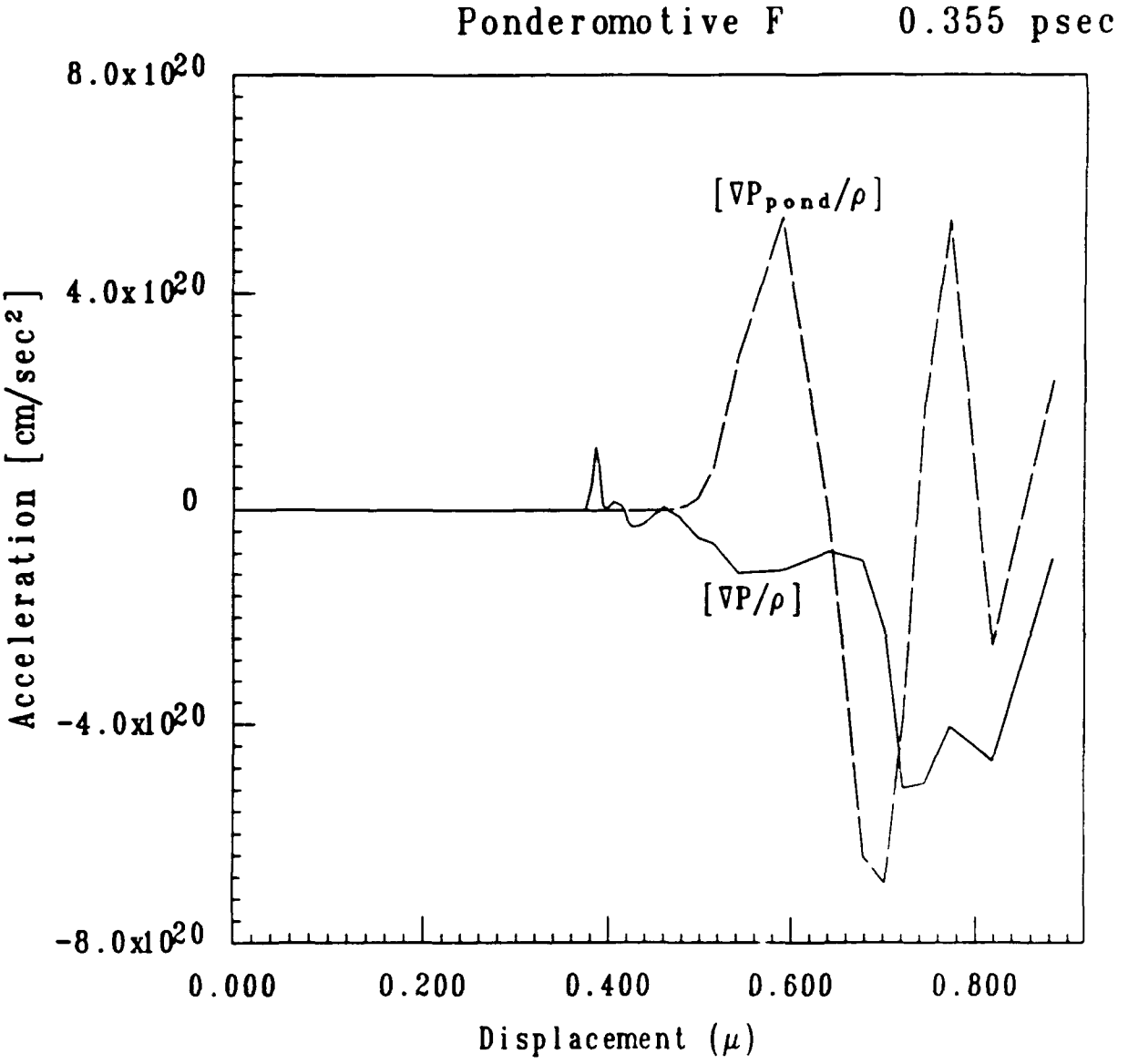

Fig. 3. Ponderomotive acceleration at 0.355 picoseconds. The magnitude of the local ponderomotive force $\omega_p^2/\omega^2 \nabla E^2/16\pi$ is compared with the magnitude of the fluid (pressure gradient) forces just after the peak of the laser pulse. The corresponding fluid accelerations are plotted.

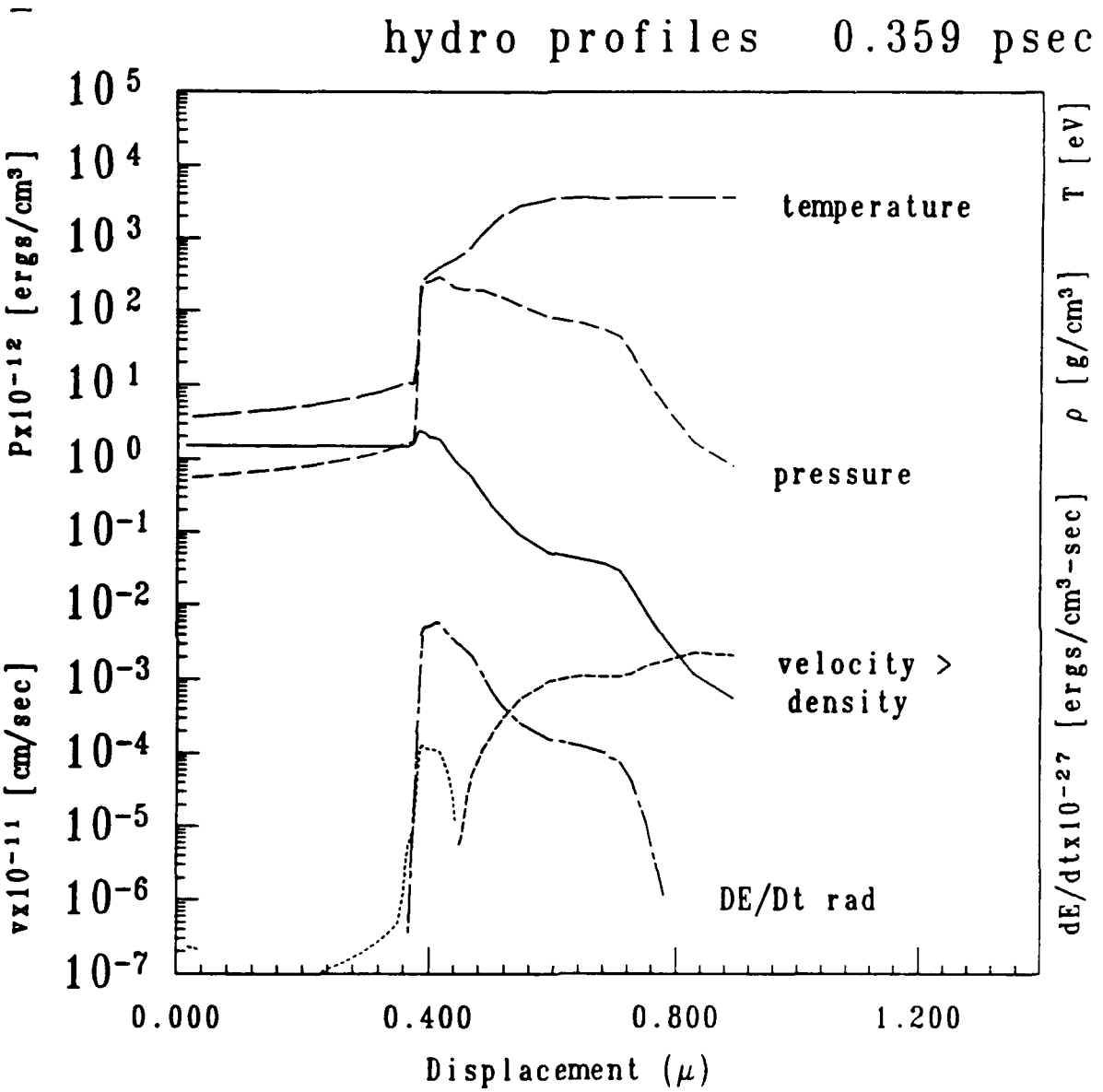

Fig. 4. Hydrodynamic profiles at 0.359 picoseconds.
Spatial profiles of mass density, temperature, pressure, velocity and radiative power are plotted near the peak of the laser pulse. These quantities are shown on a logarithmic scale, normalized as indicated above.

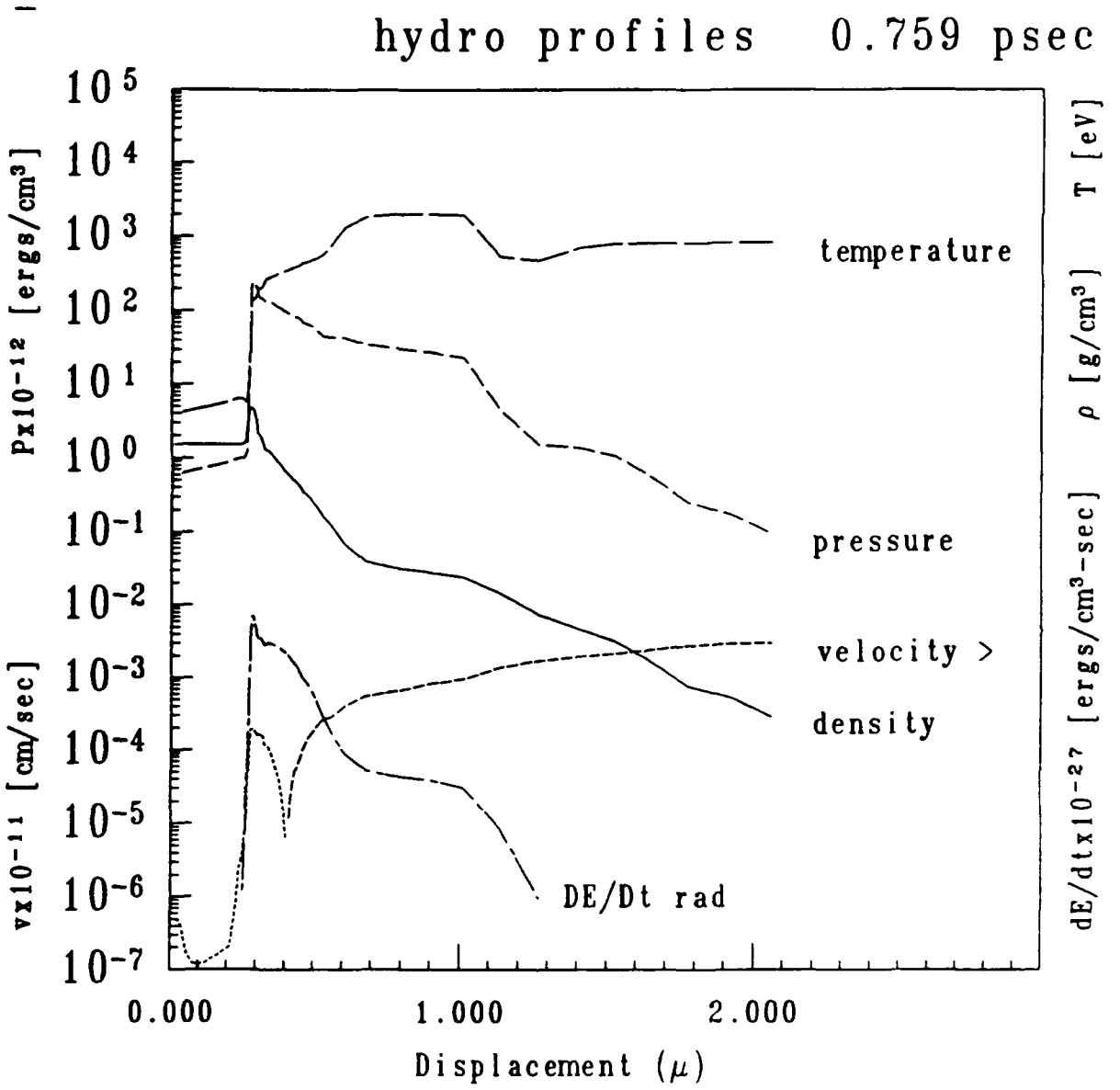

Fig. 5. Hydrodynamic profiles at 0.759 picoseconds.
Spatial profiles of mass density, temperature, pressure, velocity and radiative power are plotted near the end of the laser pulse.

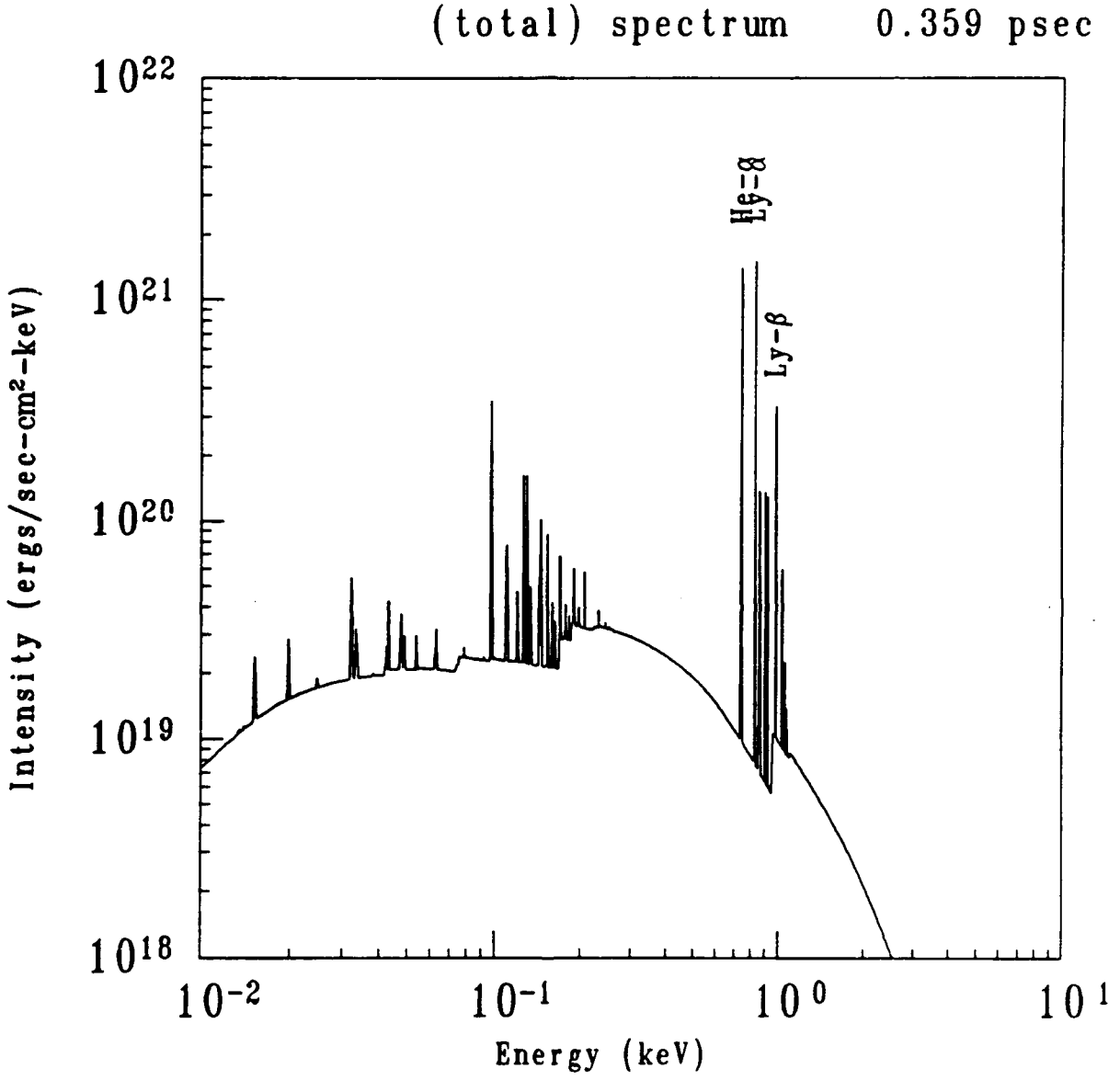

Fig. 6. Emission spectrum at 0.359 picoseconds.
Instantaneous emission spectrum after the peak of the laser pulse. Hydrogen-like Ly-α and Ly-β and helium-like He-α transitions are indicated.

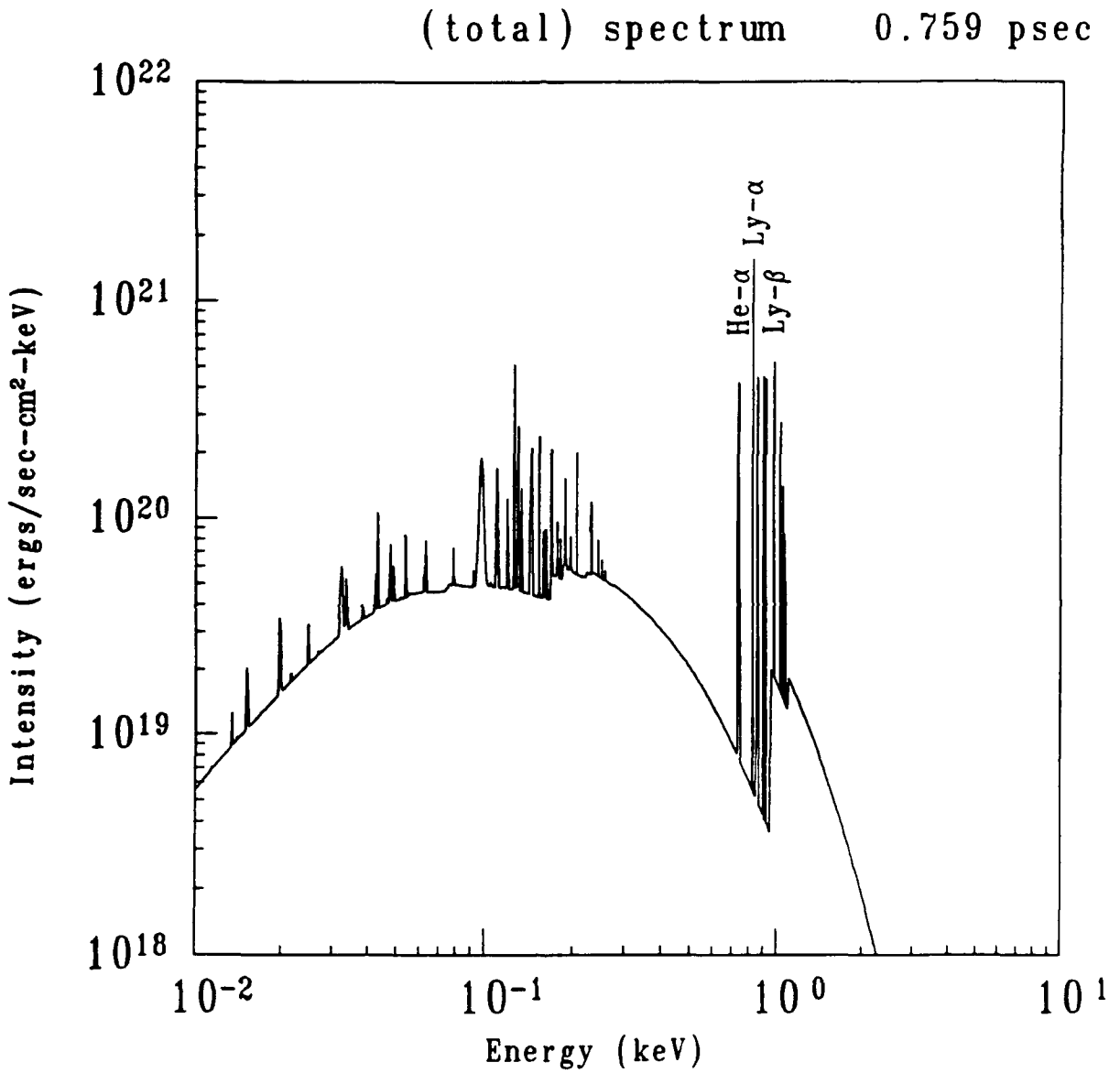

Fig. 7. Emission spectrum at 0.759 picoseconds.
Instantaneous emission spectrum near the end of the laser pulse. This spectrum is characteristic of a cooler, denser plasma than the previous case.

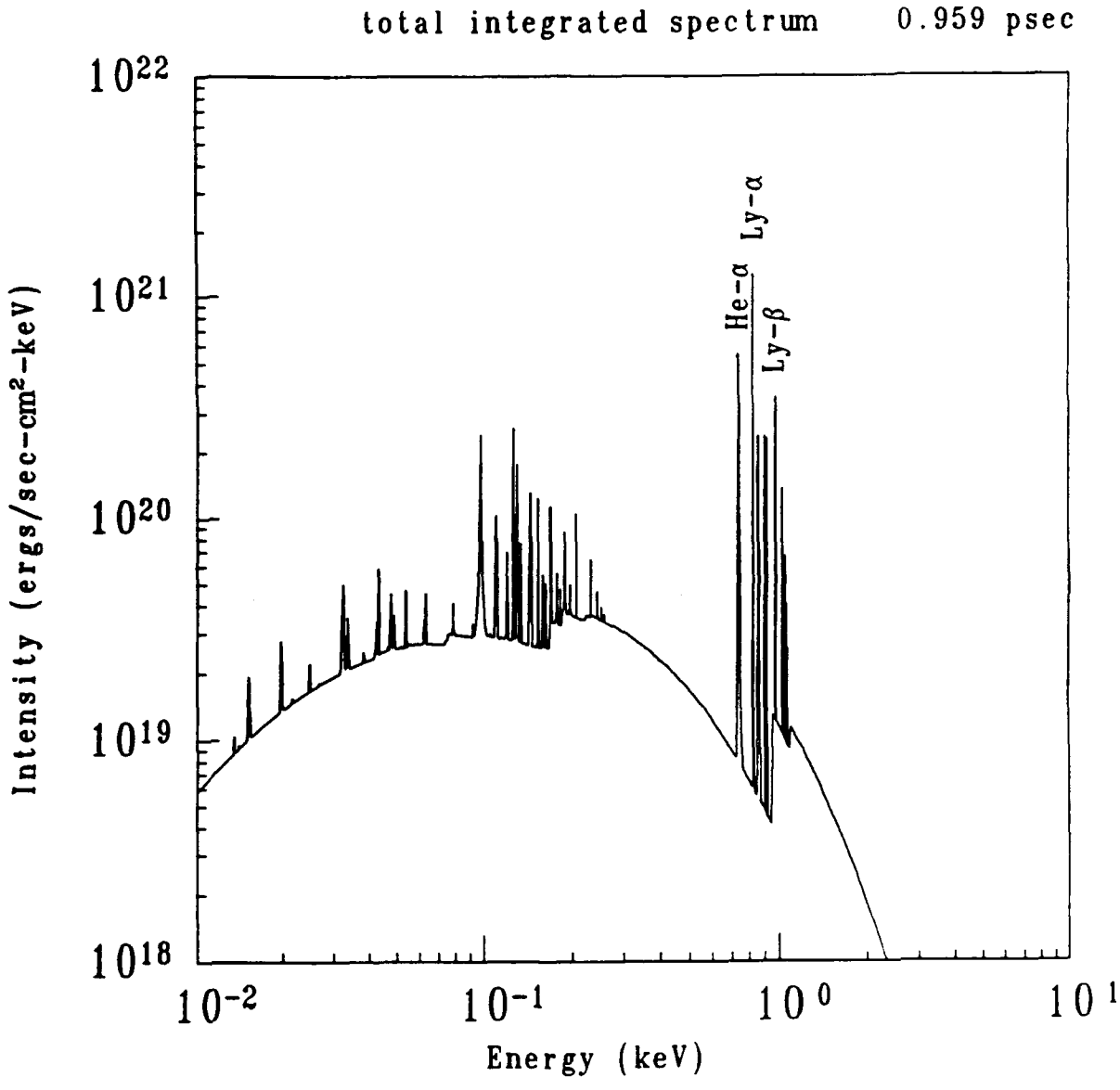

Fig. 8. Time-integrated emission spectrum.
Emission spectrum integrated through 0.959 psec. Note the similarity to the spectrum near the peak of the laser pulse.

Model for Time Dependent Radiative Transfer in Short - Pulse Laser Heated Plasmas

J. P. Apruzese
Radiation Hydrodynamics Branch

Abstract

Multiple scattering of line photons can significantly broaden the x-ray pulse emitted from ultrashort pulse laser-heated plasmas. Time-dependent radiation transport is a potentially important effect in determining both pulsewidth and intensity. A numerical, fully time dependent radiation transport model has been developed and benchmarked using the two level atom formalism. It is shown that two Gaussian quadrature rays provide sufficient accuracy, greatly enhancing its computational efficiency.

INTRODUCTION

The advent and rapid development of powerful subpicosecond lasers has stimulated a new and very recent generation of experiments producing extremely short lived plasmas[1-11] (for a review see, e.g., Ref.1). Numerous uses of such experiments are envisioned, including creation of ultrashort x-ray pulses,[1,3,4,11-15] pumping of x-ray lasers by field ionization,[16] x-ray inner shell photoionization,[17,18] rapid recombination or resonant photoionization. Subpicosecond x-ray pulses would enable unique time - resolved x-ray imaging and scattering studies of plasmas, solids, and biological subjects. Additionally, production of coherent XUV radiation by backcattered harmonics from powerful short-pulse lasers has been proposed.[19] Such ultraintense laser radiation will also facilitate basic investigations and discovery of fundamental atomic processes in the presence of field strengths equaling or exceeding those due to the Coulomb field of the nucleus.[20,21]

As expected in such a burgeoning field in its relative infancy, contradictions, questions, and apparent tradeoffs have emerged in the initial series of experiments carried out at several laboratories. For instance, it is still far from settled whether the main source of x-rays in such highly nonequilibrium plasmas will be lines or continuum, and the atomic number of the irradiated plasma can be expected to play a major role in determining the principal radiative processes. One interesting phenomenon which has been both identified and quantified is the effect of a laser prepulse on the characteristics of the emitted x-rays. Cobble et al.,[6] and, more recently, Teubner and co-workers[9] report that the presence of a laser prepulse has a strongly positive effect on the plasma x-ray yield and hence conversion efficiency. This occurs whether the prepulse is of nsec,[6] or sub-psec[9] duration. Of course, inherent in the prepulse is that the preformed plasma has time to expand. As pointed out in Refs. 13-15, hydrodynamic expansion and thermal conduction are two of the most potentially important cooling mechanisms in such plasmas. The greater the plasma scale length, the more these mechanisms tend to broaden the x-ray pulse. A tradeoff between yield and pulsewidth thus appears to be indicated by recent data. Another process

which can effect both the intensity and the width of the x-ray pulse is radiative transfer. As pointed out in Ref. 15, as line radiation becomes more important, the potential for significant opacity effects increases. This is not expected to be important for submission-sized plasmas dominated by continuum radiation.[13] However, at solid density, strong resonance lines can be very optically thick even for such small path lengths. At scale lengths of microns or longer, which have been experimentally demonstrated to produce the best laser-to x-ray conversion efficiency, opacity is even more likely to play a significant role.

In the present work, the effects of opacity on the principal resonance line of He-like Al (a commonly employed target)[4,6,9] are examined in detail using a fully time-dependent radiative transfer model accounting for the effects of photon transit time on the pulsewidth. A two-level-atom formalism is initially adopted to benchmark the results. The properties of the single line have been chosen to mimic the characteristics of the He-like Al $1s^2$-$1s2p\,^1P_1$, line at 7.757 Å. As mentioned above, Al (Z=13) has been a frequently used target in ultrashort pulse laser heating experiments. The elements of adjacent atomic number, Mg (Z=12) and Si (Z=14) have also been popular choices.[3,7,8]. Therefore, the choice to model in detail the strongest Al K shell line is clearly of experimental relevance.

RADIATION TRANSPORT MODEL

The plasma conditions considered in the present work are such that only spectral lines are likely to be optically thick. The transport of radiation is accounted for by the fully time dependent equation of transfer at frequency ν, along a ray whose coordinate is denoted by x.

$$\frac{\partial I_\nu}{\partial x} = j_\nu - k_\nu I_\nu - \frac{1}{c}\frac{\partial I_\nu}{\partial t} \qquad (1)$$

In Eq. (1) I_ν is the specific intensity, j_ν and k_ν are the emission and absorption coefficients, respectively, and c is the velocity of light. For a derivation of this equation see, e.g., Ref. 22. By convention in Eq.(1) the radiation is traveling in the direction of increasing x. Consider the space,

time point (x_o, t_o). Looking backwards along the ray x, the quantities determining $I_\nu(x_o, t_o)$ are j_ν and k_ν encountered at retarded times $t_r(x_o, t_o, x) = t_o - (x_o - x)/c$. The optical depth between x_o and x at time t_o is

$$\tau(x_o, t_o, x) = \int_x^{x_o} k_\nu (t_r)\, dx \tag{2}$$

and the solution to Eq. (1) is

$$I_\nu (x_o, t_o) = \int_{x_b}^{x_o} j_\nu \left[x, t_r(x)\right] \cdot \exp \left[- \tau(x_o, t_o, x)\right] \cdot dx. \tag{3}$$

In Eq. (3), x_b is the coordinate of the plasma boundary. In all cases considered in the present work, no external radiation is assumed incident on the plasma.

Given the emission and absorption coefficients (from previous time steps) Eq. (3) is solved on a frequency grid of 31 points per transported line and a spatial grid of 26-31 points. In the numerical solution, j_ν and k_ν are linearly interpolated between grid points in space and time. The maximum time step employed is 10 fsec. To compute photoexcitation and escape rates, angle-averaged intensity J_ν and net flux F_ν are required, necessitating, in general, the use of more than one ray. In the present work, confined to plane-parallel geometry, Gaussian quadrature is employed as described by Chandresekhar in Ref. 23. Both two rays (n=2, m=4) and four rays (n=4, m=8) have been used comparatively to obtain I_ν and F_ν as described in the (n, m) notation in Ref. 23. The escape rate is just the frequency integral of F_ν. The photoexcitation rate for a spectral line of absorption oscillator strength f from lower level l to upper level u is given by

$$W_{lu}(\mathrm{sec}^{-1}) = \frac{\pi e^2}{mc} f \int \frac{4\pi J\nu}{h\nu} \phi_\nu d\nu. \tag{4}$$

In Eq.(4) the integral is taken over the line profile ϕ_ν where the normalization is given by

$$\int \phi_\nu \, d\nu = 1 \quad . \tag{5}$$

Comparisons of solutions given by the 2-ray and 4-ray Gaussian quadrature approximations appear in the next section.

TWO-LEVEL ATOM SOLUTIONS

To aid in analysis of the phenomena revealed by fully time-dependent coupled transfer and kinetics calculations, and also as a means of benchmarking the model, it is most appropriate to consider first the case of the two-level-atom. This has been intensively studied for the time-independent approximation in the astrophysical literature (see, e.g., Ref. 24 and references therein). For reasons described in the Introduction the properties of the two-level-atom considered in the present work have been chosen to correspond to those of the principal resonance line of He-like Al, $1s^2$-$1s2p\,^1P_1$, whose wavelength is 7.757 Å and spontaneous decay rate is 2.78×10^{13} sec.$^{-1}$. Two other crucial properties of the line are a, the broadening parameter for its assumed Voigt profile and ε, the probability that the line is collisionally quenched by electron de-excitation during reabsorption. At an electron density of 10^{21} cm $^{-3}$ and temperature 200 eV, these parameters are obtained as a=0.05 and ε=0.029 from multilevel atomic data for Al described in Ref. 25. For a 100 μm thick plasma slab, the optical depth at line center for this line is 94, measured normally across the full width. These assumptions and conditions form the basic framework for the initial benchmark calculations to be described.

Following the initial collisional excitation of the upper level of an optically thick line, the emitted photon can be absorbed, usually about one optical depth away, and then re-emitted in the line with a probability (1-ε) per absorption. The probability that the line photon escapes the plasma (P_e) rather then undergoing absorption can be calculated by averaging over the line profile and has been given in useful analytic forms for Doppler,[26,27] Voigt,[28] and Stark[29,30] line profiles. The probability that the line photon remains in the plasma following emission is thus $(1-P_e)(1-\varepsilon)$. The photon is eventually

eliminated either through collisional quenching or escape. The process of absorption and re-emission of line photons is generally referred to as "scattering". Evidently, some line photons will escape after a few scatterings whereas other may require many scatterings or end up being collisionally quenched. This process has the potential to significantly broaden the x-ray pulse emitted from short-pulse laser-heated plasmas.

To examine this mechanism in detail as well as validate the numerical model the following initial excitation conditions (t=0) are assumed. The 100 μm thick plasma modeling only the Al XII principal resonance line is initially entirely in the ground state except for the innermost 12% which contains a 1% population of upper level excited states, as illustrated in Fig. 1. Very approximately, this corresponds to the laser heating of a preformed plasma near the critical surface. More importantly, it provides a well-defined escape probability as the photons have a common spatial origin. This permits analytical comparison with the numerical results and facilitates analysis of the physics. Of course, even when one employs the simplifying two-level-atom approximation there is more to the calculation than evaluations of the photoexcitation rates as per Eqs. (1-5). The full equation for the upper level population is

$$\frac{dN_u}{dt} = N_e (W_{lu} + C_{lu}) - N_u (A_{ul} + C_{ul}). \qquad (6)$$

In Eq. (6) W is the photoexcitation rate as given in Eq. (4), A is the spontaneous decay rate ($2.78 \times 10^{13} sec^{1}$) and the C's refer to electron collisional excitation and de-excitation of the upper level. The de-excitation rate is easily computed from the condition

$$\varepsilon = 0.029 \quad = \frac{C_{ul}}{C_{ul} + A_{ul}} \qquad (7)$$

The excitation rate C_{lu} is set to zero to simulate the effect of femtosecond-time-scale plasma cooling given the intial conditions described above, and the radiative transfer algorithm for calculating the W's, Eq. (6), is integrated employing the method of Young and Boris.[31]

The upper level fraction as a function of space and time is illustrated in Figs. 1 and 2 for 5 time points varying from 0 to 7 psec. These numerical

solutions to Eqs (1) - (6) are presented for both 4-ray and 2-ray Gaussian quadrature. Note first the excellent agreement between the n=2 and n=4 cases, strongly suggesting that 2 rays are adequate. Diffusion of the upper level population through the plasma through line photon absorption and re-emission is clearly evident. Of considerable interest is the rate of decay of the upper level population in the central zone. If the plasma were optically thin this population would decrease with an e-fold time of $(2.78\text{x}10^{13})^{-1}$ = 36 fsec. The actual e-fold time is much less in the optically thick medium because of re-excitation of the level by line photons, as is evident in Figs. 1 and 2. In fact, for the first 0.5 psec, the lifetime of the upper level fraction is 0.7 psec, and this lifetime increases to 1.1 psec for the final 3 psec covered by Figs. 1 and 2. A frequently used analytic approximation for line transfer is to multiply the spontaneous decay rate by the escape probability, implicitly assuming that "true" de-excitation occurs only a fraction P_e of the time. According to the calculations of Ref. 28, the escape probability for this line from the midpoint of the plasma is $8.9\text{x}10^{-3}$. Of course, collisional de-excitation also depletes the upper level. Employing the escape probability dilation method, the total decay rate is $\sim A_{ul}\ (P_e + \varepsilon) = 1.05\text{x}10^{12}\ \text{sec}^{-1}$, implying a lifetime of 0.95 psec, very close to the average e-fold time observed in Figs. 1 and 2. Time dependent delays in re-excitation result in an initially more rapid population falloff, but this transient phenomenon damps out over 7 ps, resulting in good correspondence between the analytically estimated and numerically computed upper level decay times.

The time dependent escape of the line photons is more directly relevant to the experimental achievement of optimally short plasma x-ray pulses. For the two level atom, this quantity may also be analytically estimated and compared with the present numerical calculations. Ignoring the light travel time between scatterings, each absorption and re-emission requires a time equal to the lifetime L of the upper level (36 fsec in this case). The probability that a photon escapes after an excitation is $(1-\varepsilon)\ P_e$; the probability of escape by the N^{th} scattering, P_N, is the sum of the probabilities of escape after initial excitation and each of the subsequent scatterings, viz.

$$P_n = (1-\varepsilon)P_e\left[1+\sum_{n=1}^{N,}(1-\varepsilon)^n(1-P_e)^n\right] = (1-\varepsilon)P_e\left(\frac{1-S}{1-S}^{N+1}\right) \qquad (8)$$

where in Eq.(8) $S=(1-\varepsilon)(1-P_e)$, the probability that the photon remains in the plasma after an excitation. The time required for N scatterings, i.e., associated with fractional escape P_N, is simply the level lifetime, 36 fsec, multiplied by N. In the case under consideration, $\varepsilon=0.029$, $P_e=8.9 \times 10,^{-3}$ and the analytic results obtained from Eq. (8) are plotted along with the numerical solutions in Fig. 3. As indicated in that figure, one of the plotted numerical solutions ignored the time dependent term in Eq. (1), equivalent to assuming infinite light velocity. As expected, it is this numerical curve which most closely approximates the analytic solution (which also ignores the light travel time between scatterings). Note that the numerical solutions including full time dependence were obtained for 2 and 4 Gaussian rays, and the 2-ray solutions are again in excellent agreement with those of 4-rays which are of course twice as computationally expensive. It is clear that the economical 2-ray quadrature is adequate.

The asymptotic or ultimate escape probability for a line photon is obtained by taking the limit of Eq. (8) as $N \rightarrow \infty$. For the presently considered conditions a value of 0.23 is obtained, as also seen in the analytic curve of Fig. 3. Most photons (77%) do not escape, since the quenching probability exceeds that of escape by a factor of ~ 3. The numerical solutions exhibit two important departures from the analytic result. First the photons do not emerge immediately since 170 fsec is required to traverse the 50 μm to the outer edge of the plasma. Second, about 28% of the initially created line photons escape rather than the 23% estimated analytically. This is not particularly surprising since the photons diffuse toward the boundary spatially (as seen in Figs. 1-2) and therefore do not strictly obey an escape probability calculated from the midplane. It is also seen from Fig.3 that the pulsewidth obtained from the full numerical solutions which include the time-dependent term exceeds that yielded by dropping the $1/c\,(\partial I/\partial t)$ term. For the time-dependent case, 3.1 psec is required for 90% of the photons to escape whereas 2.4 psec is needed when this effect is ignored. Clearly, the light travel time can affect the x-ray emissions when very short pulsewidths are considered and multiple photon scattering is significant in the overall x-ray energy budget. This effect can be examined in more detail by coupling the time-dependent radiative transfer to a multilevel ion kinetics model.

REFERENCES

1. M.M. Murnane, H.C. Kapteyn, M.D. Rosen, and R.W. Falcone, Science 251, 531 (1991).

2. C.H. Nam, W. Tighe, S. Suckewer, J.F. Seely, U. Feldman, and L.A. Woltz, Phys. Rev. Lett. 59, 2427 (1987).

3. M.M. Murnane, H.C. Kapteyn, and R.W. Falcone, Phys. Rev. Lett. 62, 155 (1989).

4. J.A. Cobble et al., Phys. Rev. A 39, 454 (1989).

5. J.C. Kieffer et al., Phys. Rev. Lett. 62, 760 (1989).

6. J.A. Cobble, G.T. Schappert, L.A. Jones, A.J. Taylor, G.A. Kyrala, and R.D. Fulton, J. Appl. Phys. 69, 3369 (1991).

7. A. Zigler et al., Appl. Phys. Lett. 59, 534 (1991).

8. A. Zigler et al., Opt. Lett. 16, 1261 (1991).

9. U. Teubner, G. Kuhnle, and F.P. Schafer, Appl. Phys. Lett. 59, 2672 (1991).

10. W.M. Wood, C.W. Siders, and M.C. Downer, Phys. Rev. Lett. 67, 3523 (1991).

11. M.M. Murnane, H.C. Kapteyn, and R.W. Falcone, Phys. Fluids B 3, 2409 (1991).

12. S.E. Harris and J.D. Kmetec, Phys. Rev. Lett. 61, 62 (1988).

13. M.D. Rosen, "Scaling Laws for Femtosecond Laser Plasma Interactions", in SPIE Conf. Proc. 1229, E.M. Campbell, ed., p. 160 (1990).

14. V.V. Kolchin and S.A. Shlenov, Sov. J. Quantum Electron. 21, 247 (1991).

15. H.M. Milchberg, I. Lyubomirsky, and C.G. Durfee, III, Phys. Rev. Lett. 67, 2654 (1991).

16. P. Amendt, D.C. Eder, and S.C. Wilks, Phys. Rev. Lett. 66, 2589 (1991).

17. T.S. Axelrod, Phys. Rev. A 15, 1132 (1977).

18. G.L. Olson, J.K. La Gattuta, and J.C. Comly, in Proceedings of the Second International Colloquium on X-Ray Lasers, York, England, G.J. Tallents, ed. (Institute of Physics, Bristol, 1991), pp. 329-332.

19. P. Sprangle and E. Esarey, Phys. Rev. Lett. 67, 2021 (1991).

20. G.T. Schappert et al., AIP Conf. Proc. 206, p. 217 (1990).

21. R. Grobe and C.K. Law, Phys. Rev. A 44, R4114 (1991).

22. J. Cooper and P. Zoller, Astrophys. J. 277, 813 (1984).

23. S. Chandasekhar, Radiative Transfer, (Dover, New York, 1960), pp. 61-62.

24. P.B. Kunasz and D.G. Hummer, Mon. Not. R. Astron. Soc. 166, 19 (1974).

25. D. Duston and J. Davis, Phys. Rev. A 23, 2602 (1981).

26. T. Holstein, Phys. Rev. 72, 1212 (1947).

27. J.P. Apruzese, J. Davis, D. Duston, and K.G. Whitney, J. Quant. Spectros. Radiat. Transfer 23, 479 (1980).

28. J.P. Apruzese, J. Quant. Spectros. Radiat. Transfer 34, 447 (1985).

29. J.C. Weisheit, J. Quant. Spectros. Radiat. Transfer 22, 585 (1979).

30. R.C. Mancini, R.F. Joyce, and C.F. Hooper, Jr., J. Phys. B 20, 2975 (1987).

31. T.R. Young and J.P. Boris, J. Phys. Chem. 81, 2424 (1977).

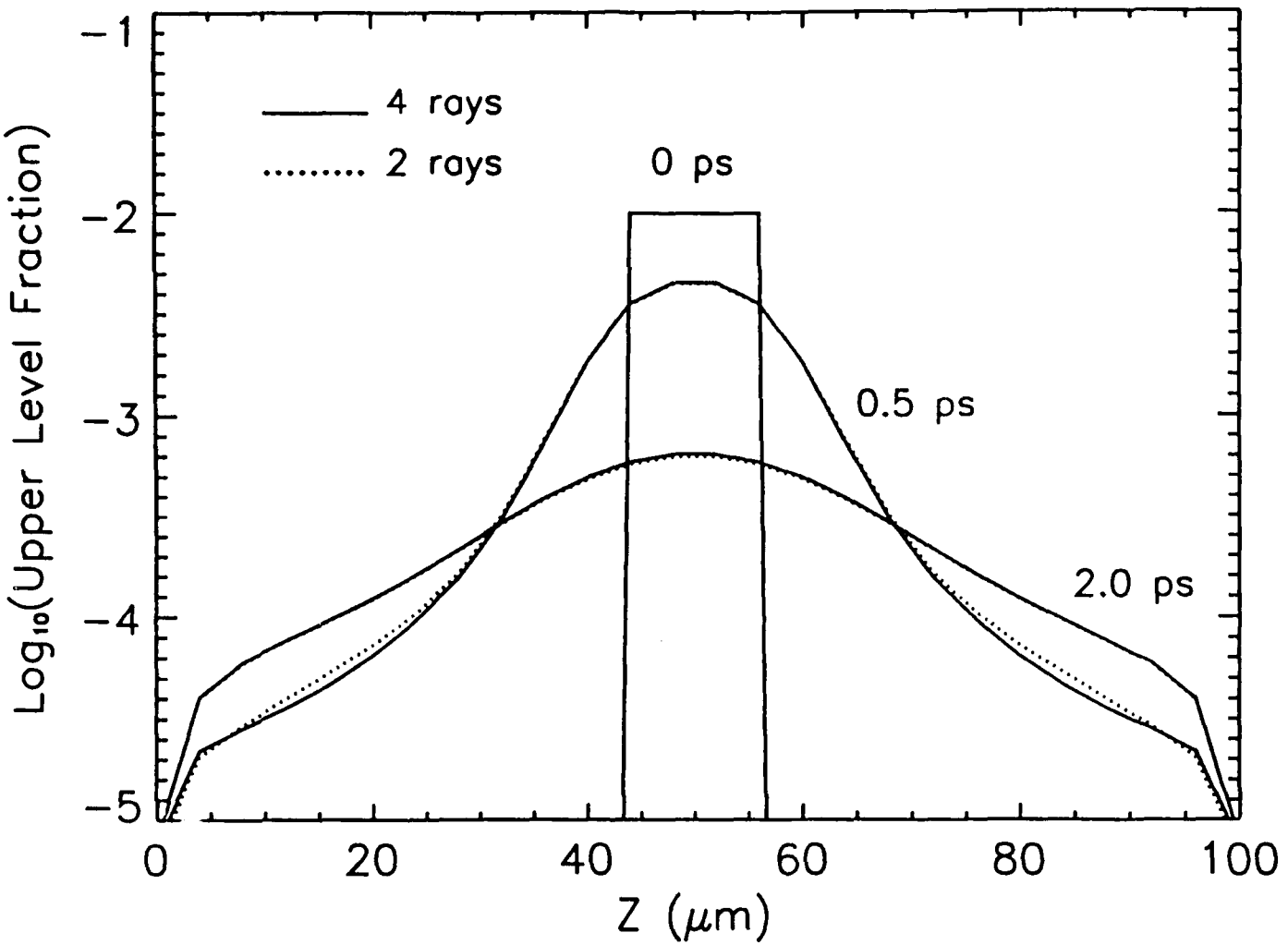

FIG. 1 Calculated upper level fraction of the Al XII $1s^2$-$1s2p\,^1P$ line is presented as a function of space and time in the two-level-atom approximation, at 0, 0.5, and 2.0 psec. Total optical depth across the plane is 94, and the probability of collisional quenching per scattering is 0.029, corresponding to an electron density of 10^{21} cm^{-3}. Solid and dotted lines indicate results using 4-ray and 2-ray Gaussian quadrature, respectively.

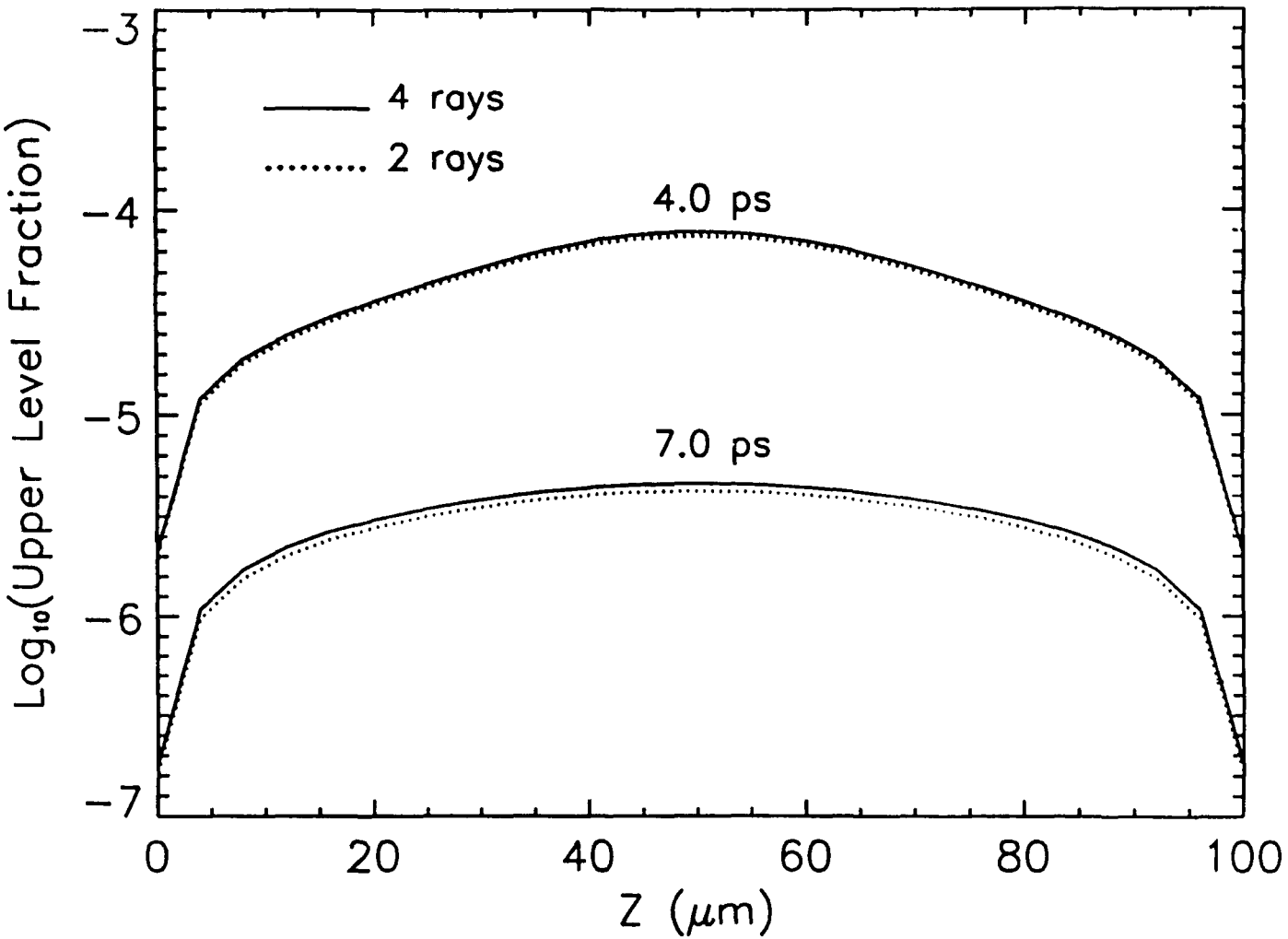

FIG. 2 As in Fig. 1, except that times of 4.0 and 7.0 psec after initial excitation are illustrated.

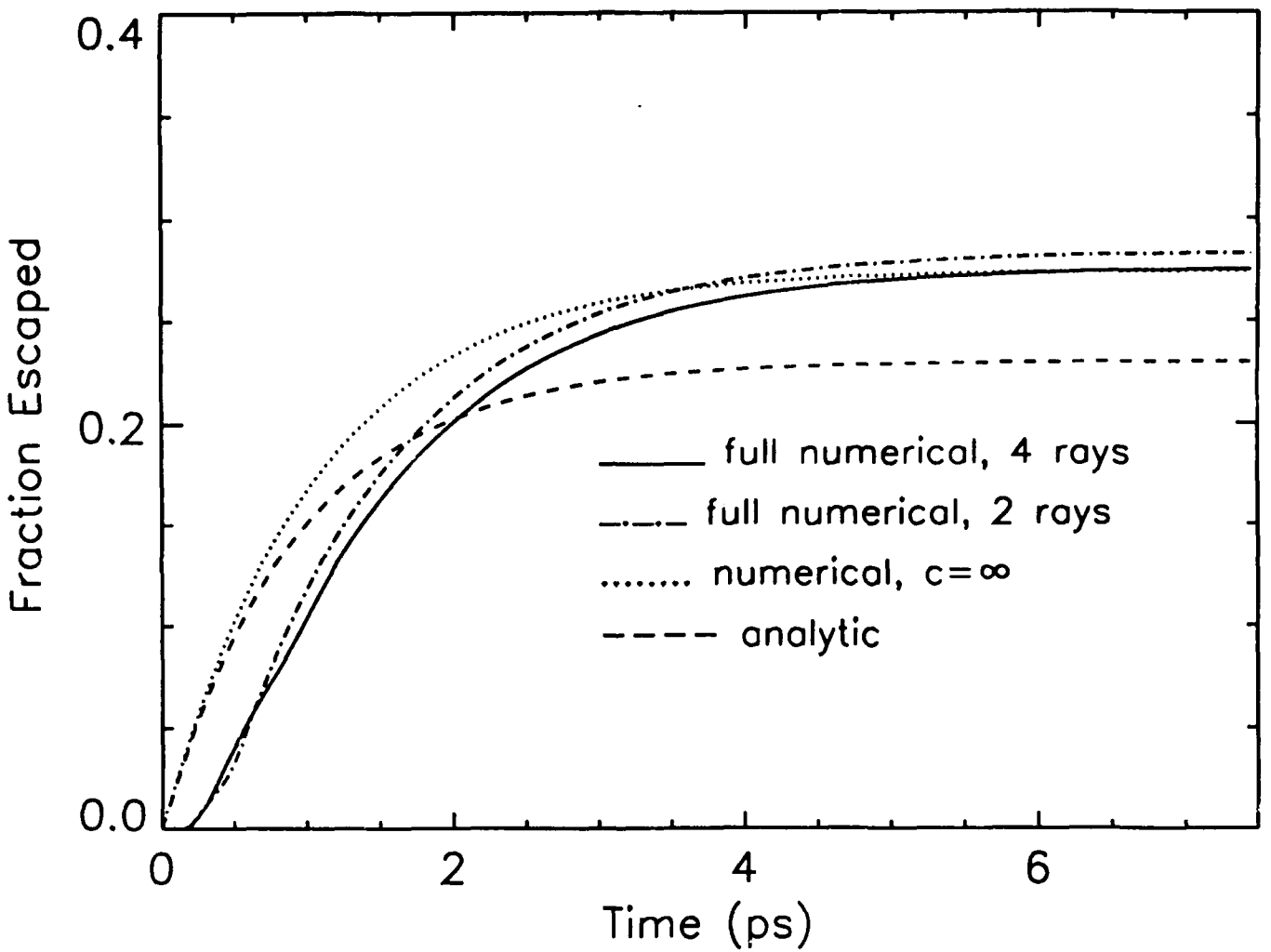

FIG. 3 Escaped fraction of the Al XII principal resonance line is illustrated for the conditions of Fig. 1 as a function of time. Numerical calculations using 4 Gaussian rays assuming both the correct and infinite light velocity are shown, as well as 2 ray and analytic approximations discussed in the text.

ANALYSIS OF PUMPING MECHANISMS AFFECTING THE GAIN OF THE J=0-1 AND J=2-1 LINES IN NEON-LIKE SELENIUM

A. Dasgupta and K. G. Whitney

Naval Research Laboratory

Radiation Hydrodynamics Branch

Plasma Physics Division

M. Blaha

Berkeley Research Associates

Springfield, Virginia

M. Buie

University of Michigan, Dept. of Nuclear Engineering,

Ann Arbor, Michigan

Abstract

We present CRE gain calculations for the important J=2-1 and J=0-1 3s-3p transitions of neon-like selenium using state-of-the-art excited state couplings and self-consistently calculated ionization and excited state abundances. An atomic model was put together containing all the most significant processes impacting the gain calculation of these transitions in order to determine the sensitivity of the gain ratio of the J=0-1 to the J=2-1 lines to the monopole excitation cross sections in CRE. It is seen that variations of a factor of 2 or 3 of these cross sections are all that are needed to reverse the calculated J=0-1/J=0-2 gain ratios. For example, a decrease in the direct excitation rate from the ground to the $(1/2,1/2)_0$, 3p level by a factor of three is sufficient to reverse the gain ratio for the J=0-1 line at 182 A^o to the J=2-1 line at 210 A^o and move it into agreement with the experimentally observed ratio for these transitions. Experimental observations would suggest that for low Z elements (Cu,Zn), this ratio is larger than one, while for high Z elements (Mo,Sr), it is less than one. At issue is where the cross-over occurs. We draw attention to another instance where the discrepancy between theoretically calculated behavior and experimental behavior can be attributed to the large size of the calculated monopole excitation rate. We also present the calculated temperature and density behavior of the J=0-1 and J=2-1 gains and discuss how this behavior might be used to determine the adequacy of present atomic models to explain experimental neon-like X-ray laser observations.

I. INTRODUCTION

Since the first demonstrations of soft X-ray lasing in neon-like selenium[1,2], a number of experimental and theoretical developments have occured leading to improved gain calculations and measurements and to the achievement of even shorter wavelength neon-like x-ray lasers. The population inversion scheme employing neon-like selenium has been thoroughly investigated because the energy multiplet structure is relatively simple, and neon-like selenium X-ray lasers have been carefully studied experimentally. However, several important issues regarding the interpretation of experimental results by these calculations remain to be adequately resolved. The 3s-3p transitions in the neon-like system were considered a good source for lasing because the $2s^2 2p^5 3s$ lower lasing levels can decay to the ground state by a dipole allowed radiative transition in less than a picosecond whereas the upper metastable $2s^2 2p^5 3p$ lasing levels can do so much more slowly only by a quadrupole transition and by collisional deexcitation. Neon-like selenium was considered to be a very good initial candidate ion for experimental study since the first theoretically predicted gains for the plasma conditions achievable in the early experiments seemed to peak around selenium[2]. In recent years theoretical calculations and experimental measurements have been carried out for many different Ne-like ions. In order to calculate the population inversion between the $2s^2 2p^5 3p$ and $2s^2 2p^5 3s$ excited states all possible mechanisms responsible for populating and depopulating these states have been considered. The different theoretical models that have been developed have varying strengths and weaknesses because they include detailed calculational data for some of the atomic processes while other processes are incorporated only in an approximate way. The major problem addressed by recent calculations is to

explain the experimental findings for the relative strengths of the strongest lasing lines. The greatest discrepancy between the experimental observations and theoretical calculations that still puzzles scientists today is the fact that the J=0-1 182 A^{o} line, which is calculated to have the highest gain, showed much less or little gain when measured. Recent improvement in experimental[3] procedures and diagnostics and more complete theoretical models and calculations[4] utilizing detailed and more accurate atomic data have lessened this discrepancy, but the disagreement persists. In accord with these developments, the work to be presented in this paper utilizes, in detail and self-consistently, an atomic model that includes the atomic processes that are known to be responsible for populating or depopulating the laser levels in order to analyze and understand systematically how significantly each process affects CRE gain calculations of the neon-like selenium 3s-3p lines in order to explain why the J=0-1 discrepancy may not be such a mystery at all.

There are two neighboring J=0 and J=2 3p levels that produce important lasing transitions in neon-like Se. We will focus specifically on these states to quantify, as best possible, the different pumping mechanisms that determine the J=0-1 to J=2-1 gain ratios and the sensitivity of these ratios, in particular, to the monopole excitation rates of the J=0 states from the neon-like ground state. Extensive experimental investigations have been carried out in recent years with the goal of accurately measuring these ratios in a variety of different experiments. These investigations include not only efforts to improve upon the experimental data for Se but other Ne-like ions as well. For example, experimental data on Ne-like yttrium[1] was obtained from the same experiments[1] in which Se was investigated. However interpretation of the measured gains was ambiguous because of line coincidence between the J=0-1 and

one of the J=2-1 transitions. The experimental data of molybdenum[5] had similarity with the Se data i.e, the J=2-1 lines were measured to have substantial gain whereas the J=0-1 line analogous to the 182 A^{o} line in Se did not show much amplification. In their observation of amplication in the 3s-3p lines in Ne-line germanium, researchers at the Naval Research Laboratory (NRL)[6] obtained measurable gain for the J=0-1, 196 A^{o} line, but the gain for the J=2-1 lines were higher compared to this J=0-1 line. Thus for all ions, the relative strengths of the measured gain for the J=2-1 lines were larger and sometimes much larger than the measured gain of the J=0-1 lines. However for copper[6], these ratios were reversed (as the original gain calculations for selenium had predicted). The J=0-1 line at 221 A^{o}, analogous to the 182 A^{o} line in Se, showed a larger gain compared to the two J=2-1 lines. More recent experiments on zinc, gallium, arsenic, and selenium[7] have also been performed at NRL. Gain measurements could not be obtained for Ne-like gallium because the lines were too weak. There were also no observed gain in arsenic for the J=0-1 line, analogous to the 182 A^{o} line in Se. In the same experiment, gains of 4.9 cm^{-1} were measured for the two J=2-1 lines for Se and a measurable (but substantially lower than theoretically predicted) gain of 2.6 cm^{-1} was reported for the J=0-1, 182 A^{o} line. In the same experiment however, the J=0-1 line for zinc showed a larger gain coefficient than the gain for the two J=2-1 lines. These observations would indicate that the relative strengths of the gains for the J=2-1 are indeed smaller compared to the gain of the J=0-1 line for sufficiently low Z ions.

Recent improved experiments[3] in Se at LLNL achieved a measureable gain for the J=0-1 182 A^{o} line. The results of this experiment are in much closer agreement with the new calculations[4] of the theoretical group at LLNL. The better agreement resulted because the gain of the J=2-1 lines increased and

the gains of the J=0-1 lines decreased in their calculation, and reanalysis of the gain data of the J=0-1 line in the measurement showed a noteworthy gain of 2.4 cm^{-1}. Very recently substantial gain has been measured for the J=2-1 transition of Ne-like strontium[8]. The J=0-1 transition, analogous to the 182 A^{o} line in Se, was not observed due to a wavelength overlap with a Na-like Sr line. Thus, from all the data available so far for the Ne-like ions there is strong indication of a systematic Z-scaling behavior of the gain ratio of J=0-1 to J=2-1 lines. This scaling was first noted by Whitten et al[9].: their calculated gains for the J=2-1 lines increased; whereas the J=0-1 gains decreased as a function of Z. The difference between the calculated and measured gain ratios appears to be in the Z value at which the ratio becomes one. In order to understand the Z scaling of the gains of the two different(J=2-1 and J=0-1) but adjacent transitions and particularly the behavior of the J=0-1/J=2-1 gain ratio as a function of Z, one has to accurately calculate the Z dependence of the relative strengths of the different pumping mechanisms that predominantly populate the upper laser levels.

Collisional excitation is the single most important mechanism for populating the J=0 levels of the 3p multiplet. The evaluation of the monopole excitation rate from the ground 2p state has received much attention. Thus most atomic models include a well calculated collisional excitation rate in their gain calculations. Although other ionization and recombination processes must also be included, their influence on the population inversion dynamics is less direct.

It was also realized that the J=2 upper lasing states could be pumped preferentially by dielectronic recombination (DR) from flourine-like ground state relative to the J=0 state pumping. Thus DR was thought to have a

significant effect on the gain calculation of the lasing levels especially for non-equilibrium plasmas, and the inclusion of detailed DR rates into the kinetic model for each of the n=3 multiplet states seemed absolutely essential[10,11]. However, such inclusion still did not fully explain the "J=0" mystery in Se. Early calculations contained only a ground-to-ground effective DR rate. The theoretical group at Livermore, in their recent improved calculation,[4] included state specific DR rates to each of the lower and upper lasing levels. These inclusions and other improvements in their atomic model were observed to be responsible for the better agreement between their calculated and observed gains[3].

Another dominant mechanism for populating the 3p levels is deexcitation from the 3d excited levels. Like DR, 3d deexcitation also favors the pumping of J=2 states over that of the J=0 states. It was pointed out by Whitten et. al.[11] that collisional and radiative cascade from the excited states into the 3d states increase the gain of the J=2-1 lines by 15-20%.

It was also shown that the rates for inner-shell ionization[12] of sodium-like ions could be comparable to electron excitation from neon-like ions in a nonequilibrium plasma. In fact inner-shell ionization also pumps 3p states while favoring the J=2-1 inversion over the J=0-1. This process might also figure into the interpretation of experimental findings, especially for short pulse experiments.

In this work, we have constructed a detailed atomic model of the n=3 states of neon-like selenium and coupled it self-consistently to a less detailed but fairly complete model of the ionization dynamics in all ionization stages of the selenium system. The model makes use of state-of-the-art atomic data and contains all of the processes known to play an important role in the excitation dynamics of the n=3 excited states.

It enables us to carry out self-consistent calculations of both the ionization abundances of the neon- and fluorine-like ground states and of the populations of each of the 26 n=3 multiplet states. With it, we have computed the collisional radiative equilibrium (CRE) behavior of the J=0-1 and J=2-1 gain coefficients and quantified their dependence on the three important competing processes for populating the 3p states from the ground neon- and fluorine-like states and from the 12 3d multiplet states. Our model produces somewhat different relative magnitudes of the different X-ray laser transitions in neon-like Se than other models that have been reported on, and we use it to evaluate the relative importance of the different pumping mechanisms in interpreting the gain calculation results.

This paper is structured as follows. In section II, the atomic model that we use for the gain calculations is described. The relative strengths of the three dominant CRE pumping mechanisms are discussed in section III. These magnitudes depend not only on the relative strength of the collision rates, but on the relative size of the populations being pumped. The parametric dependence of the J=0-1 and J=2-1 gains on temperature and density is then presented in section IV, where the sensitivity of these results to the strength of the monopole excitation rates is discussed. Finally, in section V, we summarize the results of these calculations and discuss how they bear on the problem of comparing theoretical gain calculations with experimental results.

II. ATOMIC MODEL

Our atomic model was developed to include all the important processes responsible for 3s-3p population inversions in neon-like selenium but in as economical yet complete a fashion as possible. Thus to compute the overall ionization state of selenium, we began with the hydrogenic atomic model described in Reference 13, and replaced the lumped excited state structure of the hydrogenic model with the 30 excited states shown in Fig. 1 in order to compute the detailed excitation dynamics of the n=3 states of neon-like selenium, Se^{24+}. Similarly, the fluorine-like structure of the hydrogenic model was replaced by a lumped state version of Fig. 1. As we can see from this figure, the model contains all the multiplet levels (4 levels of 3s, 10 levels of 3p and 12 levels of 3d) of valence n=3 excited states of immediate relevance to neon-like lasing as well as the 3 inner shell excited $2s2p^6 3s$, $2s2p^6 3p$, $2s2p^6 3d$ states, and the n=4 lumped excited state of indirect relevance. We include all the n=3 multiplet states and all processes coupling these levels explicitly because these populations support large inversion densities only when the levels are far from LTE, i.e., only when the metastability of the n=3 states is pronounced. The fluorine-like ionization stage was modeled using tha same atomic structure as the neon-like system but in a less detailed fashion since only its ground state populations play an important role in determining the n=3 neon-like populations. For economy, it contained a lumped description of the 57 n=3 multiplet states; thus, in all, it contained only eight excited states : the $\Delta n=0$ excited state, the 3s, 3p, and 3d lumped states, and the $2s2p^5 3s$, $2s2p^5 3p$, $2s2p^5 3d$, and n=4 states of Fig. 1. The CRE gain calculations consist of simultaneous calculations of the populations of all ionization stages surrounding the neon-like ionization

stage in addition to the populations of all the neon-like excited states in Fig. 1.

Figure 2 shows the 14 specific J levels that constitute the upper 3p and lower 3s multiplet states in neon-like selenium. The four J=0-1 and J=2-1 radiative decays along with the wavelengths for these transitions are also shown in this figure. It is drawn to scale and defines labels for each of the four J=0-1 and J=2-1 transitions, which are the focus of the theoretical investigations of this paper.

The processes that couples these levels are collisional and resonance excitation, collisional deexcitation, radiative decay, radiative recombination, and dielectronic recombination both from the fluorine-like ground state and its $\Delta n=0$ excited state. It is crucial to obtain these couplings as accurately as possible in order to calculate the population dynamics of these states accurately. We have obtained this data from a variety of sources; all of it, to the best of our knowledge, is state-of-the-art. For example, we used the collision strengths calculated by Zhang et al.[14] to couple the n=3 states to the neon-like ground state. The collisional excitation rate coefficients were then obtained by fitting the collision strength data points (see Fig. 8) and using the fits to integrate the cross sections over a Maxwellian electron distribution for each required temperature. The resulting rate coefficients to the most important upper and lower lasing levels are shown in Fig. 3. It shows by how much the collisional excitation rates to the upper J=0 levels are larger than the rates to the J=2 levels or to the lower J=1 levels. Collisional ionization and recombination rates from the 3s sublevels were obtained from Golden et. al.,[15] and the ionization and recombination rates from the 3p and 3d sublevels were taken from Moore et. al.[16].

Because collisional deexcitation from the 3d excited levels to the 3p states is a major contributor in populating the J=2 upper lasing levels and because 3p-3p collisions tend to equalize the gain of the two J=0-1 lines,[17] it is important that these collisional couplings be accurately calculated in our model. We have used the relativistic distorted wave 3s-3s, 3s-3p, 3p-3p, 3s-3d, 3p-3d, and 3d-3d collision strengths calculated by P. Hagelstein and R. Jung[18]. Again, we used algebraic fits to the data given in their paper to carry out the integration over a Maxwellian electron distribution to obtain the rate coefficients coupling the n=3 states.

Additional coupling of the neon-like excited states to the fluorine-like system occurs by radiative and dielectronic recombination (DR). Only a total ground-to-ground radiative recombination coupling of the fluorine-like to the neon-like ionization stage was included in our model. The DR rates, on the other hand, were calculated[19] from a detailed calculation of the needed doubly excited energy levels, stabilizing radiative rates, and autoionization rates using the HFR (Hartree-Fock with relativistic correction) method of R. D. Cowan[20]. The inclusion of ground-to-ground effective DR rates into the rate equation dynamics had been argued early on in the history of the the neon-like Se x-ray laser, and more recently the importance of state specific (for each excited multiplet level) DR processes had been claimed by London et. al.[4]. We have taken into account a complete set of doubly excited states in calculating the DR rates[19]. For low lying doubly excited states, the DR branching ratios were explicitly calculated, while for higher Rydberg states the states were lumped and the $1/n^3$ falloff of the DR rates was used, where n denotes the principal quantum number of the Rydberg electron. Our total ground to ground DR rate coefficients compared very well with the detailed multi-configuration Dirac-Fock (MCDF) calculation M. C. Chen[21]. The DR rate coefficients that were

obtained from our calculations connecting the ground state of F-line selenium to the most important upper 3p and lower 3s lasing levels are shown in Fig. 2 of Ref. 19. This figure shows that coupling strengths from the F-like ground state are in reverse order to those from the neon-like ground state, i.e., the J=2 levels of the 3p states are pumped more strongly by dielectronic recombination (DR) than the J=0 levels are. The rate coefficients for the missing multiplet level $2p^5 3p\ (3/2,3/3)_0$ in that figure are approximately of the same magnitude as those for the $2p^5 3p\ (1/2,1/2)_0$ level.

Besides direct collisional excitation, the excitation of neon-like ions can proceed via intermediate autoionizing resonances which can often have contributions comparable to or even larger than those due to direct excitation. These resonances are produced when a neon-like ion captures a target electron into a doubly excited sodium-like state, which may either radiatively decay or autoionize. The radiative channel leads to dielectronic recombination to sodium-like states but when doubly excited states autoionize to excited neon-like states, they act as intermediaries in the resonance excitation (RX) of the neon ion. We calculated these rates in the resonance approximation following Cowan[22] in a way that was very similar to the DR rate calculation. Their importance to the 3s-3p gain calculation is illustrated in Fig. 4, which shows not only that the RX rates to the 3s levels are much larger than those to the 3p levels but, by comparison to Fig. 3, that the 3s RX rates are larger than the direct excitation to these states. The inclusion of these processes therefore will increase the J=1, 3s populations slightly and decrease the calculated gain coefficients. When we compared these level specific RX rates with those of Chen[23], we found that our calculated RX rates to the 3p multiplet levels are lower than his, but our rates to the 3s multiplet states compare quite well with his rates.

Because accurate DR rates are also important to the calculation of the ionization balance, which indirectly has a large influence on the 3s-3p neon-like gain calculations, we have also included in our model a detailed calculation of the DR rates from the 0-like ground and $\Delta n=0$ excited states to all levels of the singly excited F-like ion. The inclusion of these processes has a significant impact on reducing the oxygen-like fractional populations, and hence, in turn, on shifting the CRE ionization balance and influencing the strength with which the neon-like states are pumped.

Finally, to complete the collisional couplings in our Ne-and F-like models, we have also calculated excitation and deexcitation collision rates between all the other lumped states of our model and each of the lower multiplet levels by again integrating cross-sections over Maxwellian electron distributions. The corresponding cross-sections were calculated in a non-relativistic distorted-wave approximation using atomic wave functions and data generated by the computer code of R. D. Cowan[20]. Intermediate coupling and configuration mixing were taken into account. The rates from the n=4 lumped state to all lower n=3 multiplet states were obtained from individual J-J' rates with the assumption that the population of individual upper J levels is proportional to 2J+1.

III. PUMPING MECHANISMS

Collisional excitation from the Ne-like ground state, dielectronic recombination from the F-like ground and $\Delta n=0$ excited states, and collisional deexcitation from the 3d excited states are the most important competing atomic processes that are responsible for directly populating the upper 3p lasing levels. Fig. 5 shows an energy level diagram, which applies to either of the two neighboring J=0 and J=2 upper lasing level pairs, that summarizes the situation in which these three pumping mechanisms compete to populate the two states. The dark arrows designate which of the two rates to the J=0 and J=2 states is the strongest in each case. Note that the J=0 level is pumped preferentially only by collisional excitation from the ground Ne-like state, while the J=2 level, on the other hand, is pumped preferentially by both collisional deexcitation from the 3d excited state and by recombination (DR) from the F-like ground state. Note also that the populations of the 3d states, which most directly affect the population of the J=2 level, are themselves directly populated by collisional excitation from the Ne-like ground state, and by direct and cascade recombinations as indicated in this figure. Two of the 3d states are depopulated by strong radiative decays to the ground state, while the other 10 have no strong decays and, like the 3p states, are metastable (see Fig. 10).

Fig. 5 partially explains why the gain ratio of neighboring J=0-1 to J=2-1 lines can turn out to be larger or smaller than unity. The relative strengths of the two gains will also depend on the relative strength of the three pumping rates into the J=0 and J=2 levels. Since these pumping rates are each the product of the total rate coefficient for a given process times the population of the state undergoing the transition, the total pumping strength

depends on the fractional population that is calculated for each state as a function of the plasma conditions. Thus, on the one hand, the total pumping strengths to the two J=0 upper levels may be small if the strong collisional excitation rate coefficient multiplies a small fractional population of the Ne-like ground state. (This effect was argued early in the history of the selenium X-ray laser[10,24].) Similarly, the total pumping strengths to the J=2 upper levels depend not only on the relative strengths of the deexcitation rates from the 3d excited states to those of DR from the fluorine-like states but also on the relative ion populations that are calculated for these states. In CRE, on the other hand, we find there is a large abundance of ions in the neon-like ground state and that they contribute strongly to the excitation of the J=0 levels. However, in CRE, we find that the pumping of the J=2 states is due predominantly to deexcitation of the 3d states, and that it is also competitive with the collisional excitation of the J=0 states. These points are illustrated in Figs. 6 and 7, which show the calculated pumping strengths in CRE to the (1/2,1/2) J=0 and (1/2,3/2) J=2 lasing levels as a function of temperature at the fixed ion density of 10^{19} ions/cm^3.

When we compare Figs. 6 and 7, we see that, even though the contribution of DR pumping to the J=2 state is comparatively much larger than its effect in populating the J=0 level, the strengths of DR pumping to both of these levels are much smaller than collisional excitation from the ground state. Fig. 2 of Ref. 19 shows how dielectronic recombination feeds the upper and lower lasing levels and how the J=2 levels can be substantially populated directly from the fluorine-like ground state via DR when there are enough F-like ions. The DR rate coefficients from $\Delta n=0$ F-like to J=0 and J=2 upper 3p levels and J=1 3s lower lasing levels are such that inclusion of these rates also tend to increase the rate coefficients to the J=2 levels compared to that of the J=0

levels. However, when we compare Fig. 2 of Ref. 19 to Fig. 3 of this work, it is evident that the dominance of collisional pumping from the neon-like ground state over DR pumping from the fluorine-like ground states that is seen in Fig. 7 is attributable to the preponderance of neon-like ground states to fluorine-like ground states in CRE under plasma conditions relevant to selenium X-ray lasing. When we include detailed calculations of DR from oxygen-like to fluorine-like states, this effect is increased. To further understand the magnitudes of the curves shown in Figs. 6 and 7, we turn to Figs. 8-11.

Fig. 8 shows the collision strengths used in our calculations for all the multiplet levels of the 3p state that were obtained from Ref. 14. This data directly explains the differences in the strengths of the J=0 and J=2 collisional excitation pumping rates seen in Figs. 6 and 7. Since collisional excitation to both J=0 and J=2 levels is from the same neon-like ground state, the relative magnitude of the collision strengths to these two states determines the relative strength of the pumping rates. As can also be seen from Fig. 8, the collision strengths to the other 3p levels fall off very rapidly with energy and consequently have even smaller excitation rates than do the J=0 and J=2 levels.

The situation regarding deexcitation pumping from the 3d states is more complex. In this case, the degree of metastability of the 3d states is an important factor in the 3p-3d coupling. If we ignore this feature initially and examine the coupling to the 3p states by summing over the 3d states, then we obtain the results shown in Fig. 9 for the 3p-3d collision strengths to the J=0 and J=2 levels as obtained from Ref. 18. It is seen from this figure that 3d collisional couplings to the J=2 3p levels are about an order of magnitude higher than those to the J=0 3p levels. However, the pumping rates due to 3d

deexcitation to the J=2 levels in Figs. 6 and 7 are about two orders of magnitude larger than the 3d pumping rates to the J=0 levels. In order to explain this behavior we have to understand how each of these 3p (J=0 and J=2) levels are coupled to each of the 3d levels and also how each of these 3d levels are populated in CRE. Any reduction in 3d populations will give lower deexcitation pumping of the 3p states.

A detailed examination of the coupling strengths between the 3d and 3p states shows the pattern depicted in Fig. 10; namely, each 3d state, while collisionally coupled to each 3p state, is predominantly coupled to only one as indicated in Fig. 10. Moreover, under the plasma conditions shown in Figs. 6 and 7, the 3d states are depopulated predominantly by collisional deexcitation rather than by radiative decay to the 3p states. The J=0, 3p states, in particular, are strongly coupled only to the two ($^3D_1$ and $^1P_1$) 3d states that strongly radiate to the ground state; whereas, the J=2 states are strongly coupled to metastable 3d states. (The rate coefficients for the two 3d to ground state radiative decays are also shown in Fig. 10). Thus the J=2 3p levels receive substantial population from the 3d metastable states compared to the J=0 3p levels because the populations (as well as the coupling strengths) of these metastable states are much larger than the populations (and coupling strengths) of the decaying J=1 states that populate the J=0 3p levels. To quantify these statements, the relative fractional populations, $f_i = f_i^{3d}/\Sigma f_i^{3d}$, of the five highest lying 3d J levels are shown in Fig. 11 as a function of ion density at an electron temperature of 1 keV. This figure shows that the fractional populations of the metastable J=3 3d levels are approximately an order of magnitude larger than the populations of the J=1 3d levels at a plasma density of 10^{19} cm^{-3}, and that the 3d populations only begin to equilibriate at ion densities larger than 10^{21} cm^{-3}.

We see from the above discussion how the calculated populations of the states responsible for populating the laser levels play a major role in determining the relative and absolute population inversions. Thus it is crucial to determine these populations as accurately as possible for the time dependent plasma conditions that are generated in each experiment. Accurate comparisions between theoretically calculated and experimentally inferred gain coefficients require accuracy in each of these three calculations: rate coefficients, ion populations, and plasma conditions. For this reason, X-ray lasers provide an important challenge to our theoretical ability to calculate and comprehend the plasma dynamics necessary to produce them efficiently.

IV. GAIN CALCULATIONS

It follows directly from the discussion of the previous section that in order to produce the maximum gain for the important lasing lines one must generate the right plasma conditions of temperature, density, and ionization where an abundance of neon-like or fluorine-like ground state Se ions exist. In CRE, the total fractional abundances of Na-,Ne-, and F-like selenium ions as a function of electron temperature at an ion density of 10^{19} cm^{-3} that are calculated by our model are shown in Fig. 12. These populations were obtained by summing over all states in each ionization stage. We note from this figure that only at electron temperatures well beyond 1 keV, the temperature most relevant to the Ne-like Se x-ray laser, do the populations of F-like ions become comparable to and larger than those of the Ne-like ion in CRE. Nevertheless, it is important to calculate and include accurate atomic data for the F-like ion from mechanisms such as excitation, ionization and recombination in order to accurately calculate the neon-like as well as F-like populations.

One way to evaluate the quality of the CRE calculations resulting from our model is given in Fig. 13. In this figure, the gain curves that are computed from the CRE population inversion generated between the total number of 3p and 3s states in each of the F-like and Ne-like ionization stages are compared as a function of density at an electron temperature of 1 KeV. To obtain the Ne-like curve, we summed over the individually computed populations of the 3s and 3p states. In this and all the other gain curves to be shown in this section, we used a Doppler linewidth calculated by assuming that the ion temperature T_i equalled the electron temperature T_e. In Fig. 12 the 3s-3p gain coefficient for the Ne-like ion is much larger than that for F-like. This result is

consistent with recent gain calculations of P. Hagelstein[24] and with experimental observations. Hagelstein calculated gain coefficients between 2 and 4 cm^{-1} for the four 3s-3p J-J transitions in F-like selenium. No amplification of these lines has yet been measured, however, which is in keeping with Fig. 13, where the calculated gains in F-like Se are significantly smaller than those calculated for neon-like Se at, for example, 10^{19} ions/cm^3. Hagelstein's calculation was performed for the same plasma conditions as quoted in the Livermore experiment[3] i.e., at the electron density of $5x10^{20}$ cm^{-3}. Note, also, in Fig. 12 that the gain in the F-like ion peaks and falls off at a slightly higher density than that of the Ne-like ion. Thus to observe amplification of F-like lines, one may require plasma densities higher than those yet achieved. On the other hand, while the results in Fig. 13 are suggestive, they are not definitive. To obtain a more accurate description of the population dynamics, one must calculate the gain for each of the specific transitions among the F-like J levels.

Fig. 14 shows the gain coefficients that are calculated for the four J=0-1 and J=2-1 lasing transitions in Se^{+24} as a function of temperature at an ion density of $1x10^{19}$ cm^{-3}. The coefficients are labeled according to Fig.2. The temperature dependence of the gain was calculated at this particular ion density because it is of the same order of magnitude as the density that was inferred in the Livermore experiment. Because the gain coefficients of these four J=0-1 and J=0-2 lines all peak at 1 keV at this density, we used this temperature to calculate the density dependence of these gain coefficients, which is plotted in Fig. 15. Fig. 15 shows that the gain curves for all the four lines peak at a larger ion density than $1x10^{19}$ cm^{-3} and that the gains for different lines peak at different densities. Thus if all four lines are amplified during an experiment, one may infer an upper bound on the density

depending on the reliability of the atomic model.

While the sizes of the gain coefficients in Figs. 14 and 15 are in general agreement with recent calculations of London et. al. at the temperature and density of their calculation, there is one noteworthy difference. In our calculation, only the upper of the two J=0-1 lines has a larger gain than its neighboring J=2-1 line. Our calculated gain for the 169 A^{o} line is small and in general accord with the early experimental observations. Only the calculated gain of the 182 A^{o} line would appear to suggest problems in our model because of its unusally large size.

Because the J=0-1 182 A^{0} line is calculated to have a much larger gain than the J=2-1 lines, which may contradict experimental observations, we were led to investigate the sensitivity of this gain coefficient to the strength of the monopole collisional excitation rate. Moreover, there are other instances in the literature where the accuracy of calculated monopole rates have been called into question. It was shown by Machado et al[25], for example, that, while the calculated differential and integral cross sections for electron-impact excitation of all $2p^{5}3s$ levels were very close to experimental measurements, a strong disagreement with experimental data[26] could be found for the cross sections of the $2p^{5}3p$ levels of neon. In a different calculation of the excitation of argon, Bubelev et al[27] showed that the cross sections for excitation of $3p^{5}4p$ J=2 levels had quite good agreement with experimental data[28], but that the cross sections of the $3p^{5}4p$ J=0 levels were calculated to have an order of magnitude higher values than those measured experimentally. In another example, Griffin et. al[29] calculated the electron impact ionization cross sections of Na-like ions using distorted wave approximation in order to investigate the effect of excitation-autoionization on these cross sections. Their calculations indicated that the largest contributions came from the 2p-

3p excitations for all the ions they considered. Again, when they compared their results with experimental data, there was substantial disagreement. They concluded that the primary discrepancy arose due to their overestimation of the magnitude of the monopole-dominated 2p-3p (and to a lesser extent the 2p-4p) transition. All this evidence suggests that it is plausible that the calculated monopole excitation rate coefficient to the upper J=0 level that we employed in our model could also be in error by at least a factor of three.

In order to test this hypothesis, we reduced the collisional excitation rate to the upper J=0, 3p level by a factor of three and used this modified rate in the CRE calculation to repeat the gain calculations of Fig. 15. As expected, the gain for the J=0-1 182A^{o} line was reduced, but, additionally, the reduction was significant. The gains for the four J=0-1 and J=2-1 lines using the reduced monopole rate to the $(1/2,1/2)_0$ level is shown in Fig. 16 as a function of density at an electron temperature of 1 keV. Comparing Fig. 16 with Fig. 15, we see that the strengths of the gain coefficients for both sets of J=0 and J=2 levels are now in the same relation. The J=2-1 line near 206A^{o} now has the highest overall gain, and the gain curves for the two J=0-1 lines are very close to one another. The relative strength of the gain curves in this figure would appear to be in much closer accord with the early expermental observations than any of the calculations performed to date. By contrast, if we increase the collision excitation rate to the lover of the two J=0 levels by only a factor of two, the gain ratio for both of the J=0-1 to the J=2-1 lines at densities above 10^{20} ions/cm^{3} can be reversed from that in Fig. 16. This effect is shown in Fig. 17.

From the results of these gain calculations, it is apparent that one must have accurate monopole collisional excitation rates in order to accurately calculate gain ratios involving the J=0 levels of the neon-like 3p states. It

is also apparent that a realistic calculation of the ionization balance will rely on an accurate knowledge of plasma conditions. For these reasons, it may be easier and more meaningful to make experimental and theoretical comparisons between the gain ratios of lines than it is to compare the absolute values of calculated and measured gains.

V. SUMMARY

The problem of comparing calculated with experimentally inferred gain coefficients in order to confirm our understanding of the dynamics of X-ray laser schemes is complex yet decipherable in general. The complexities are due, in part, to the fact that experimental plasma conditions vary rapidly both spatially and temporally, and the x-ray laser beam may be refracted, partially absorbed, or receive non-uniform amplification. In a recent pair of papers[30,31], it was suggested, moreover, (1) that the observed ratio of gains between the J=0-1 and J=2-1 lines of neon-like germanium would vary depending on the geometry that was used to carry out the X-ray laser experiment and (2) that the average temperatures or densities reached in X-ray laser experiments were not necessarily those predicted by hydrodynamics calculations. To this list of potential difficulties in making calculational/ experimental comparisions, one can add the problems of (1) calculating accurate rate data for each atomic process, (2) building a complete atomic model from which both excited state populations and ionization abundances can be self-consistently obtained and (3) accurately calculating the ion populations for different specific sets of rapidly changing plasma conditions. In spite of all these difficulties , however, there are several issues concerning the behavior of X-ray laser gain coefficients that can be fruitfully examined jointly by experiments and by a variety of supporting calculations. One involves the design of experiments to promote one pumping mechanism over another in order to preferentially amplify one set of lines over another. Another involves experiments designed to explore the density dependence of the gain coefficients of different lines. Finally, a third involves experiments systematically carried out to determine the atomic number scaling of the

relative strengths of the gains of neighboring lines. In this paper, we have presented results of gain calculations in neon-like selenium that bear on these latter two issues and examined in detail the relative strengths of the neon-like pumping mechanisms in CRE that bear on the first issue.

A complete selenium atomic model consisting of 30 neon-like and eight lumped F-like excited states was used to calculate self-consistent populations, pumping rates, and gain coefficients for the 3s-3p lasing transitions in CRE. The model utilized state-of-the-art collision, DR and RX rates in both Ne-like and F-like ionization stages and was able to reproduce all of the essential aspects (with some important differences) of previous gain calculations for all of the 3s-3p lasing transitions. The collisional excitation rates to the n=3 states were the same as those used by the Livermore researchers and our DR rates compared very well with those of M.Chen[20] (although we could only compare total ground-to-ground DR rates with those of Chen). We found that the inclusion of state specific DR rates had only a minor direct impact in CRE on the gain calculation of the J=2-1 lines presumably in contrast to Livermore findings[4]. Even though these rates were calculated in a very accurate and detailed way, the variation of the gain curves as a function of the strength of the J=2 3p DR rates was not significant when these rates were varied by up to a factor of three. The reason for this insensitivity was that in our CRE calculation, collisional excitation and 3d deexcitation pumping dominates DR pumping and so the latter will have a major influence only in a non-equilibrium plasma.

Another apparent difference between our results and other published results was that our model predicted the gain ratio J= $(1/2,1/2)_0$ - J= $(1/2,1/2)_1$ / J=$(1/2,3/2)_2$ - J= $(1/2,1/2)_1$ to be larger than one while J= $(3/2,3/2)_0$ - J= $(3/2,1/2)_1$ / J=$(3/2,3/2)_2$ - J= $(3/2,1/2)_1$ was less than one.

However, a decrease in the size of the calculated $(1/2,1/2)_0$ monopole excitation cross section by only a factor of three was sufficient to reverse the J= $(1/2,1/2)_0$ - J= $(1/2,1/2)_1$ / J=$(1/2,3/2)_2$ - J= $(1/2,1/2)_1$ ratio to values less than one. Moreover, in this case, the low density ($<5x10^{19}$ ions/cm^3) gains for both J=2-1 lines became approximately equal. The same was true for the J=0-1 lines. This is an important finding since it is generally believed that cross section calculations are no more accurate than a factor of two or three. Equally important, we pointed out that this is not the first instance when the size of a calculated monopole cross section was suspect. In a previous instance,[27,29] it was believed that the calculated monopole cross section was too large by a factor of ten. We hope that these findings will provide sufficient motivation for other researchers to more accurately recalculate or measure the rates for processes exciting the J=0 3p states. The results of our calculations would suggest that the collisional excitation rate for populating the upper level of the mysterious "J=0-1" 182 A^o line needs the most attention, either theoretically or experimentally. A thorough measurement of this rate using the electron beam ion trap (EBIT)[32] at Lawrence Livermore Laboratory, for example, would provide an important benchmark for theoretical atomic models of the neon-like system.

A second method for benchmarking gain calculations against experiment is provided by the predicted density behavior of different models. Without any modifications of the monopole excitation cross-sections, the gain of the J=0-1 line at 182 A^o peaked above $100cm^{-1}$ at $3x10^{20}$ ions/cm^3, and it had values larger than 10 cm^{-1} up to densities of $2x10^{21}$ ions/cm^3, well past those densities where the other lines can be amplified. These results are very sensitive to the strength of the $(1/2,1/2)_0$ monopole excitation rate since a factor of three reduction in its magnitude caused the peak gain of the 182 A^o

line to be reduced by a factor of 5 and its gain to vanish above 5×10^{20} ions/cm^3. Another important feature of our calculations was that the gain of the J=2-1, 210 A^o line vanished near or below 2×10^{20} ions/cm^3 in all of the cases we studied. This behavior suggests that if experiments could be carried out in which the density of the gain medium could be systematically increased (with care to avoid refraction problems), then not only could greater amplification be achieved but variations in the relative strengths of the amplified lines could also be used to test the accuracy of the rate data used in the calculations.

REFERENCES

1. D. L. Matthews et al., Phys. Rev. Lett. 54, 110 (1985).

2. M. D. Rosen et al., Phys. Rev. Lett. 54, 106 (1985).

3. C. J. Keane, N. M. Ceglio, B. J. MacGowan, D. L. Matthews, D. G. Nilson, J. E. Trebes and D. A. Whelan, J. Phys. B., At. Mol. Opt. Phys. 22, 3343 (1989).

4. R. A. London, M. D. Rosen, M. S. Maxon, D. C. Eder and P. L. Hagelstein, J. Phys. B., At. Mol. Opt. Phys. 22, 3363 (1989).

5. B. J. MacGowan et al., J. Appl. Phys. 62, 5234 (1987).

6. T. N. Lee, E. A. McLean and R. C. Elton, Phys. Rev. Lett. 59, 1185 (1987).

7. T. N. Lee, E. A. McLean, J. A. Stamper, H. R. Griem and C. K. Manka, Bull. Am. Phys. Soc. 33, 1920 (1988).

8. C. J. Keane et al., Phys. Rev. A 42, 2327 (1990).

9. B. L. Whitten et al., Proceedings of the Intl. Conf. on Lasers '88 90 (1989)

10. J. P. Apruzese, J. Davis, M. Blaha, P. C. Kepple and V. L. Jacobs, Phys. Rev. Lett. 55, 1877 (1985).

11. B. L. Whitten, A. U. Hazi, M. H. Chen and P. L. Hagelstein, Phys. Rev. A 33, 2171 (1986).

12. W. H. Goldstein, B. L. Whitten, A. U. Hazi and M. H. Chen, Phys. Rev. A 36, 3607 (1987).

13. K. G. Whitney and M. C. Coulter, IEEE Trans. Plasma Sci. 16, 552 (1988).

14. H. Zhang and D. H. Sampson, Atomic Data and Nuclear Data Tables 37, 17 (1987).

15. L. B. Golden, D. H. Sampson and K. Omidvar, J. Phys. B 11, 3235 (1978).

16. D. L. Moores, L. B. Golden and D. H. Sampson, J. Phys. B 13, 385 (1980).

17. B. L. Whitten, R. A. London and R. S. Walling, Opt. Soc. Am. B5, 2537 (1988).

18. P. Hagelstein and R. K. Jung, Atomic Data and Nuclear Data tables 37, 121 (1987).

19. A. Dasgupta and K. G. Whitney, Phys. Rev. A 42, 2640 (1990).

20. R. D. Cowan, "The Theory Of Atomic Structure and Spectra (Univ. California Press, Berkeley, 1981)".

21. M. C. Chen, Phys. Rev. A 34, 1079 (1986).

22. R. D. Cowan, J. Phys. B 13, 1471 (1980).

23. M. C. Chen, Phys. Rev. A 40, 2292 (1989).

24. P. L. Hagelstein, Phys. Rev. A 34, 924 (1986)

25. L. E. Machado, E. P. Leal and G. Csanak, Phys. Rev. A 29, 1811 (1984).

26. D. F. Register, S. Trajmar, G. Steffensen and D. C. Cartwright, Phys. Rev. A 29, 1793 (1984).

27. V. E. Bubelev and A. N. Grum-Grzhimailo, J. Phys. B., At. Mol. Opt. Phys. 24, 2187 (1991).

28. A. Chutjian and D. C. Cartwright, Phys. Rev. A 23, 2178 (1981).

29. D. C. Griffin, C. Bottcher and M. S. Pindzola, Phys. Rev. A 25, 154 (1982).

30. S. Nakai et al., " Soft-Xray Laser Experiments with GEKKO XII-Amplification Collimation and Coherence", Bull. Am. Phys. Soc. 36, 2431 (1991).

31. H. Baldis, J. Dunn, D. Villenevue, G. Enright and H. Pepin, "Electron Density and Temperature Calculation and Measurements for Neon- and Plasma", Bull. Am. Phys. Soc. 36, 2431 (1991).

32. R. E. Marrs, M. A. Levine, D. A. Knapp, and J.R. Henderson, Phys. Rev. Letters 60, 1715 (1988).

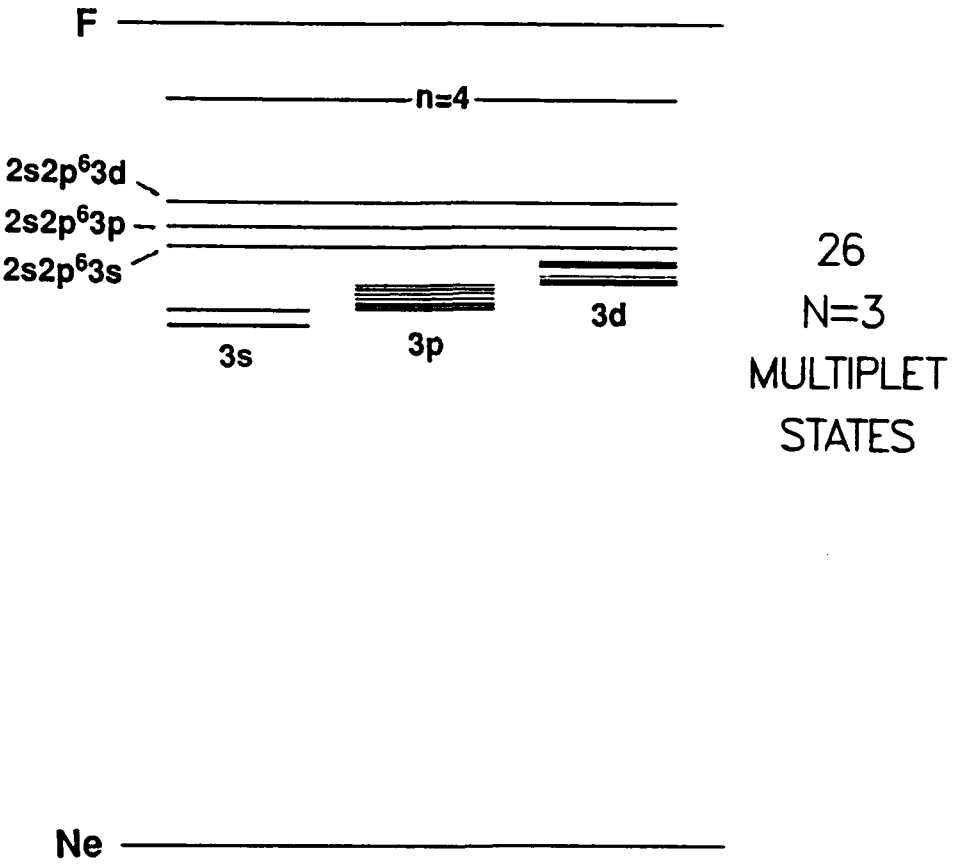

FIG. 1 Energy level diagram for Ne-like selenium as used in our atomic model.

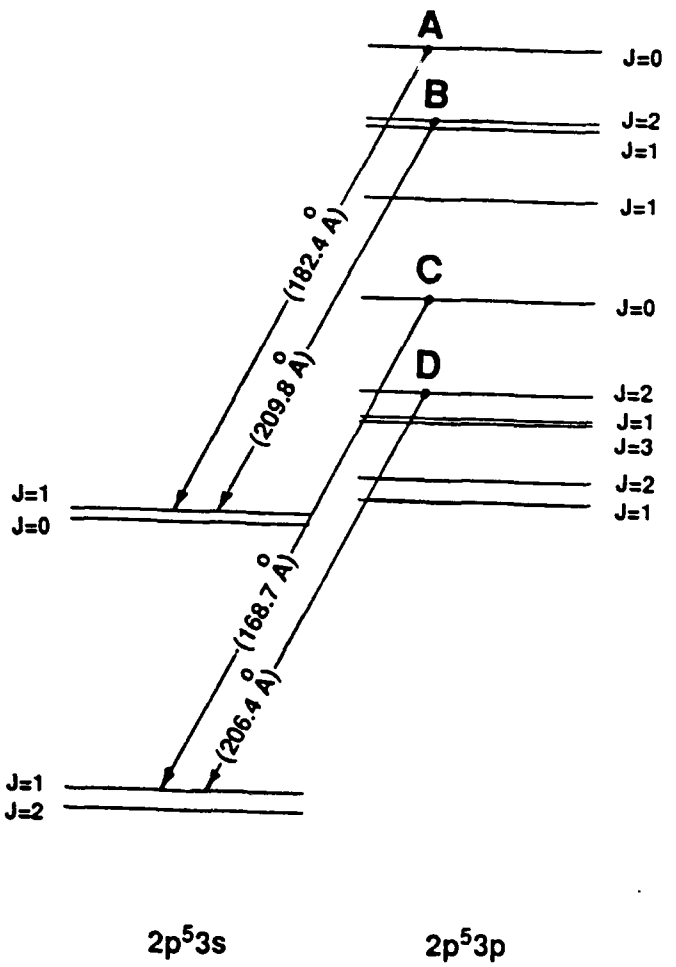

FIG. 2 Energy level diagram for the 3s and 3p multiplet levels of neon-like selenium. The important lasing lines are labeled and shown along with their corresponding wavelengths.

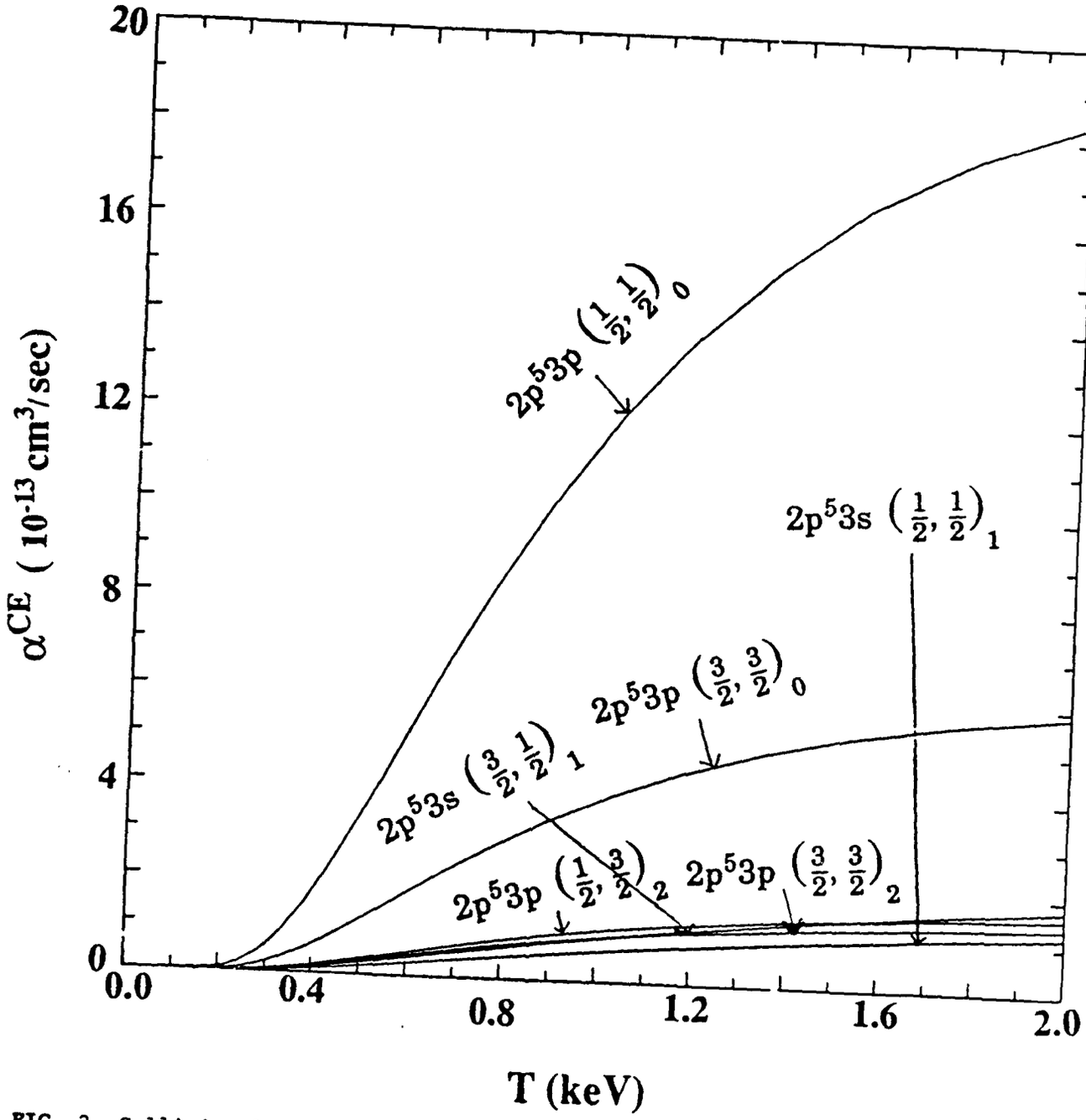

FIG. 3 Collisional excitation rate coefficients from the ground state to the observed upper $2p^5 3p$ and lower $2p^5 3s$ lasing levels of Ne-like selenium.

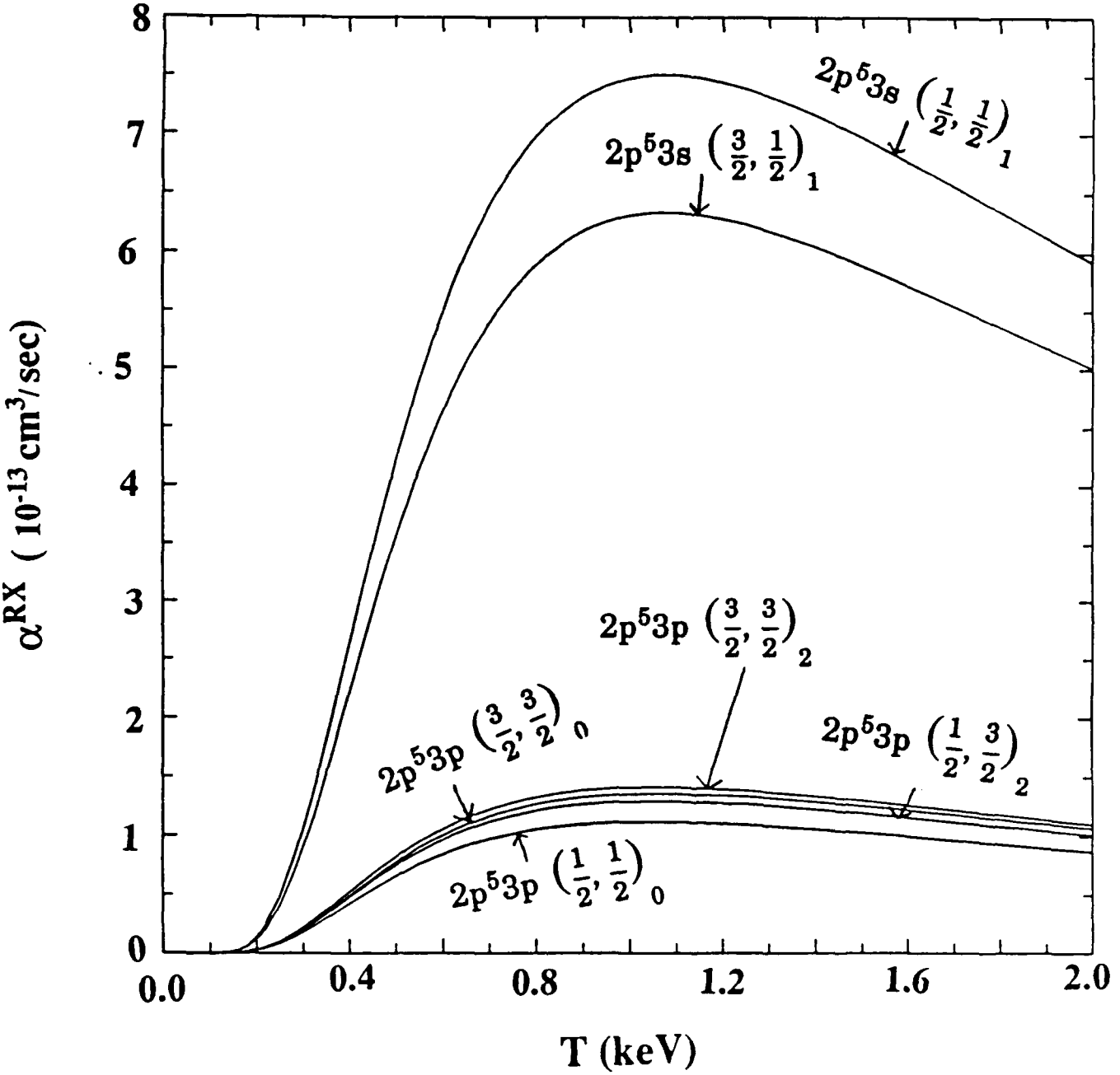

FIG. 4 Resonance excitation rate coefficients from the ground state to the observed upper $2p^5 3p$ and lower $2p^5 3s$ lasing levels of Ne-like selenium.

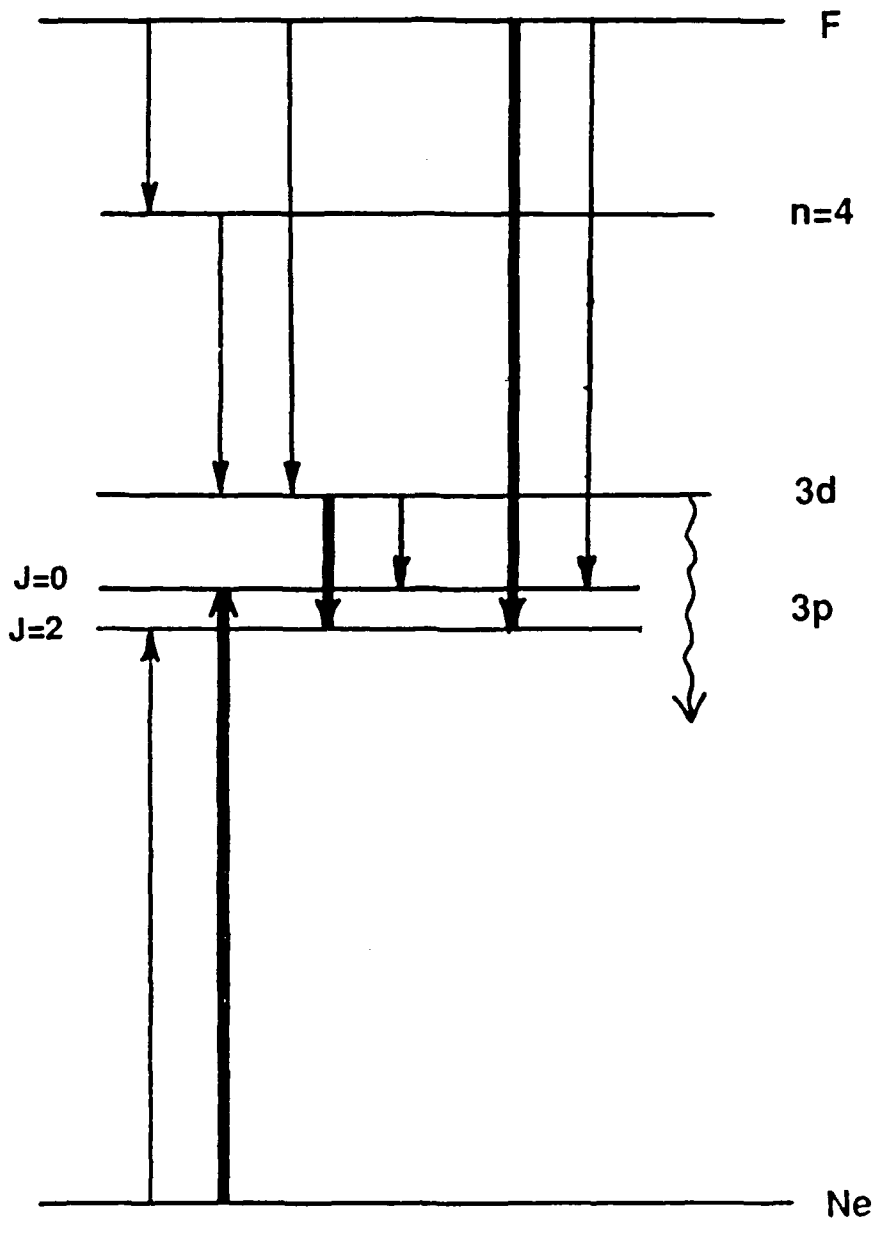

FIG. 5 Energy level diagram showing the relative strengths for populating the J=0 and J=2 3p levels from the F-like ground, Ne-like ground, and 3d excited states. The dark arrows indicate the strong pumping channels.

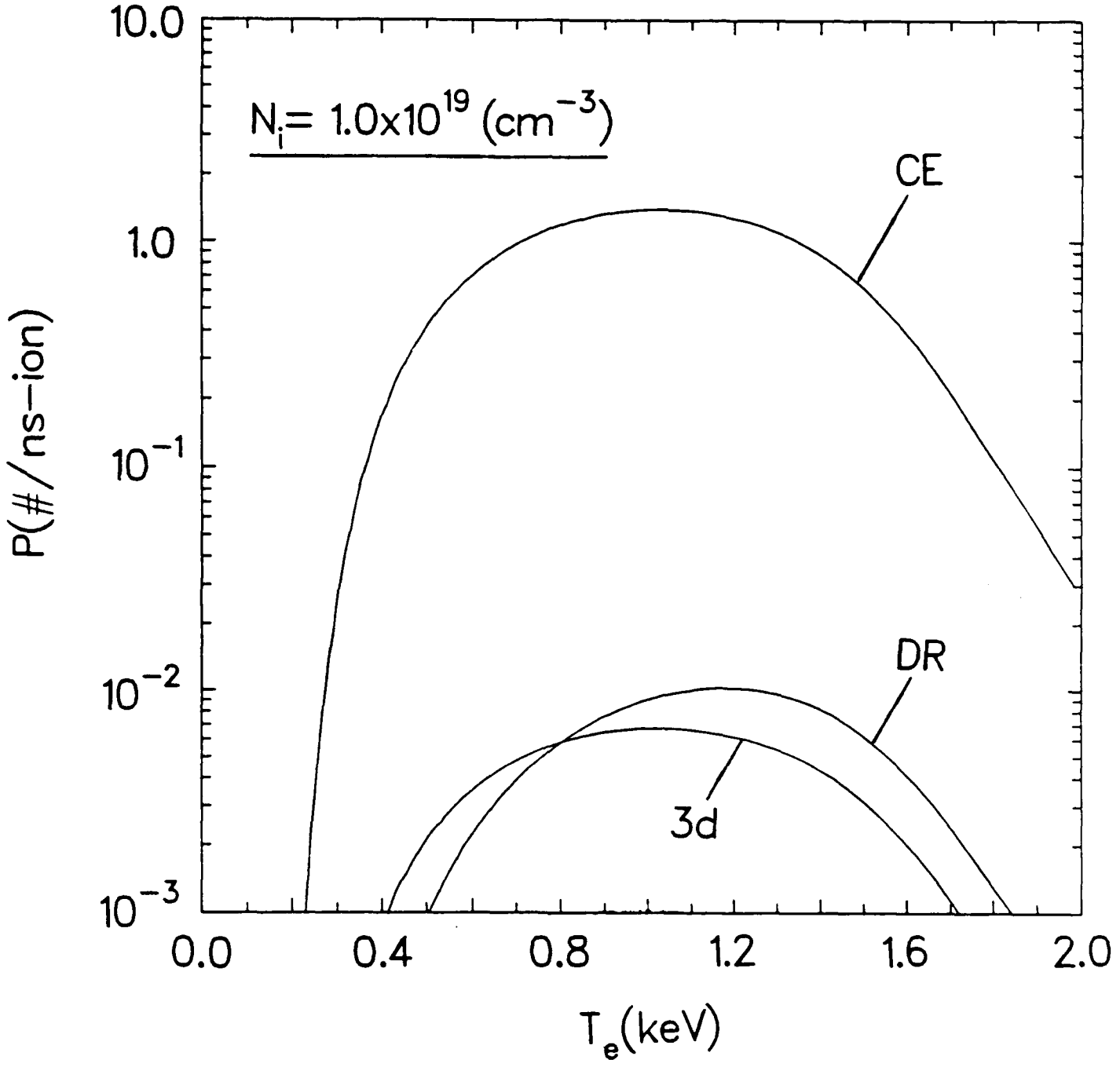

FIG. 6 Pumping rates of different processes populating the $(1/2,1/2)_{J=0}$ upper lasing level as a function of electron temperature at an ion density of 10^{19} cm^{-3}.

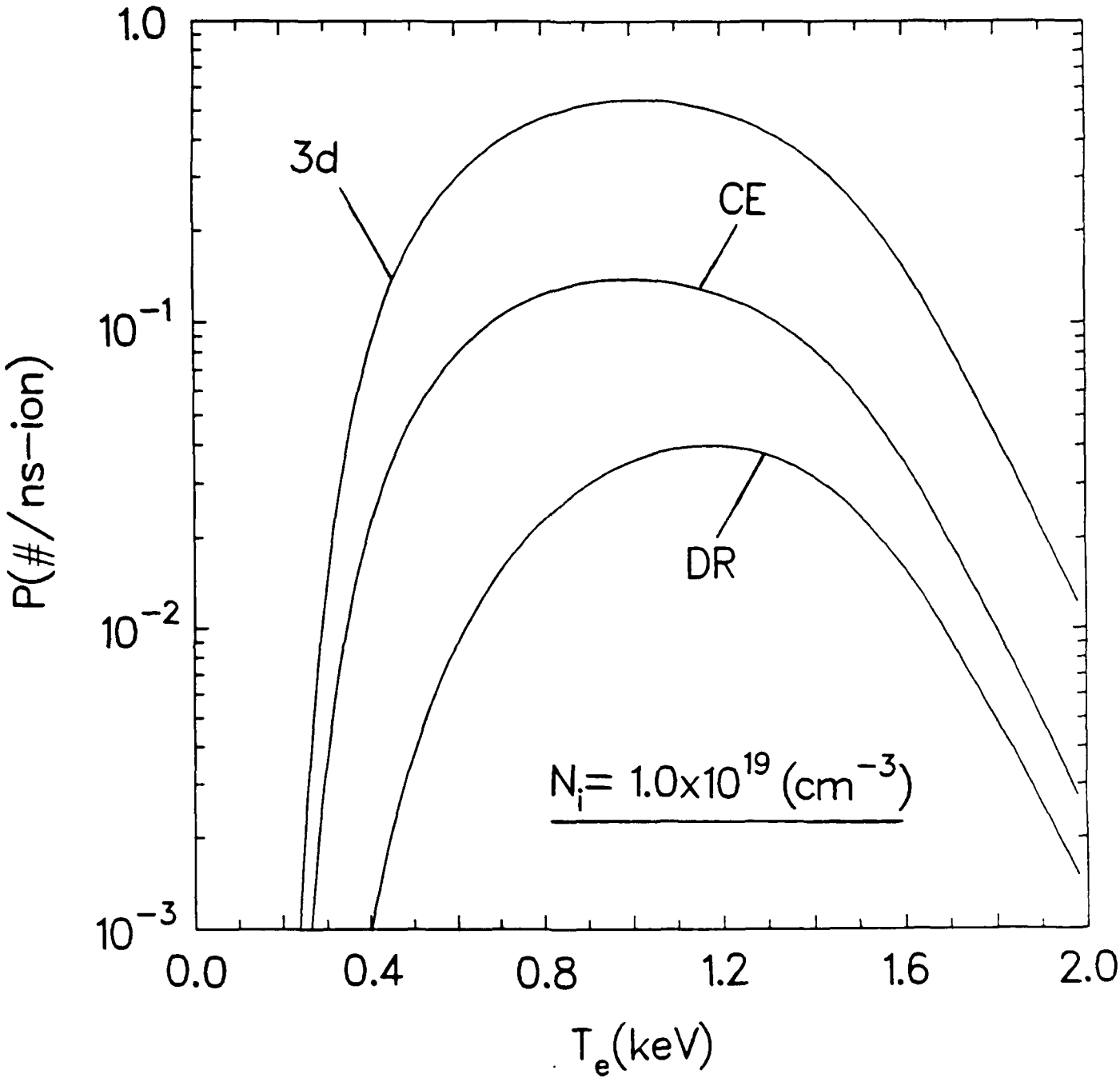

FIG. 7 Pumping rates of different processes populating the $(1/2,3/2)_{J=2}$ upper lasing level as a function of electron temperature at an ion density of 10^{19} cm^{-3}.

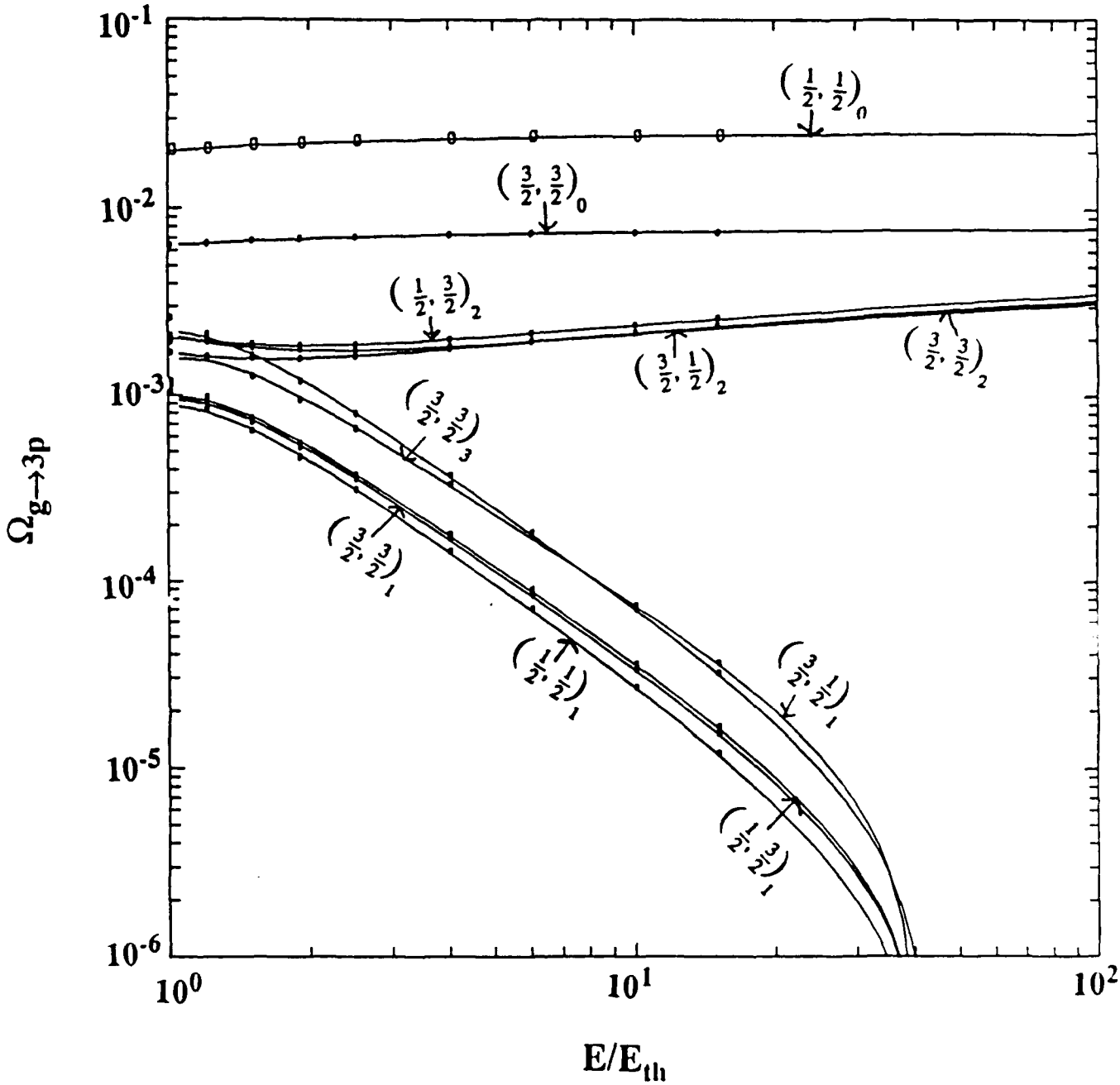

FIG. 8 Collision strengths of the ten 3p multiplet levels for excitation from the ground state of Ne-like selenium as a function of electron energy relative to the threshold energy. The circles are data points from Zhang and Sampson (Ref. 14).

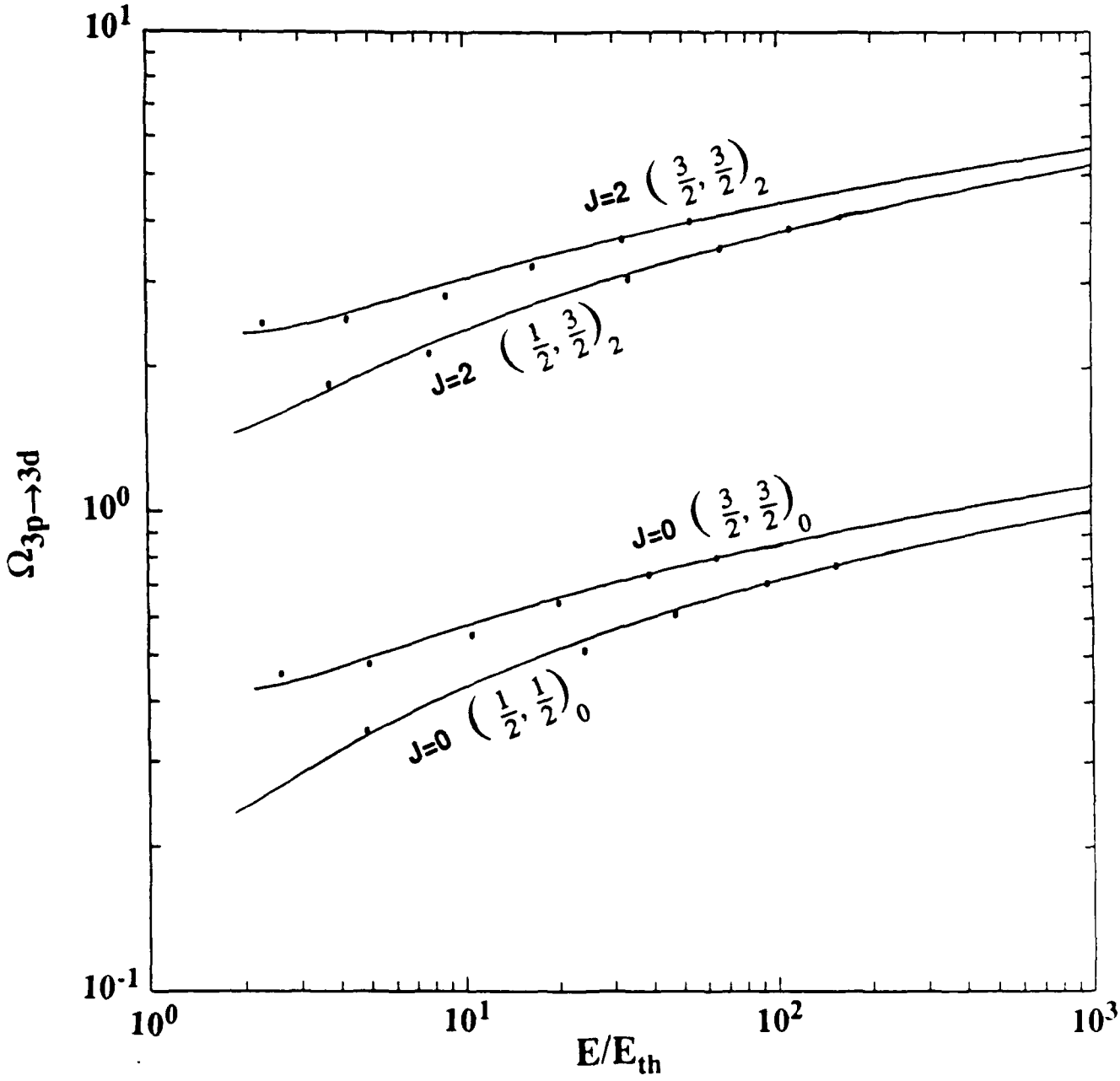

FIG. 9 Total collision strengths of the important four excitations from the J=0 and J=2 levels of the 3p state to the lumped 3d state. The circles are data points from Hagelstein and Jung (Ref. 18).

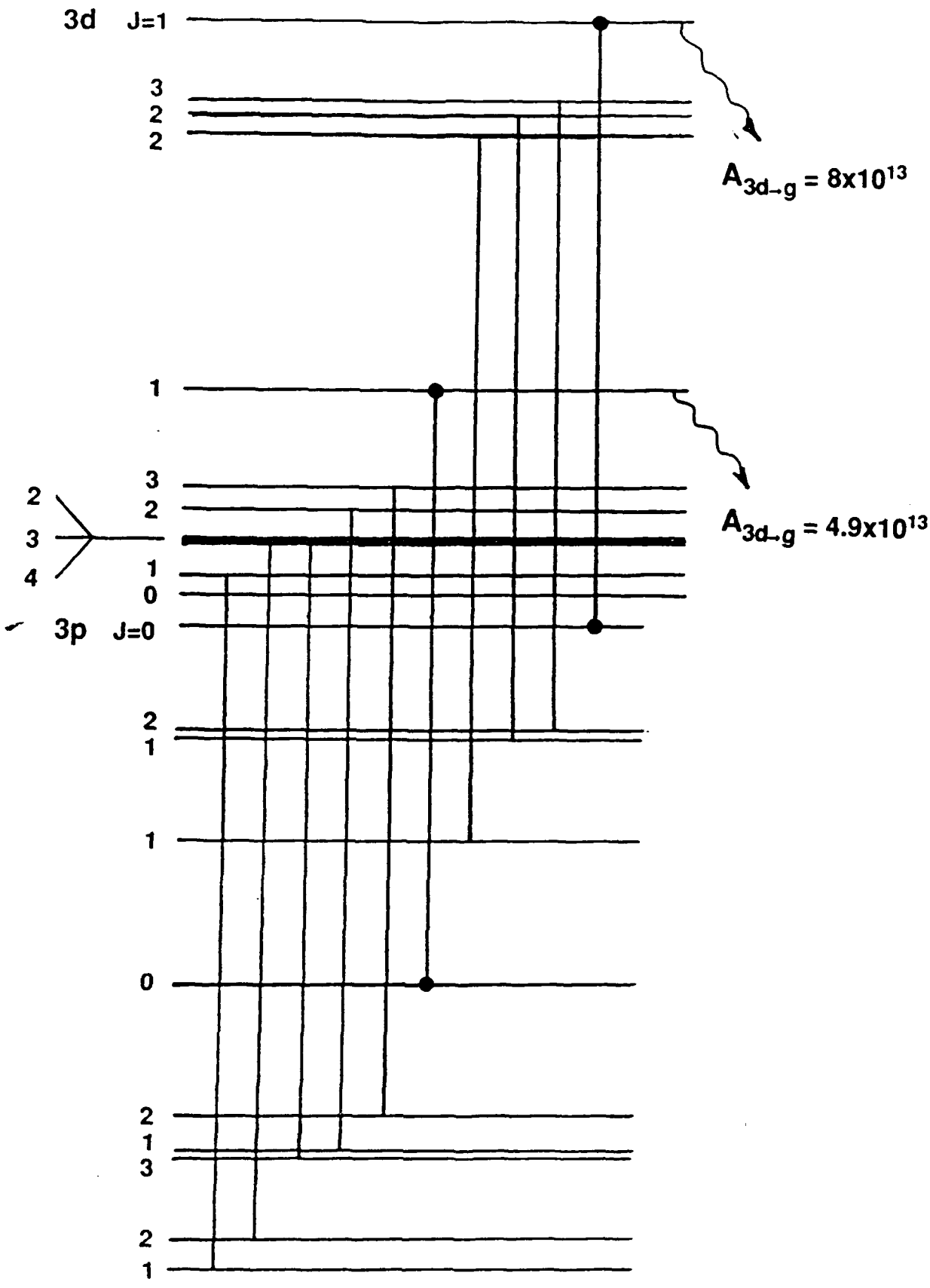

FIG.10 Energy diagram showing the strongest pumping channels of the 3p multiplet levels by deexcitation from the 3d levels. The channels coupling to the two strongly decaying 3d states are indicated by lines with dark dots.

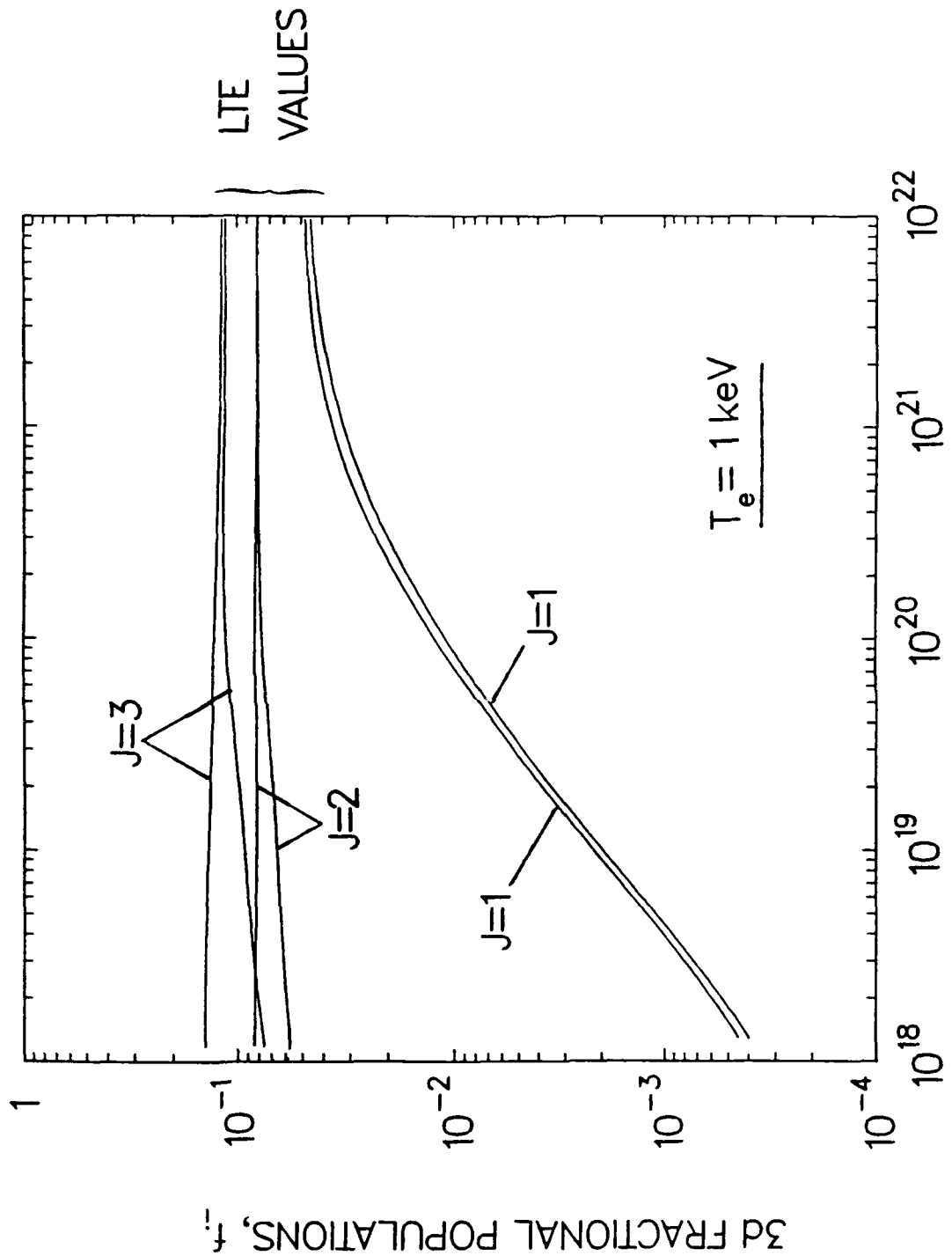

FIG.11 Fractional populations of the five 3d levels as a function of ion density at an electron temperature of 1 keV.

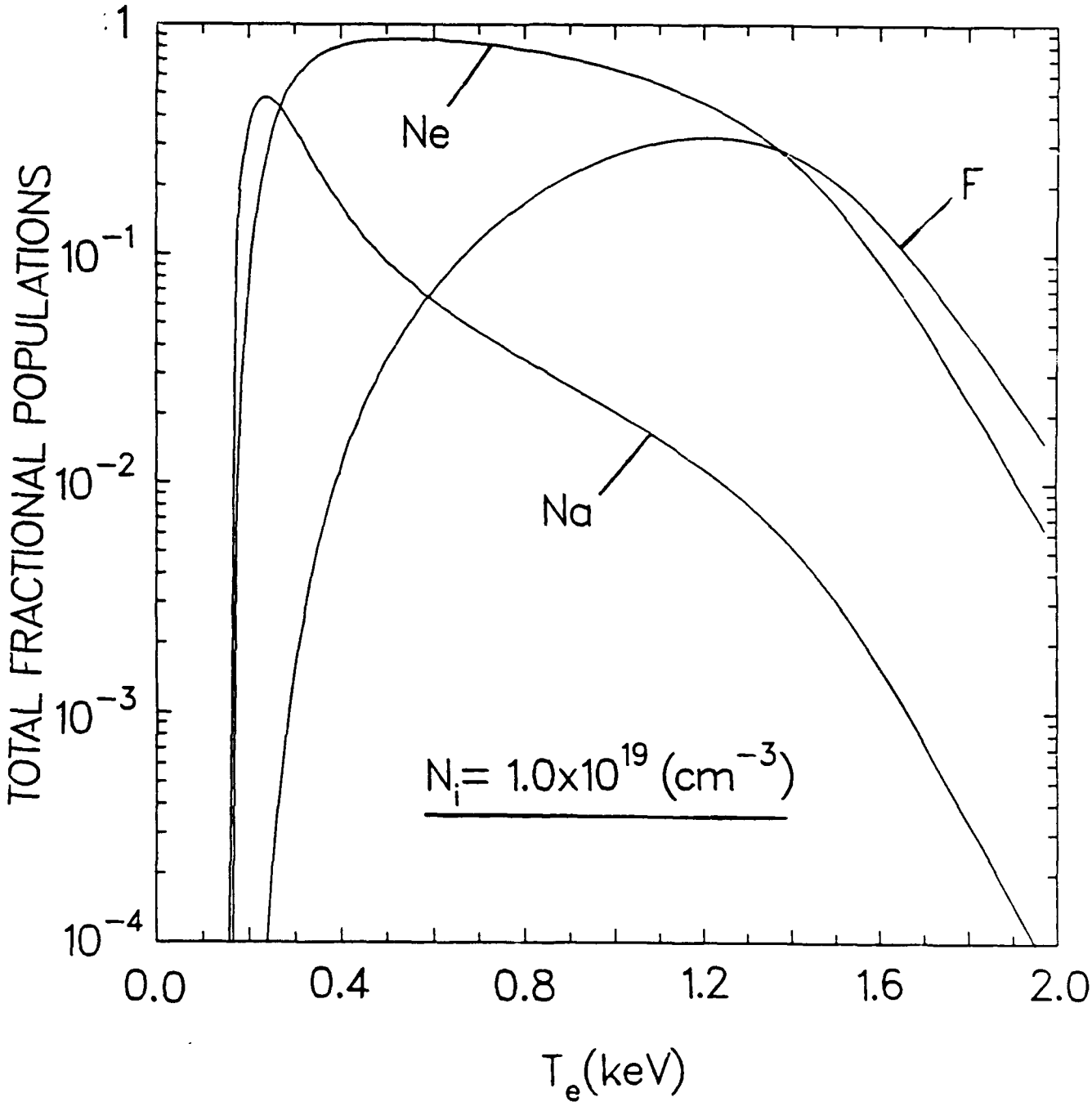

FIG.12 Total fractional populations of F-, Ne-, and Na-like selenium ions as a function of electron temperature at an ion density of 10^{19} cm^{-3}.

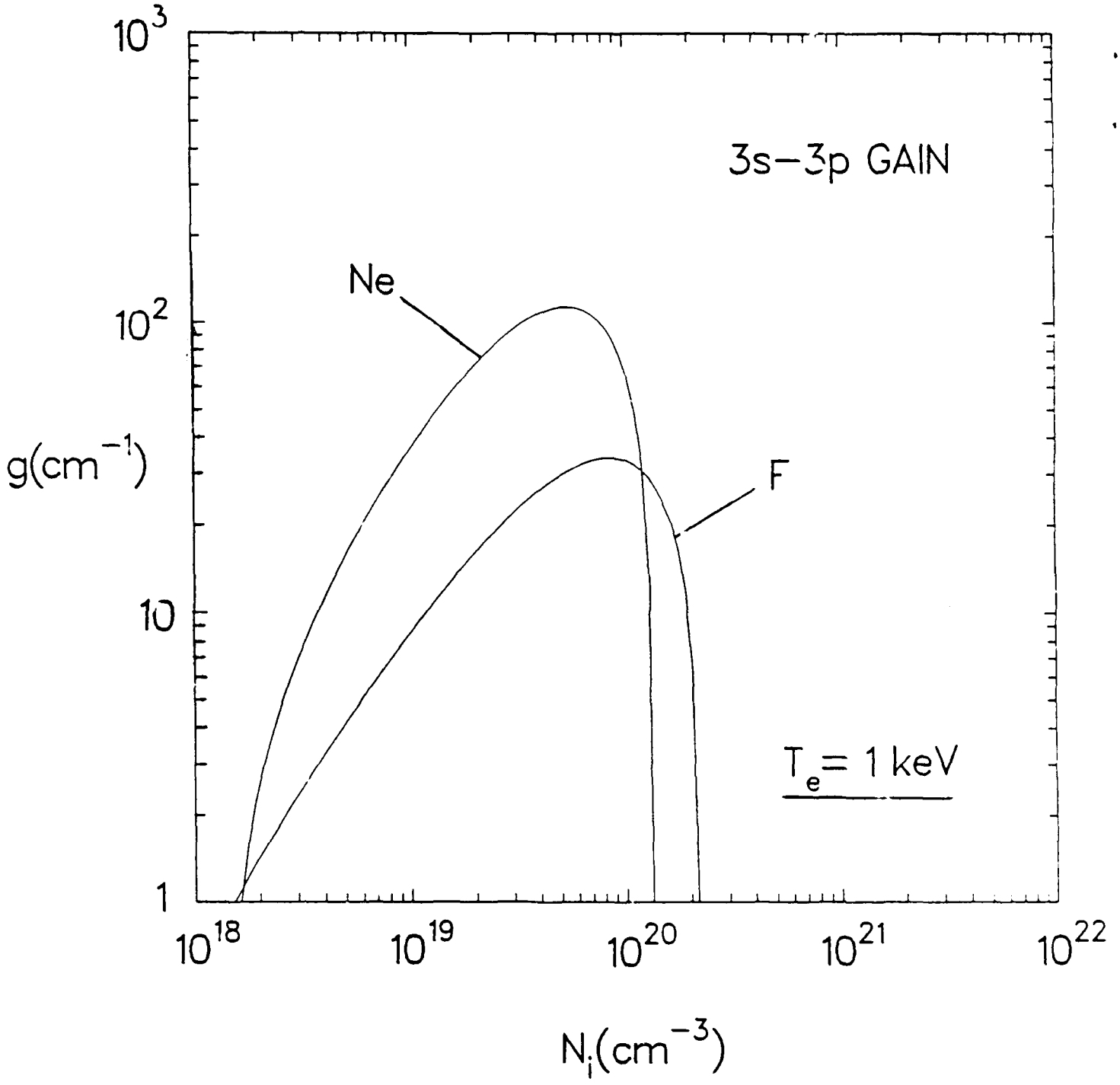

FIG.13 Total gain coefficients for the 3s-3p transition in F- and Ne-like selenium as a function of ion density at an electron temperature of 1 keV.

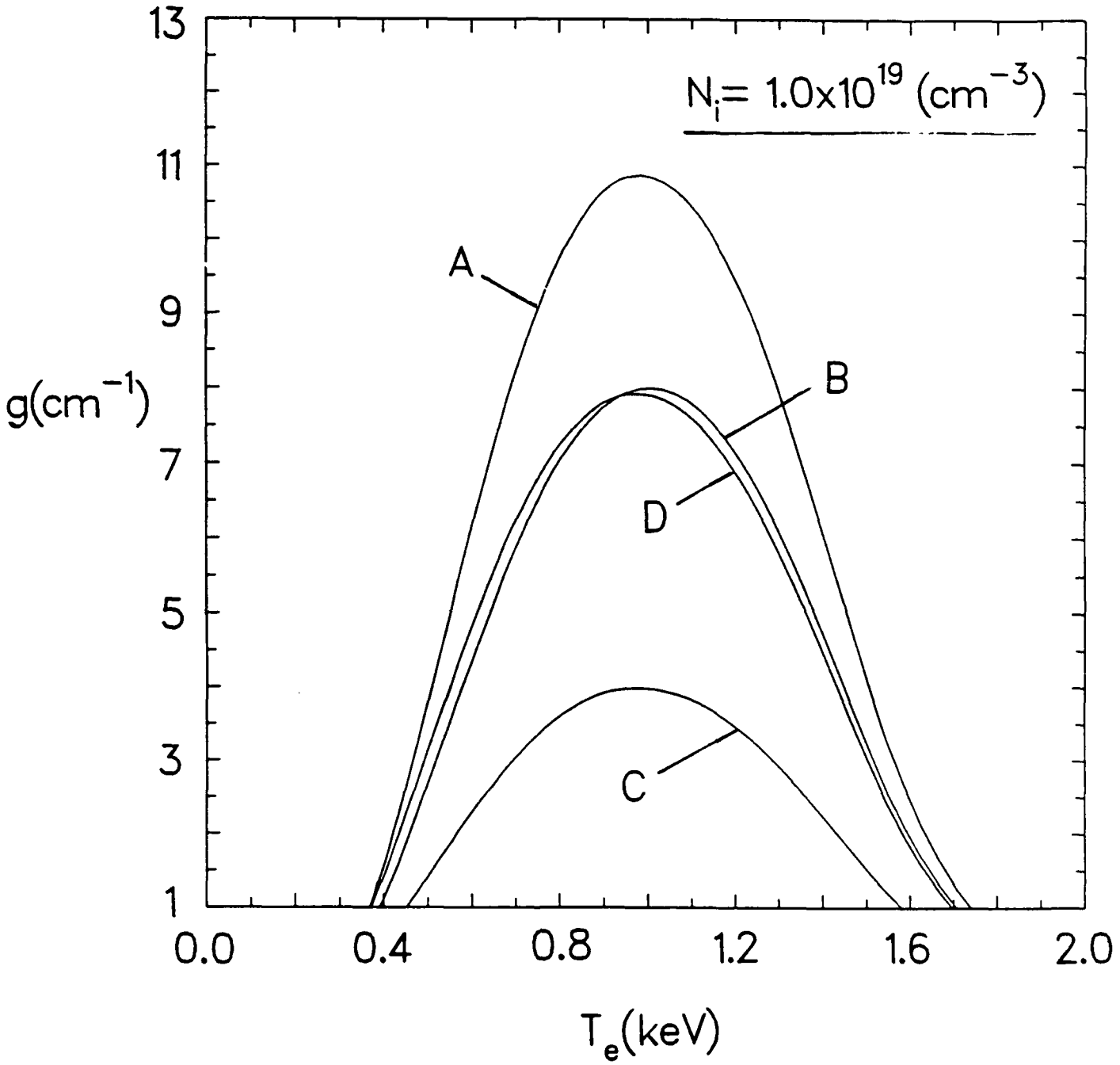

FIG.14 Gain coefficients (in cm^{-1}) for the four J=0-1 and J=2-1 3s-3p lasing transitions of neon-like selenium as a function of electron temperature. The curves are labeled as in Fig. 2.

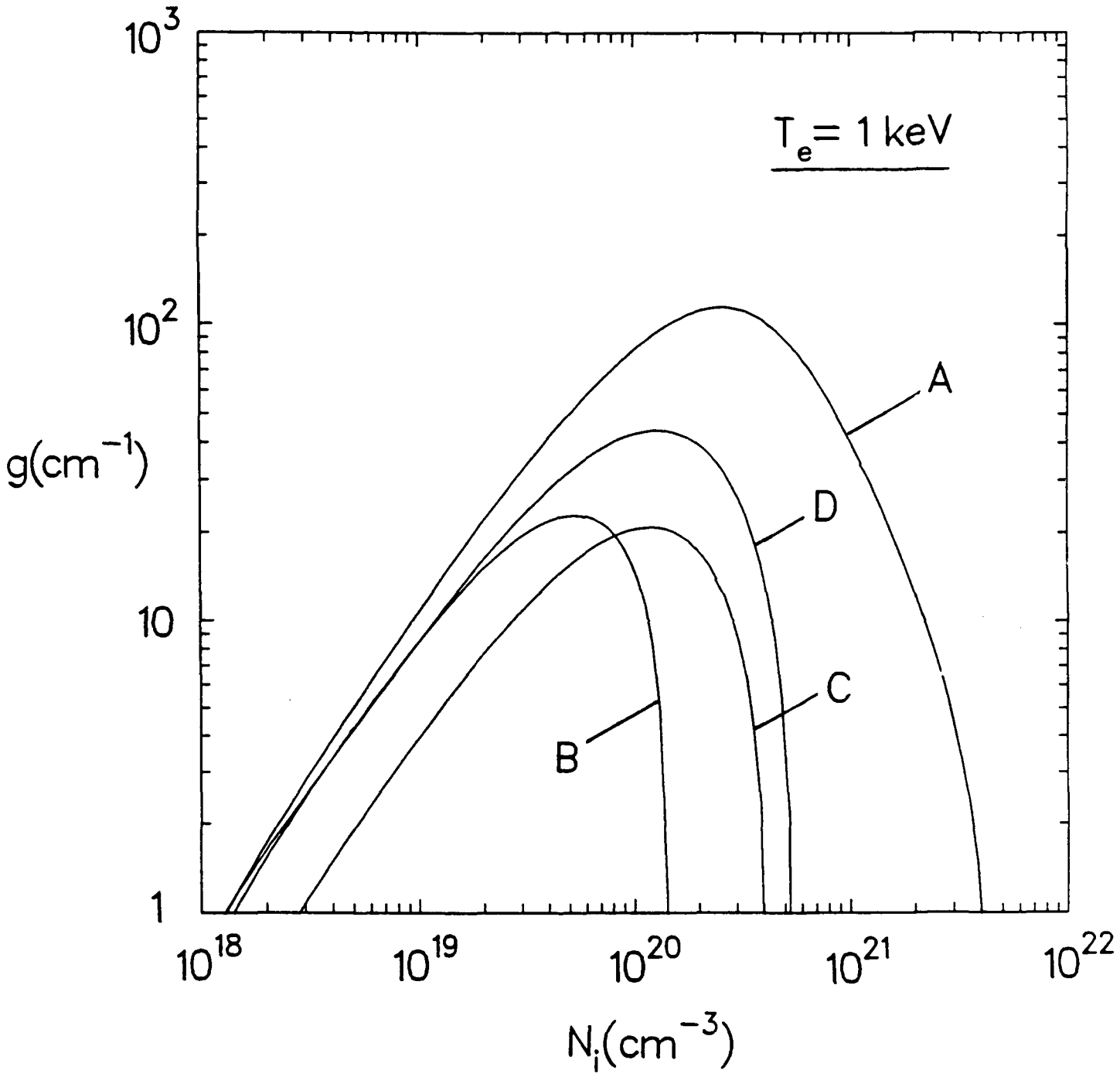

FIG.15 Gain coefficients (in cm^{-1}) of the J=0-1 and J=2-1 3s-3p lasing transitions as a function of ion density at an electron temperature of 1 keV.

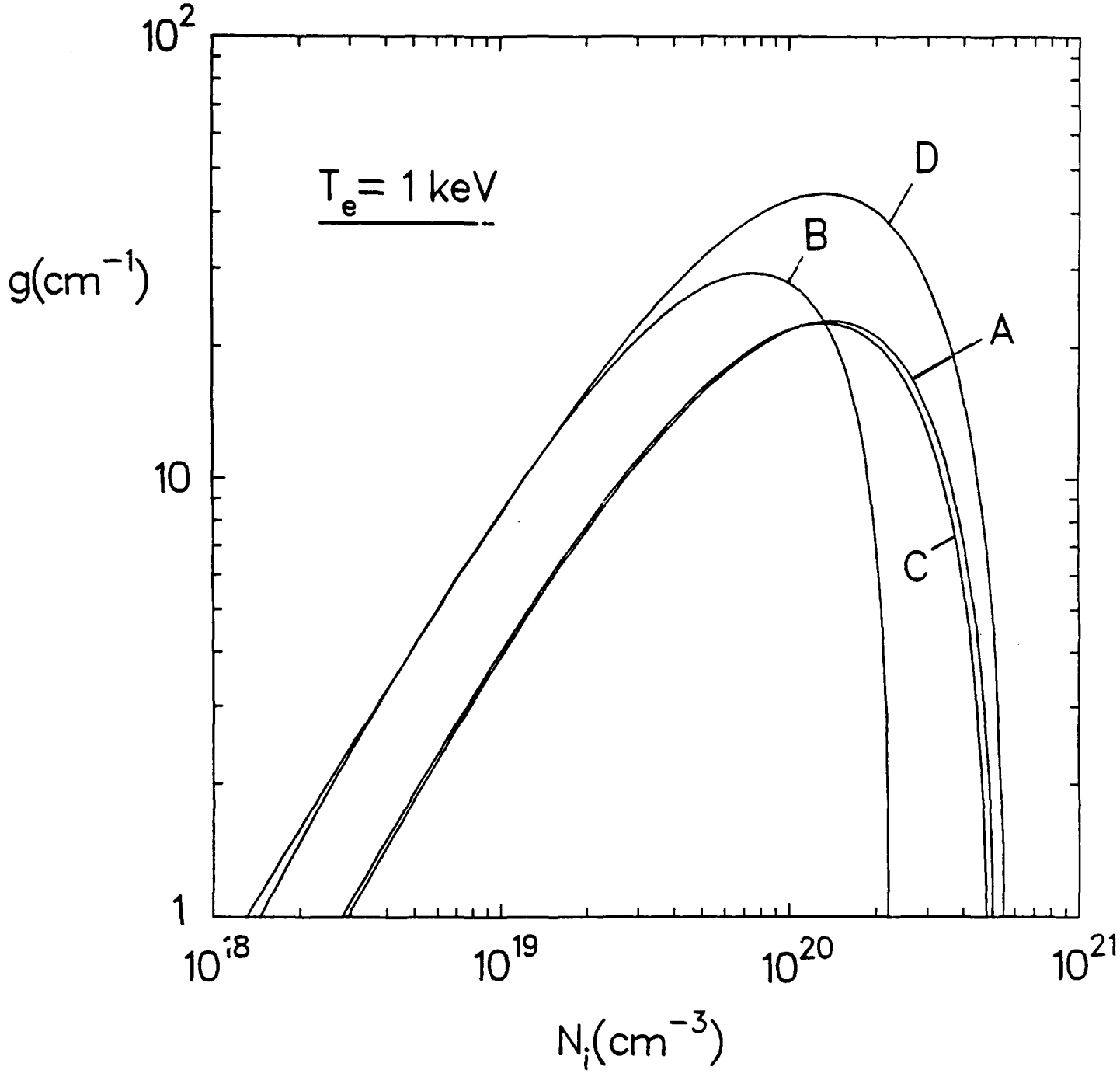

FIG.16 Gain coefficients (in cm^{-1}) of the J=0-1 and J=2-1 3s-3p lasing transitions as a function of ion density at an electron temperature of 1 keV. These coefficients were calculated using a modified atomic model in which the magnitude of the monopole excitation rate to the $(1/2,1/2)_0$ level was reduced by a factor of three.

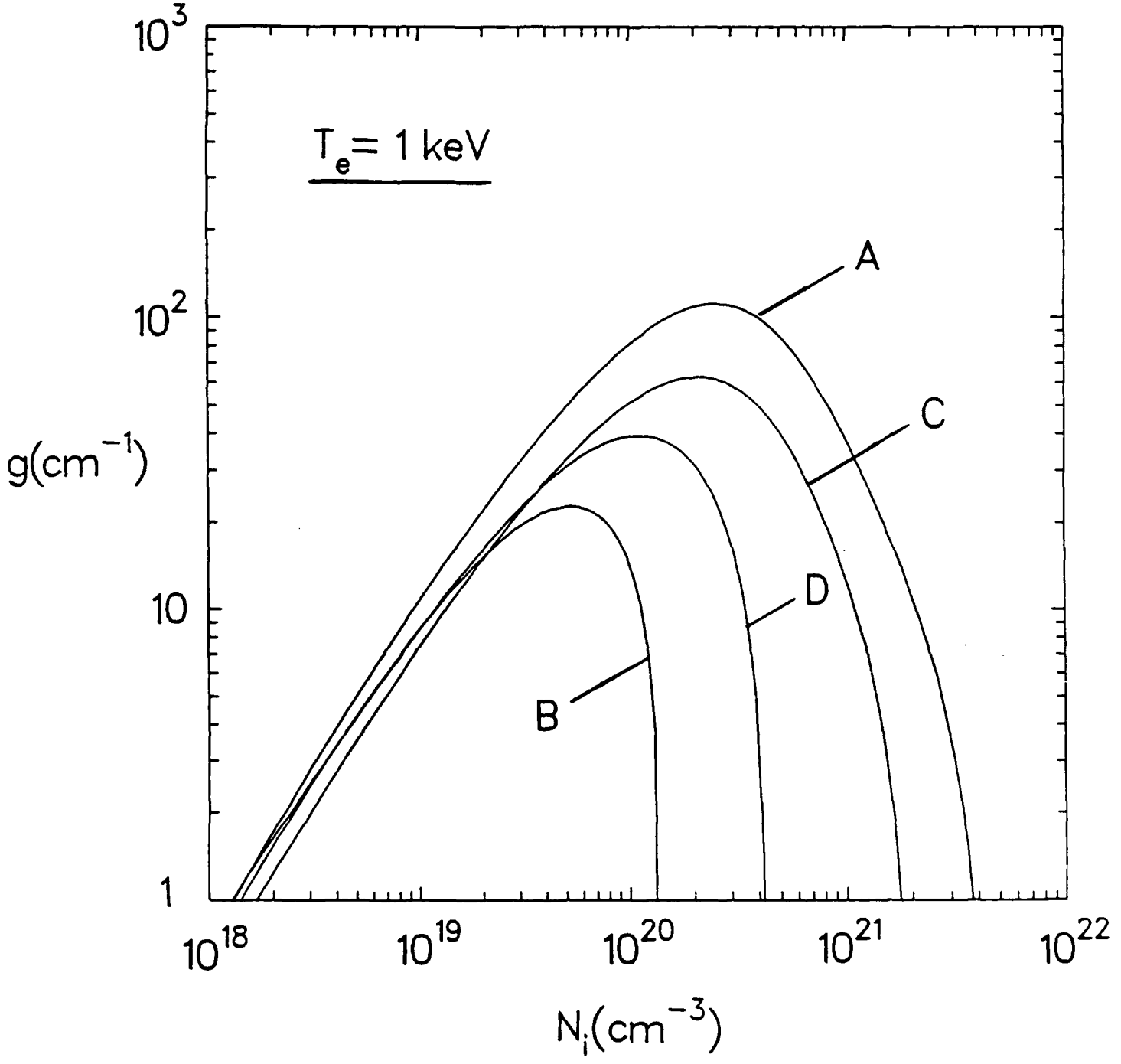

FIG.17 Gain coefficients (in cm^{-1}) of the J=0-1 and J=2-1 3s-3p lasing transitions as a function of ion density at an electron temperature of 1 keV. These coefficients were calculated using a modified atomic model in which the magnitude of the monopole excitation rate to the $(3/2,3/2)_o$ level was increased by a factor of two.